School of Environment

Engineering geological investigation of a recent mud volcano eruption, Waimata Valley

By

Alex Leighton

A thesis submitted in fulfilment of the requirements for the degree of

Master of Engineering Geology

The University of Auckland

2020

ABSTRACT

Mud volcanoes typically form in sedimentary basins both onshore and offshore, by localized expulsion of mud that has been remobilized from the subsurface. The extrusion of mud forms topographic features that are representative of the release of fluids and mud and overpressure.

The research that is presented in this thesis focuses on the recent formation of a mud volcano within the Waimata Valley near Gisborne from a single eruptive event on 15 December 2018, extruding approximately 11,200m^3 of mud at the surface. The eruption occurred from a completely new location though it is inferred that this feature is part of a mud volcano system that has previously formed other nearby mud volcanoes. The eruption of a mud volcano from the day of its occurrence is only something that has been documented a handful of times in New Zealand's written history.

Prior to eruption, this new eruptive centre had gained the attention of local scientists following a significant M_W7.1 earthquake that occurred offshore of Te Araroa in northern Tairawhiti region on 2 September 2016. It was also noted that following the earthquake many other mud volcanoes within the region demonstrated increased activity whilst others remained quiescent, highlighting an obvious relationship between mud volcanism and seismic activity.

Through utilising an engineering geological investigation of the site, an insight into the processes and mechanisms that trigger mud volcanism, as well establishing a database of the geological and geotechnical properties of the associated materials has been achieved. The materials were identified to contain a significant clay fraction, contributing to their low permeabilities and strength. These properties are inferred to have an important influence on how the that materials withstand significant overpressures remaining unconsolidated at depth leading to their migration toward the surface.

By developing this greater understanding of the mud volcano, multiple potential geohazards were identified and can be applied to future events that will inevitably continue to occur throughout the region. The most significant hazard identified resulting from this eruption was the formation a several highly mobile mud flows that led to the formation of a small lake.

ACKNOWLEDGEMENTS

Firstly, I'd like to thank my supervisor Associate Professor Martin Brook for his constant availability, guidance and support throughout every stage of this research. It was a daunting topic to undertake due to my limited prior knowledge, though it has proved to be an exciting and rewarding journey into the world of mud volcanoes.

I'd also like to thank Dr Murry Cave from the Gisborne District Council for the coordination and information he provided. Murry's local knowledge and enthusiasm regarding the subject was invaluable to my research.

To the landowners, the Utting and Hall families. Thank you for letting me access your land and I hope I managed to leave as little of a trace as possible. I enjoyed our conversations over the fence and your knowledge of the event was an essential part of my research.

To the many university staff who helped me throughout the many hours spent in the various laboratories: Dave Wackrow, Brendan Hall, Catherine Hobbis, Stuart Morrow, Jeff Melster and Mike Rowe. All your technical knowledge and guidance was essential to my research.

At last, but certainly not least, to my loving and supportive partner Ash. Her organisation and sacrifice were fundamental to getting this across the line. As an unexpected bonus for her, listening to my ramble about mud volcanoes late at night proved to be an effective lullaby and falling asleep was never an issue.

TABLE OF CONTENTS

LIST OF FIGURES

LIST OF TABLES

CHAPTER ONE: INTRODUCTION

1.1 Introduction

Mud volcanoes typically form in sedimentary basins both onshore and offshore, by localized expulsion of mud that has been remobilized from the subsurface (Odonne et al. 2020). Sediment mobilization is driven by the migration of gas and liquids resulting from compaction, diagenetic transformation, and thermal maturation of sediments (Brown, 1990; Dimitrov, 2002; Kopf, 2002; Deville et al., 2003; Manga et al., 2009; Mazzini and Etiope, 2017). A distinction can be made between mud volcanoes constructed from individual mudflows to emplaced during a single eruptive event, and mud volcanoes built over hundreds or thousands or years from multi-eruptive activity events (Odonne et al., 2020). Indeed, the emission of mud is an episodic phenomenon; phases of eruption can last from time intervals lasting only a few days, that can then be separated by longer intervals of quiescence that can last over several years, or even decades (Kopf, 2002; Deville, 2009; Mazzini and Etiope, 2017).

In New Zealand, >250 fluid and/or gas seeps and at least 4 oil seeps have been reported and studied from the eastern North Island over the last few decades (Ridd, 1968, 1970; Field et al. 1997; Pettinga, 2003). Some of these fluid seeps are associated with diapiric mud extrusion along fault zones and the formation of mud volcanoes (Ridd, 1970; Mazengarb, 1997; Pettinga, 2003). Most recently, on a farm in the Waimata Valley close to Gisborne, around 8am on 15 December 2018, approximately 11,200 m^3 of white mud was ejected from the ground covering an area of ~ 2.1 ha (Fig. 1.1). Later that afternoon, the ejected material was discovered by landowners Jim and Sharon Hall who had returned from Gisborne township. The ejected material was not unfamiliar to the Halls as they already had several other mud volcanoes on neighbouring paddocks. The other volcanoes on the farm had been relatively well documented due to their repeated eruptive history, but the December 15 2018 event had occurred from a completely new eruptive centre.

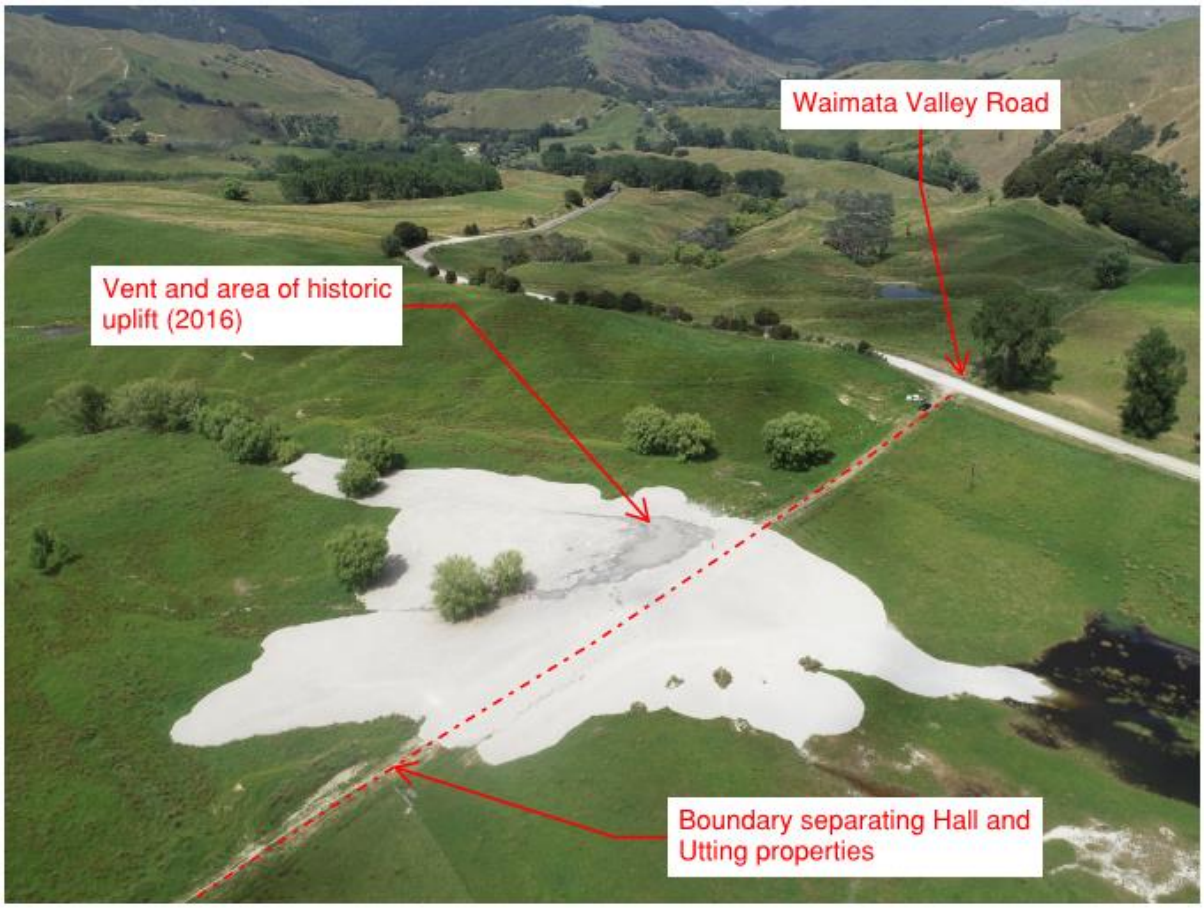

Figure 1.1: *Recently erupted Mud Volcano taken on 8 January 2019, at the boundary of the Uttings and Halls properties, Waimata Valley.*

Prior to the eruption, this new eruptive centre had gained the attention of local scientists following a significant M_W7.1 earthquake that occurred offshore of Te Araroa in northern Tairawhiti region (Fig 1.2) on 2 September 2016. The earthquake had caused the site to uplift by about 1 m and a formed a raised dome feature on the boundary of the Hall and Uttings farms. An image of the site taken immediately after the earthquake events is shown in Fig. 1.3 (below). The resulting uplift blocked a small stream that ran through the properties where excavation works had to be undertaken to restore its gradient.

As highlighted above, mud volcanoes are not unique to the Waimata Valley (e.g. Ridd, 1970; Field et al., 1997; Pettinga, 2003). As research becomes more technologically advanced, it is very likely that many more mud volcanoes within the region will be discovered, and that eruptions will continue to occur in the future (Mazzini and Etiope, 2017, Blouin, 2019). These features pose many hazards to people and structures, particularly for areas that are more densely populated. The well-known mud volcano field surrounding Wheatstone Road is located on the

outskirts of Gisborne township and the popular coastal suburb of Wainui (Ridd, 1970; Mazengarb, 1997, Speden, 2004). The field is considered active with multiple permanent seeps (Mazengarb, 1997, Speden, 2004).

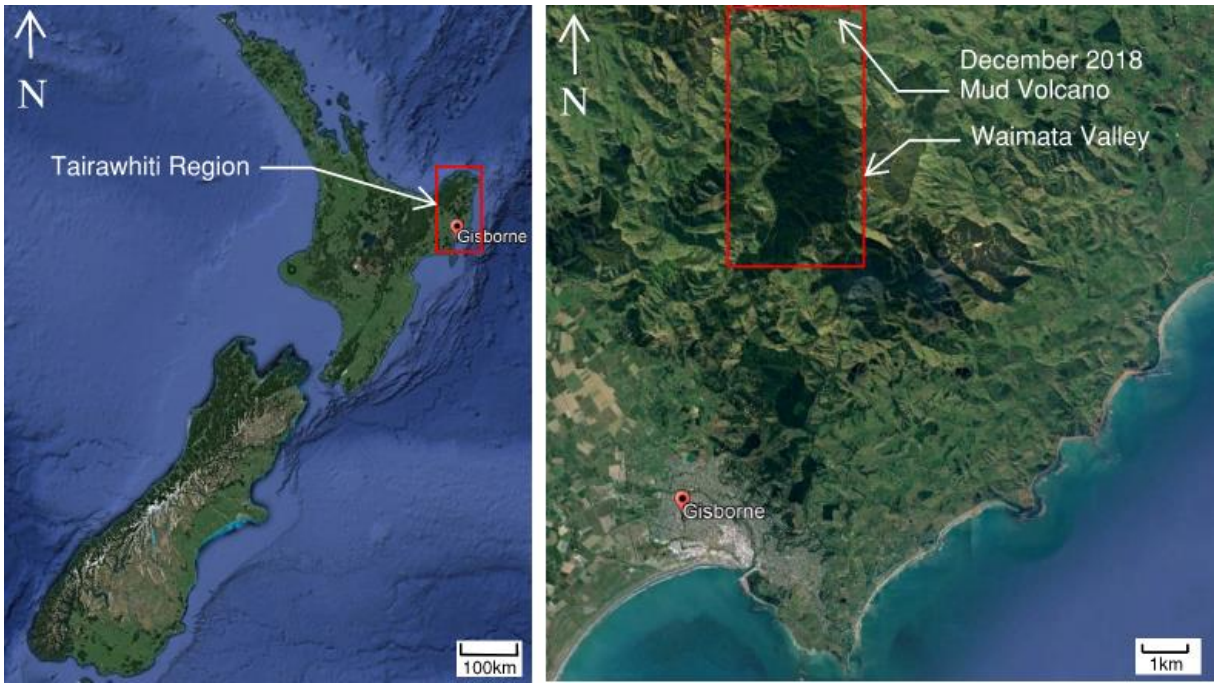

***Figure 1.2**: Study area in context of New Zealand (left) and the Waimata Valley (right)*

This 2018 event presents a unique opportunity to document the mud volcano and its continued behaviour from the initial eruption, something that has been only done a handful times in New Zealand's written history. There is also a significant lack of information in available literature regarding the engineering behaviour of the materials produced by mud volcanoes in New Zealand. This information is particularly important for understanding how the material manifested at the surface, and subsequently how it might behave once it has erupted.

Mud volcanoes and the erupted materials appear to demonstrate variable behaviours across the world (e.g. Brown, 1990; Kopf, 2002; Deville, 2009; Mazzini and Etiope, 2017; Dupuis et al., 2019; Odonne et al., 2020). An understanding of the geomorphological occurrence of the December 2018 mud volcano, as well as the engineering behaviour of the erupted material, will help to understand future events and associated hazards that they pose.

Figure 1.3: *Uplift and rupture on boundary separating the Uttings and Halls properties, Waimata Valley September 2016*

1.2 Thesis outline

Chapter One introduces the research and provides a scientific background on the phenomenon of Mud Volcanoes. This involved an extensive literature review of both local and international research, largely focusing on what are mud volcanoes, where are they and how do they occur? The engineering properties of the material associated with mud volcanism is also briefly reviewed.

Chapter Two introduces the Mud Volcano that is to be the main subject of the research. This involves providing detail of its location and the eruptive event, as well as introducing the regional and local geology which are the driving force of these features.

Chapter Three focuses on the investigative and laboratory methods used to collect data on the Mud Volcano and the extruded material. *Chapter Four* reports the results, including the geological and engineering behaviour of the extruded material.

Chapter Five is the Discussion chapter, which provides a contextualisation of the results presented in Chapter Four, in a regional and global context.

Chapter Six summarises and presents a critical evaluation of the research. This includes its limitations and what could be the focuses of future research concerning the topic.

1.3 Aims and Objectives

The aim of this research is to develop an understanding of the subject mud volcano to give insight into the mechanisms that occur to cause migration of deeply buried sediments to manifest at the surface. It is also the aim to understand the engineering behaviour of the extruded material at the surface which can be used to predict how this, and other mud volcanoes might behave in the future. This is primarily achieved by characterising the feature and extruded materials using various investigative and laboratory techniques and tests.

It is a unique opportunity to document a mud volcano eruption from the day of its occurrence, which can be used to help to understand and mitigate the hazards they present within a region where they are prevalent.

1.4 Review of Mud Volcanism

1.4.1 Definition of Mud Volcanoes

A mud volcano (MV) is the surface or seafloor expression of a subsurface transfer of fluidised clayey sediments. It is expressed as a vent, acting as a fluid outlet, allowing degassing and dewatering of deeply buried sediments (Dimitrov, 2002, Kopf 2002, Odonne et al., 2020). MVs were inherently named due to their similar geometry to igneous volcanoes, though that is where the similarity ends (Fig. 1.4). The geological and sedimentological processes controlling MV generation are vastly different to the magmatic process producing igneous volcanoes (Kopf, 2002).

Mud volcanism can be defined as the range of physical and sedimentological processes leading to the extrusion of the clayey material forming the mud volcano. The extruded mud is a mix of three or four different phases: gas (methane), water, sediment (mainly clay) and in some cases oil (Kopf, 2002; Deville, 2009; Mazzini and Etiope, 2017; Blouin, 2019). In rare cases, the gas

involved can be CO_2 or N_2 where hydrocarbon systems are within the source area of the mud (Mazzini and Etiope, 2017). The different phases that constitute the mud may have different stratigraphic sources, which are dependant of the geological context of the mud volcano i.e. tectonic setting, stratigraphy, maturity of source formations. Furthermore, mud volcanoes within the same sedimentary basin may vary greatly in their source and constituents (Mazzini and Etiope, 2017). The proportion of each phase will determine the properties of the mud, particularly the viscosity of the mud, which has a strong influence on the surface expression of the mud volcano (Kopf, 2002; Mazzini and Etiope, 2017).

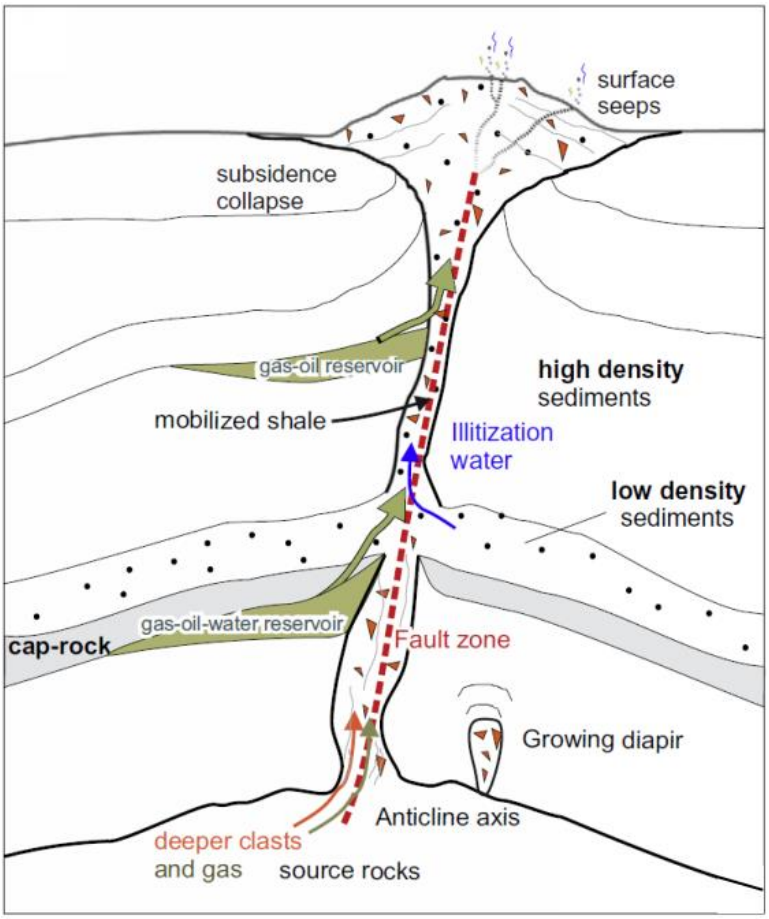

Figure 1.4: *Schematic diagram summarising the main elements characterising most MVs as well as the main sources of fluids (from Mazzini and Etiope, 2017).*

The sediment within the mud is generally composed of clay and silt-sized particles, often containing other mineral fractions such as quartz, mica and albite. Organic or biogenic particles often allow the main source of the grains to be identified, which is commonly related to the detachment level (Kopf, 2002). The source mud is combined with larger-size particles which are up ripped from the walls of the conduit during its ascension. The larger sized particles can

be several meters in size (Roberts, 2011). The water within the mud can may originate or be generated from three various sources: formation water, clay dehydration or mineral diagenesis reactions, and meteoric waters and can be generated by different mechanisms and reactions (Mazzini and Etiope, 2017). The origin of the gases within the mud are generally thermogenic or from a deep hydrothermal system, and are rarely biogenic (Kopf, 2002; Deville, 2009; Mazzini and Etiope, 2017). It has been recognised that during quiescent periods of mud volcano activity, lighter gas such as methane is often expelled from the vent, whereas heavier gases are often expelled after eruptive events (Etiope et al., 2009).

The morphology of MVs at the surface is variable and highlights the various properties that control the mechanisms of eruption (Mazzini and Etiope, 2017). The activity of a MV is largely periodic, but commonly irregular. Many large eruptions have occurred after long periods of quiescence (Brown, 1990; Mazengarb, 1997; Roberts, 2011).

1.4.2 Occurrence of Mud Volcanoes

Mud volcanoes occur in geologically similar settings across the globe (Fig. 1.5) with several thousand structures identified onshore or offshore (Dimitrov, 2002; Deville, 2009; Mazzini and Etiope, 2017). They are mostly associated with tectonically active areas such as accretionary margins, deep sedimentary basins, thrusts, and overthrust belts; and less commonly in tectonically passive areas such as major river deltas (Yassir, 1989; Dimitrov, 2002; Mazzini and Etiope, 2017). Fig. 1.5 below shows the global distribution of mud volcanoes.

Figure 1.5: *Global distribution of known mud volcanoes (from Mazzini and Etiope, 2017).*

1.4.3 The Mud Volcano System

The complete subsurface network and the consequential MV at the surface is collectively named the Mud Volcano System. This system can be subdivided in series of 'structural domains' which each control a characteristic set of processes. The basic mud volcano system consists of three principal structural domains; the deepest 'source domain', overlain by the 'intrusive domain' and finally the extrusive domain (Steward and Davies, 2006; Roberts, 2011; Blouin, 2019). Fig 1.6 (below) shows the basic subsurface architecture of a mud volcano.

The source domain includes the origin of the remobilised sediment as well as any other deeper sourced fluids. The upper boundary of the source domain (or lower boundary of intrusive domain) is classified by the deepest stratigraphic unit that has been intruded by the allochthonous fluids (Roberts, 2011). The source domain is usually comprised of a thick sequence of under compacted clays or shales and is generally Paleogene to late Neogene in age (Kopf, 2002). The composition of the sediment within the mud can easily be related to the stratigraphic formations at depth by using chemical analysis, identified of mud matrix, clast type or microfossil assemblages (Kopf, 2002).

The intrusive domain connects the and source domain to the extrusive domain. It comprises the conduit system responsible for transporting the sediments, fluid, and gas from the source domain to the surface. There are many different architectures and mud flow processes that have been suggested by various authors, though they are still poorly understood due to the lack of exposures of these conduit systems (Roberts, 2011; Blouin, 2019).

The extrusive domain of the mud volcano system is the location where the mud is extruded or erupted at the surface. Due to their exposure, the domain has been extensively studied in many locations across the globe both onshore and offshore and is perhaps the most well understood. The morphology of the edifice (outcropping or buried) depends largely on the mud composition and the subsurface architecture (Kopf, 2002; Mazzini and Etiope, 2017). It typically forms a conical to biconical shape and summit crater. The sizes and shapes are highly variable, spanning from centimetres to kilometres (Kopf, 2002). A summit crater or vent is the surface expression of the conduits through which the mud is expelled. Fluid and gas tend to continue to expel at the crater following the mud (Kopf, 2002).

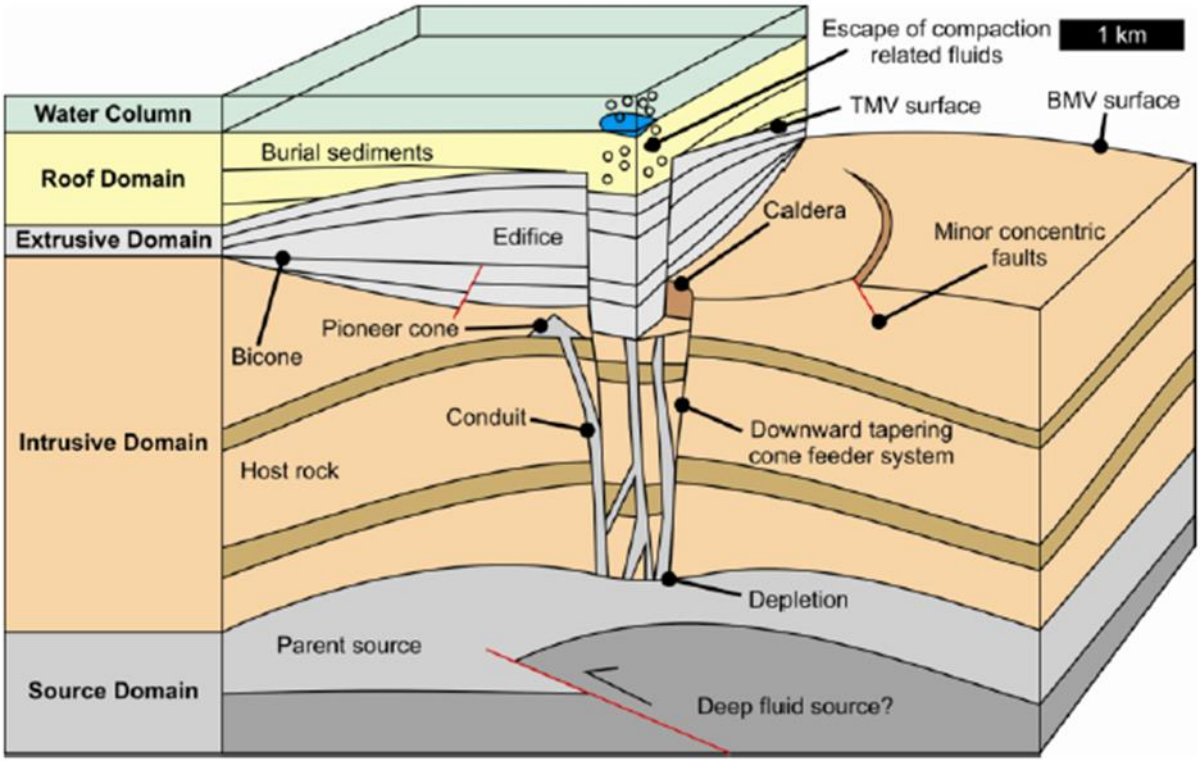

Figure 1.6: *Summary Diagram outlining the basic subsurface structure configuration and structural domains of a large mud volcano system. Onshore mud volcano systems are usually lack a roof domain and are not below sea level (Roberts, 2011).*

1.5 Mud Volcano Genesis and Activity

The formation of a mud volcano is dependent on a variety of preconditioning factors and parameters that could trigger mud generation and mobilisation (Kopf, 2002; Mazzini and Etiope, 2017). These include overpressure of strata at depth, gravitative instability and hydraulic fracturing, which are also sequenced as a chain of events leading to a mud extrusion or eruption. Fig. 1.7 (below) shows a conceptual model of a potential chain of events that may lead mud mobilisation and mud volcano formation (Deville, 2009).

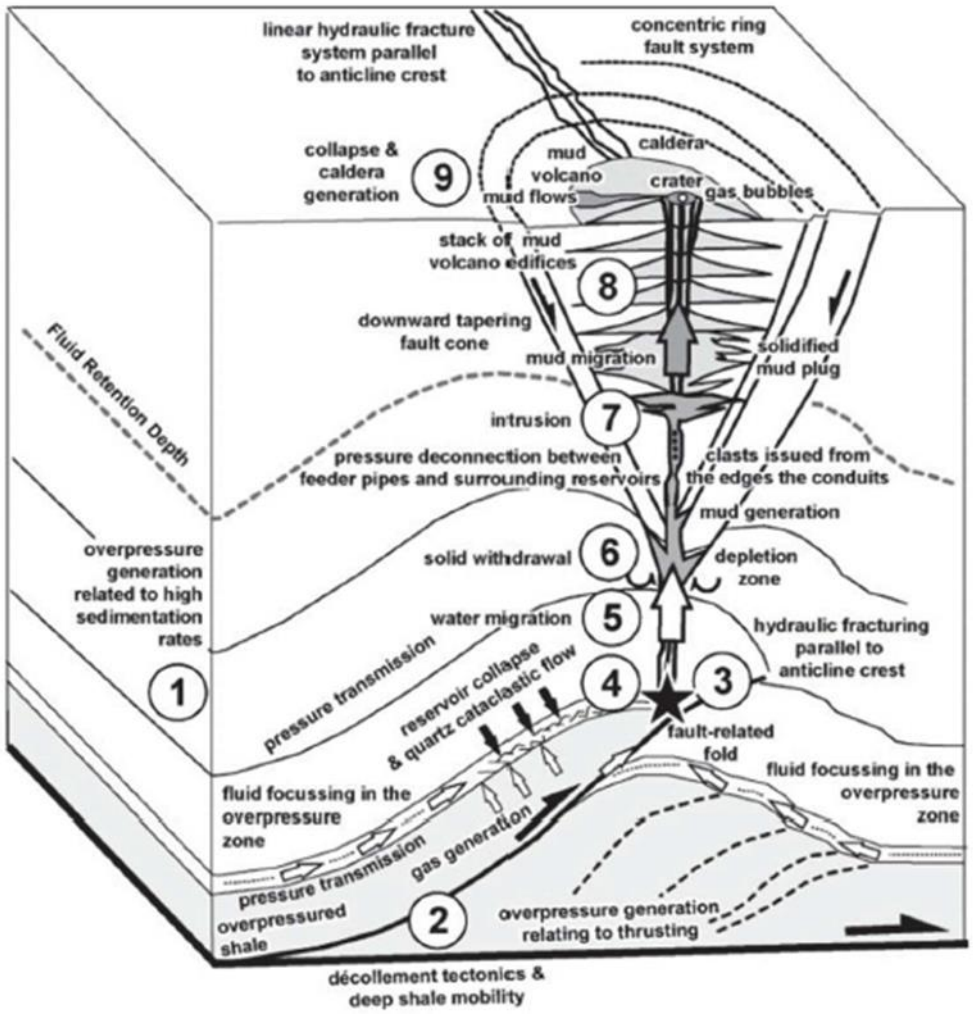

Figure 1.7: *Conceptual mud volcano system model showing a potential chain of events lead to mud remobilisation and mud volcano formation (Deville, 2009).*

1.5.1 Overpressure

Subsurface mud mobilisation is controlled by the development of overpressure at depth which provides sufficient energy for layers of strata to be breached and allows mud (fluid sediment mixing) to be transferred to the surface (Deville, 2009). Overpressure is defined by pore water pressures exceeding hydrostatic pressure. It is caused by the inability of connate pore water within strata to escape as surrounding strata compacts under lithostatic pressure at depth (Fig. 1.8). This is generally due to increased stress from tectonic loading, and/or rapid sedimentation rates where the efflux of pore water is not sufficient to maintain hydrostatic pressure (Mazzini and Etiope, 2017). The fluids may be impeded by surrounding impermeable layers. Overpressure cannot exceed the strength of the rock and is therefore highly dependent the host rock properties.

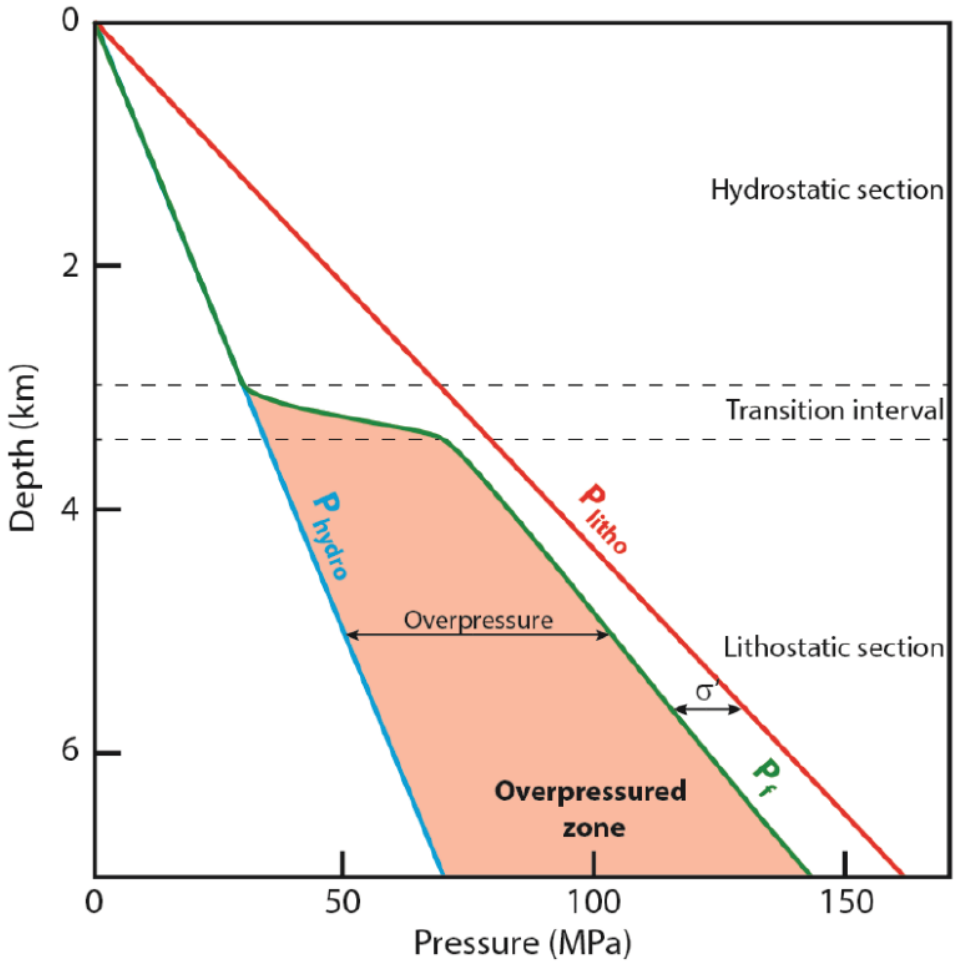

Figure 1.8: *Pressure vs depth plot showing hydrostatic pressure and lithostatic pressure. The green line is the measured pressure. The difference between pressure and hydrostatic pressure represents the overpressure and difference between the lithostatic and measure pressive gives the effective stress (Blouin, 2019).*

Mechanisms that induce overpressure induce the cracking of hydrocarbons with increased temperature at depth (Deville, 2009). Additionally, it may be induced by dehydration, increased temperature, and clay transformation reactions such as smectite-illite (Blouin, 2019).

Earthquakes have commonly been associated with mud volcano activity. They induce changes in the stress field and therefore pore pressure. Fault reactivation and fracture opening may trigger overpressured strata at depth to migrate to less pressured areas, leading to the rapid overpressure of strata at more shallow depths. This increase in pressure may be sufficient to cause mud mobilisation from already overpressured strata, or at least to reactivate dormant structures (Rogozhin, 2005; Manga et al., 2009).

1.5.2 Gravitative Instability

Gravitative instability arises due to differences of pressure between stratas, allowing low density clay bearing units to become buoyant in the surrounding units. (Mazzini and Etiope, 2017). This density inversion may come from intrinsic properties of the strata, or externally from low-density fluid and gas input, hydrocarbon generation, diagenetic reactions or tectonic processes (Kopf, 2002; Roberts, 2011). The instability is necessary to initiate mud mobilisation though it cannot be the sole factor.

Clay rich strata are prone to mud remobilisation due to their porosity and ability to adsorb water. The source layer may be overpressured or under compacted which causes a density contrast within the overlying, normally compacted sediments (Kopf, 2002). Most commonly, the input of low-density fluids and gases will increase the gravitative instability. This is also enhanced during the ascent of the mud as the effective stress is reduced, therefore the porosity increases, ultimately lowering its density leading to acceleration of the ascent (Deville, 2009).

Some MVs are associated with 'mud diapirs' as they develop at the crest of such structures. Diapirism is caused as connate water becomes trapped after deposition with concomitant gas (predominantly methane), leading to high pore pressures and weakly compacted strata (Neef and Bottrill, 1992). This is frequently observed in environments with high sedimentation rates leading to under "compaction". To facilitate mud volcanism and extrusion from mud diapirs, several secondary processes are also required (Kopf, 2002). These presence of mud diapirs within the Tairawhiti region of New Zealand's North Island have long been documented and associated with mud volcanism, though not entirely understood (Ridd; 1970; Mazengarb, 1998; Pettinga, 2003). With the help of more advanced imaging techniques, more recent international studies have shown that many previously inferred mud diapirs are in fact the occurrence of ascending clay-masses forming diapiric-like structures and canopies (Blouin, 2019). The mud volcanoes of the Tairawhiti Region are commonly suggested to result from diapiric activity (Ridd, 1970; Mazengarb, 1997).

1.5.3 Hydraulic Fracturing

The progressive deformation within the overpressured strata is susceptible to be transferred laterally by permeable horizons towards areas where strata thickness and load is lower, leading

to hydraulic fracturing (Deville, 2009). This is commonly observed in rock fragments expelled by mud volcanoes, occurring as angular blocks with no preferentially orientated fractures representing isotropic cracking. Hydraulic fractures propagate hundreds of meters above the overpressured source, establishing a pathway for the remobilised mud. The expelled rock fragments often contain calcite filled fractures signifying that water (will dissolved carbonates) is responsible for the hydraulic fracturing and precedes mud ascent (Deville, 2009). Fracturing may also be a result from tectonic stresses, fault reactivation and seismicity (Mazzini and Etiope, 2017).

1.5.4 Mud Volcano Activity

The final stage of the mud volcano growth is its manifestation to the surface which happens in a gradual or sudden manner. A gradual extrusion is progressive with a slow release of mud and subsequent gas and fluids. A sudden eruption arises when a critical depth is reached, where the overburden weight is not sufficient to balance the pressure of the ascending mud and growth of the mud toward the surface (Mazzini and Etiope, 2017). At this depth fracturing and breaching of the upper most strata occurs, sometime facilitated by external factors such as earthquakes (Kopf, 2002).

Following an eruption or extrusion, depletion of the mud volcano system occurs as faults and fractures close to the surface provide inherent weaknesses that are exploited by ongoing fluid and gas migration following mud volcano formation (Deville, 2009). In some cases, the edifice area surrounding the mud volcano, as well as the underlying strata, may collapse leading to the formation of a caldera. This is attributed to the removal of sediment and fluid from within the ground forming a void and leading to a depression at the surface (Roberts, 2011). This mud volcano structure is observed at the Mangaehu mud volcano in the Waimata Valley, New Zealand (Ridd, 1970; Mazengarb, 1997).

The mud volcano is considered dormant when activity at the surface ceases and a period of quiescence and build-up is entered. This may occur within the same system for thousands of years however, overpressure may continue to accumulate within the source domain and the cycle is re-established (Roberts, 2011).

1.6 Mud Volcanism in New Zealand and the Tairawhiti Region

Mud volcanoes in New Zealand have been documented since the start of the 20th century. They mostly occur with the East Coast Basin of the North Island but there are also examples in Northland and Canterbury. The mud volcanoes of the East Coast Basin extend from the top of the Raukumara Peninsula to the southern Hawkes Bay. Offshore, submarine mud volcanoes have been identified off the East Coast though studies are limited. It is considered there is likely to be many more undiscovered in the area (Mazengarb, 1997).

Similar to mud volcanoes around the world, the mud volcanoes of New Zealand are associated with thick sequences of overpressured sediments dominated by smectite clay. These sediments accumulated at the convergent plate margin during a time of low tectonic activity through the Late Cretaceous to Paleogene. The sediments contain large amounts of pore water, together with dissolved volatile hydrocarbons from the decay and alteration of organic matter (Pettinga, 2003). Due to the lack of information on the features in the area, there is a lack of understanding how the mud volcanoes manifest at the surface, though it is commonly concluded that the sediments migrate to the surface along clay-rich fault zones (Pettinga, 2003). There is also a common association rising diapiric structures that contain cores of broken melange and smectite clays. The diapirs are either associated with faults or in the cores of Neogene anticlines. Neogene strata are commonly steeply dipping in the vicinity of these diapirs and as well there is an increased incidence of calcite veining highlighting the presence of migrating fluids (Mazengarb, 1998). Mud volcanoes occur at the crest of the of these anticlinal structures.

Within the Tairawhiti region, the mud volcanoes are distributed from Hangaroa in the south to the Waikura Valley in the north. There is a cluster of these features in an east-west line on the northern edges of Gisborne from Knapdale to Sponge Bay, as well as another cluster in the Waimata Valley. There have been new mud volcanoes identified at Te Puia, while the Otopotehetehe Mud Lake in the Waikura Valley is also classified as a substantial diapir and mud volcano field. New unerupted diapirs have also been identified near Tolaga and adjacent to Gisborne City.

Some of the East Coast Basin mud volcanoes have been erupted explosively, notably the Mangaehu Stream mud volcano in the Waimata Valley. This mud volcano has been documented to have erupted explosively on two different occasions in 1908 and 1930, both times throwing

mud and large fragments of rock hundreds of metres in the air and away from the vent (Ridd, 1970; Mazengarb, 1997). The activity of this mud volcano has been declining since the eruptive events, with only a saline marsh and sparse gas bubbling remaining (Monroe, 1999).

Less explosive mud extrusion events are also associated with mud volcanoes in the region such as the Hangaroa, Sponge Bay and Arakihi Road. One of the better documented events occurred in southern Hawkes Bay detailed by Pettinga (2003). The extrusion formed a large mud flow which subsequently dammed a nearby river. Other mud volcanos have also been documented to have produced mud flows following the eruption. The time at which these flows may form could be immediately after the eruptions or up to years later (Ridd, 1970).

Quiescent vents seeping gas and mud rich fluids are also common throughout the region. Such features form gentle 'volcanic like' cones called gryphons up to 1-2m in height. These features are commonly seen within the Waimata Valley and Wheatstone Road (Ridd, 1970). The activity of some of these mud volcanoes has been associated with earthquake events, notably the Hangaroa eruption and Sponge Bay uplift in 1931 following the Hawkes Bay earthquake, and more recently renewed activity and eruption at a completely new locale in the Waimata Valley following the 2016 Te Araroa earthquake (Cave, 2017).

1.7 Engineering Properties of Mud Volcano Material

An understanding of the engineering properties of the material associated with mud volcanism helps to establish the mechanisms occurring at depth that lead to the manifestation of the material at the surface. Properties such as the mineral and grain structure, composition, permeability, and shear strength of the material help to explain how the sediments at such depth withstand high pore pressures and remain under consolidated, which is a significant driving force of mud mobilisation (Kopf et al., 1998; Kopf et al., 2005).

In high porosity clays associated with mud volcanism, the undrained shear strength can be associated with high pore pressure generation. The factors that affect this property and subsequent failure of the material include: consolidation, shear stresses induced on the material, material properties such as plasticity, and the diagenetic reactions that occur within the buried sediment that contribute to high pore pressure generation (Yassir, 1989). A sediment that has failed at depth would not necessarily migrate to the surface, unless conditions in the overlying

strata allowed it to do so, highlighting the structural importance for mud volcanism (Yassir, 1989; Mazzini and Etiope, 2017).

These properties of the mud volcano material can also be used to explain and predict how the material behaves at the surface after an eruption or extrusion. Low strength material is vulnerable to collapse of the mud volcano edifice leading to the formation of a mud flow. This is particularly important for the sediment accumulated on angled slopes. This was evident in the mud flow generated following the mud volcano formation at the Brookby gas seep (Pettinga, 1993). Highly saturated, low permeability clays are also susceptible to consolidation and settlement at the surface when subjected to loading (Mazzini et al., 2007; Istadi et al., 2009; Istadi et al., 2012; Etiope, 2015).

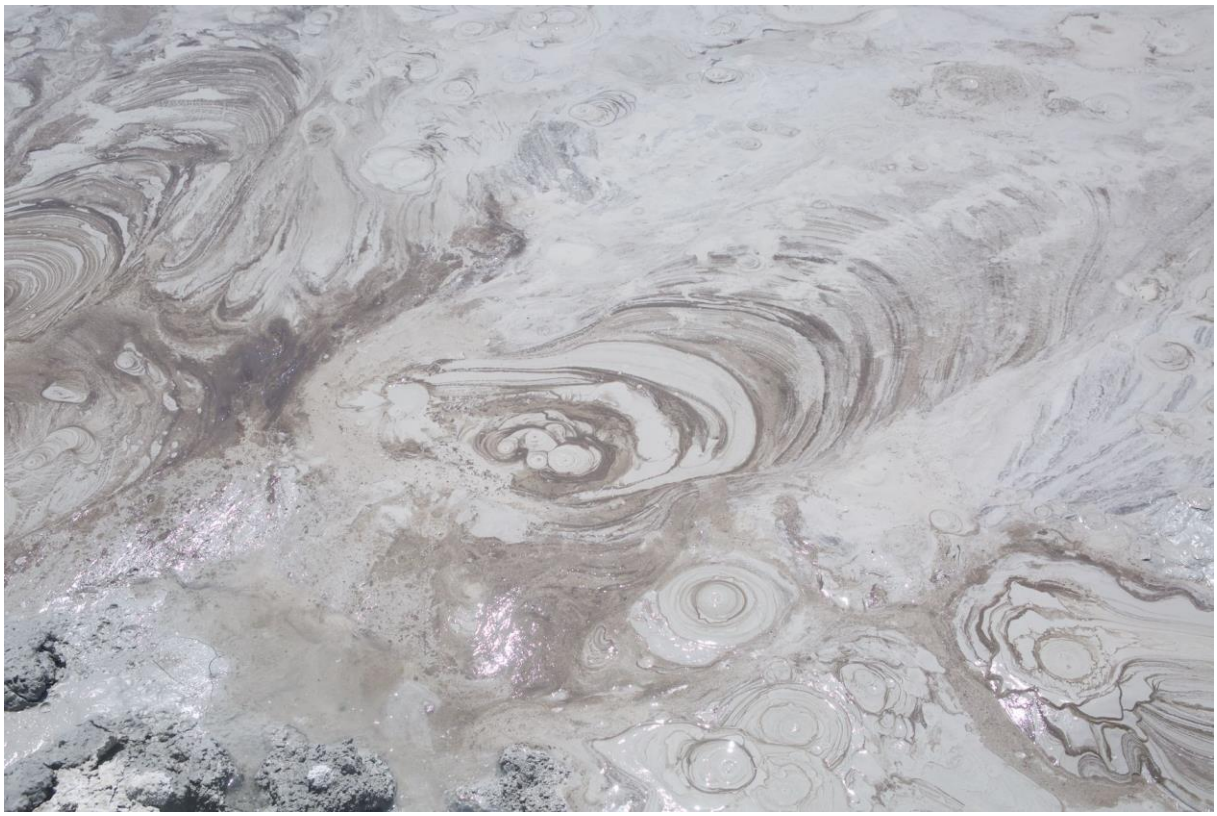

Figure 1.9: *Typical mud emanating from vent at Waimata Valley mud volcano. Taken on 6 January 2019 (three weeks after eruption).*

CHAPTER TWO: STUDY AREA

2.1 Site Description

The site is located at the northern extents of the Waimata Valley, approximately 20km north of Gisborne on the east coast of New Zealand's North Island (Fig. 2.1). It occupies the boundary between two sheep and cattle farms, owned by the Hall family to the north, and by the Utting family to the south. The Hall's farm residence is located approximately 250m north of the site. The site forms an elevated vista at the boundary and slopes gently between 5-10˚ to the north and south.

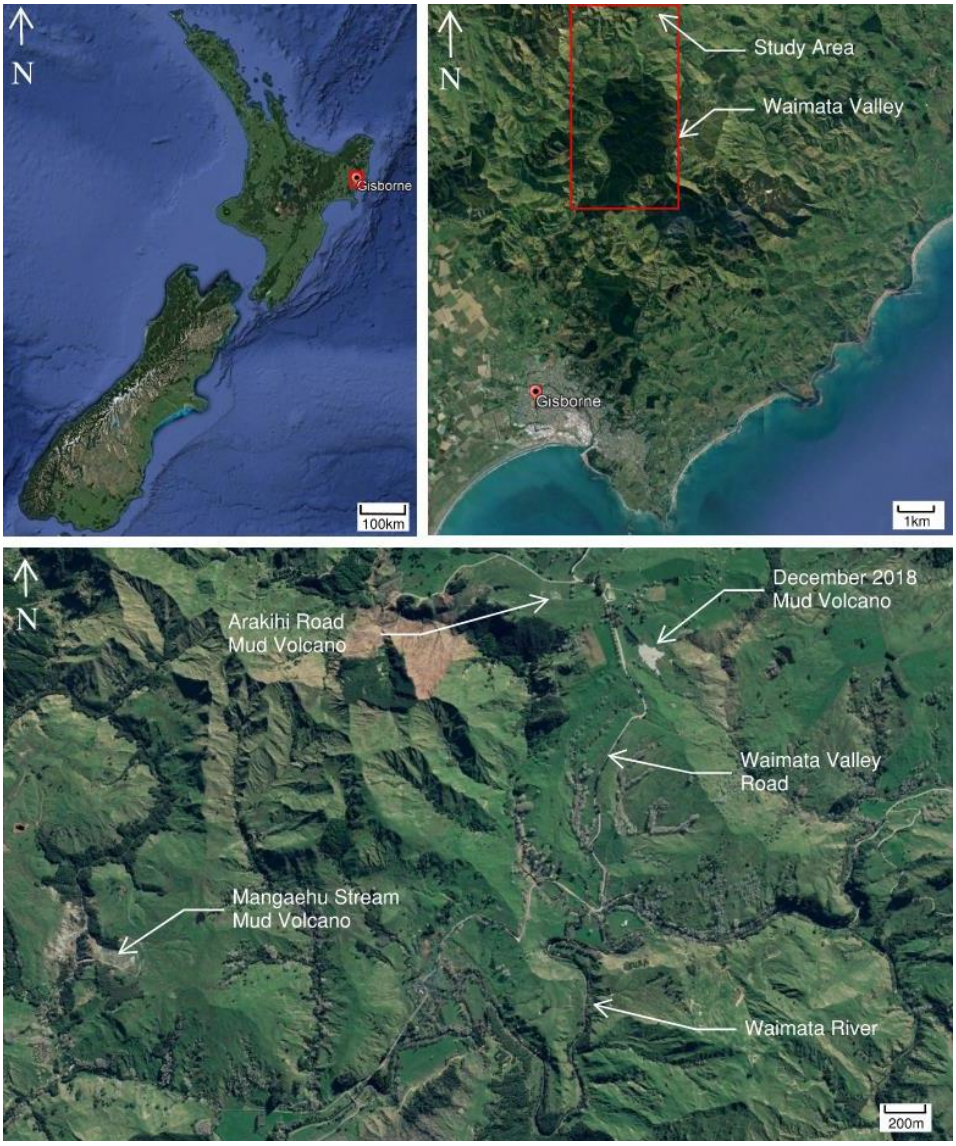

Figure 2.1: *Study area in context of New Zealand (top left) and the Waimata Valley (top right). Mud volcanoes of the Waimata Valley shown in the bottom image.*

Immediately west of the site, Waimata Valley Road runs along a north-south alignment. The road services a large pine forestry area, so it is frequently busy with large logging trucks. Several minor streams flow through or close to site, serving as tributaries to the Waimata River which is located approximately 1.5km to the south.

Within the Halls property also, approximately 600m northwest of the site, is another area of mud volcano activity. These mud volcanoes are characterised by a saline marsh area with occasional gas and clay-rich fluid seeps from several minor vents. The existence of these mud volcanoes has been documented since the early 20th century and have previously been named the Arakihi Road mud volcanoes (Ridd, 1970).

2.2 Site History and Eruptive Event

As there was no one present at the site during the time of the eruption, the precise timing of the event is unknown. The farm owners, the Hall's, left their residence at 8am on 12 December 2018 and drove to Gisborne City in what seemed like a regular morning. On their return at 1pm that afternoon, what had been a raised dome at their property boundary with the Utting's, was now an area covered in a thick layer of white mud (Fig. 2.2). By the time the newly formed mud volcano was discovered, it appeared as though the extrusion of thick mud material had ceased, though gas and fluid seepage at vent remained constant. A distinct hydrocarbon odour of the gases was noted, contrasting the odourless gas seeps at the mud volcanoes in the adjacent paddock. There was an increase in activity reported of these mud volcanoes prior or following the event.

The erupted material had covered approximately 2.1 ha of land spanning the two properties, completely burying, and damaging the boundary fence. Mud flows propagated radially from a vent area downslope, concentrating within small topographical depressions formed by streams. Immediately north of the vent, one of these flows had blocked a small stream leading to the formation of new lake. The newly-erupted mud proved to be hazardous to curious stock, where some had to be rescued after becoming stuck knee deep.

Days after the eruption, a crust along the top of the material had formed in the dry summer heat, sufficient enough to allow the feature to be traversed. The material surrounding the vent remained highly viscous with minor vents continuing to seep gas and fluid (Fig. 2.3).

Due to the lack of visual evidence at the time of the event, the way of which the material was expelled from the ground is unknown. There was no evidence of extruded material outside of the areas formed by the mud flows suggesting that the event was not explosive, and fragments of mud and rock were not thrown from the vent. Rather, a viscous mud was extruded from the ground effusively, forming a series of radial flows as a vent was progressively built. The mud flows carried large fragments of rock up to boulder size, tens of metres away from the vent. There is a lack of impact marks on the mud and area surrounding the vent further suggesting its effusive activity.

Figure 2.2: *Unmanned Aerial Vehicle (UAV) image of Waimata Valley mud volcano between the Hall's and Utting's properties. Image taken January 2019, three weeks after the eruption.*

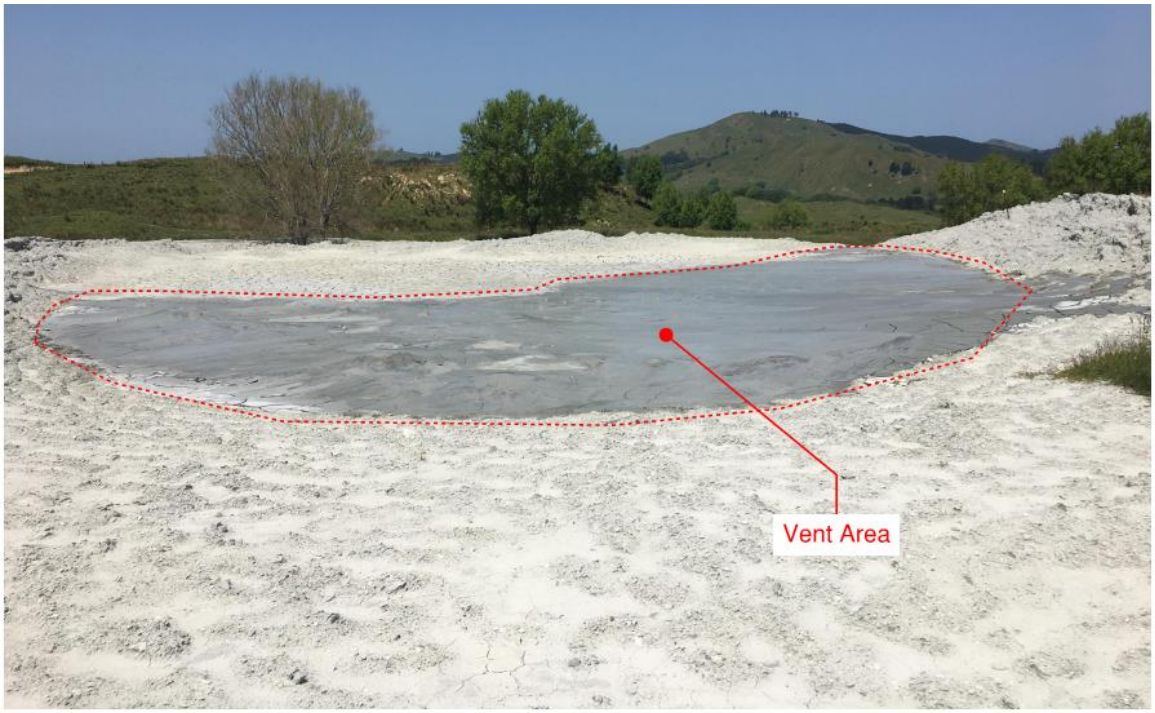

Figure 2.3: *Image of mud volcano vent taken 24 November 2019. Note the arcuate shape of the vent similar to the shape of rupture shown prior to the event.*

The extruded mud comprises of a highly sticky clay matrix, with occasional fragments of rock. These rock fragments range in a variety of sizes and composition. Within the vent area, the material has a more consistent fine-grained nature, and is of high-water content. The composition and origin of the different components of the mud are discussed in a later section of this research. The vent appeared to form in an arcuate shaped, mirroring the rupture pattern formed by the uplift following the Te Araroa earthquake (Fig. 2.4). The minor gas vents also generally followed this trend.

The eruption came as no surprise to local scientists who had been regularly monitoring the site following the Te Araroa earthquake event that occurred on 2 September 2016. Although the epicentre of the shaking was 175 km to the north, uplift had occurred at the site forming an elevated dome with associated rupturing. Other mud volcanoes in the region also demonstrated increase activity following the earthquake which included the mud volcanoes in the neighbouring paddock and further down the valley at the Mangaehu Stream mud volcano, as well as the well-known Hangaroa mud volcano west of Gisborne City. Other well-known mud volcanoes closer the east coast such as Kirkpatrick, Knapdale, Wheatstone Road, Goodwins and Taumoto remained quiescent.

As per the Geonet database, there were no significant earthquake events recorded in the region immediately prior to the December 2018 event. The closest earthquake to occur prior to the event with a magnitude greater than 5.0 was recorded 8 months prior on 10 April 2018.

Figure 2.4: *UAV image of boundary separating Utting's and Hall's properties showing uplift caused by Te Araroa Earthquake. Excavation works pictured were necessary to restore gradient of blocked stream.*

2.3 Geological Setting

2.3.1 General Overview

The North Island of New Zealand sits along the Hikurangi margin, a continent-ocean convergence zone where the east-bound Pacific Plate has been subducting obliquely beneath west-bound Australian plate for at least 25 million years (Ballance, 1975; Lichfield et al., 2007; Sutherland et al., 2009). The seafloor expression of this plate boundary is the Hikurangi Trough, approximately 90km east of the North Islands easternmost coastline. The oceanic crust of the subducting Pacific plate is anomalously thick due to the presence of a 12 to 15 km thick Cretaceous Large Igneous Province known as the Hikurangi Plateau (Lichfield et al., 2007; Sutherland et al., 2009). Figure 2.5 shows the regional tectonic setting for the eastern North Island.

On land, a large north-east south-west trending mountain range has formed which runs through the whole eastern North Island geologically known as the Frontal Arc. To the northwest of the frontal arc is the active volcanic arc known as the Taupo Volcanic Zone (TVZ), and to the southeast is the forearc which comprises of the forearc basin and accretionary wedge (Pettinga, 2003; Lichfield et al, 2007; Sutherland et al., 2009).

The oblique movement drives the forearc southwards relative to the frontal arc forming a dextral shear zone between them known as the North Island Shear Zone. This shear zone is collectively made up of a few major faults on which the displacement is concentrated (Ballance, 1975; Pettinga, 2003).

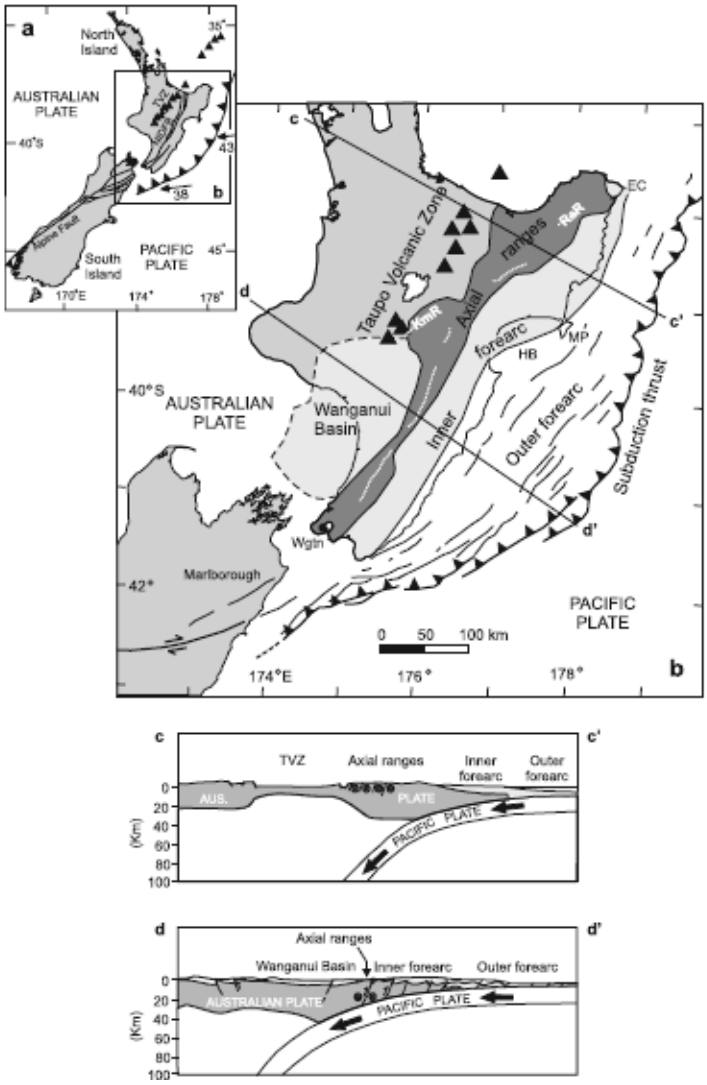

Figure 2.5: *(a) Regional tectonic setting. A black triangle represents active volcanoes in TVZ. Numbers by arrows are plate convergence rates (mm yr^{-2}). (b) Structural elements of the Hikurangi (subduction) Margin. (c) Cross-section across northern Hikurangi Margin. (d) Cross section across the southern Hikurangi Margin (Lichfield et al., 2007).*

The north eastern extension of the frontal arc forms the Raukumara Range which cover the mountainous area of the East Cape. The ranges comprise of cretaceous aged greywacke basement rock which formed at the forearc of the Gondwana supercontinent (Adams and Kelley, 1998). The ranges are being uplifted and deformed by actively moving faults of the shear zone over the past 5 million years following a change in the movement pattern of the Pacific Plate (Lichfield et al., 2007). The current rate of convergence is approximated to be 45 mm per year. Seismic studies estimate the thickness of the continental crust beneath the northern forearc (Raukumara Ranges) to be 20 km, thickening to 35 km to the south (Lichfield et al., 2007).

Bound to the east of the frontal arc is the present day forearc basin which extends from Palliser Bay at the bottom of the North Island, terminating in Northern Hawkes Bay. North of this boundary is an older basin that extends to the top of East Cape. The older Basin, which includes the Gisborne and study area, comprises a 4 km to 5 km Late Cretaceous to Pliocene sedimentary sequence, which has been deformed and uplifted during the Neogene subduction processes (Kamp, 1999). The forearc is 125 km wide at the sediment-starved northern most part of the East Cape and expands to >200 km wide at the more sediment-rich south end at the bottom of the North Island (Lichfield et al., 2007).

Between the forearc basins and the Hikurangi Trough is the accretionary wedge which is shortening under pressure and is cut by thrust faults and folds which make it thicker by way of uplift (Pettinga, 2003). This wedge exposes itself on shore in the southern Hawkes Bay region, whereas further north accretionary slope basins lie offshore (Lichfield et al., 2007).

2.3.2 Tectonic History and Structural Setting

The Late Jurassic to Early Cretaceous basement rocks accumulated at a convergent continental margin at the edge of the Gondwana supercontinent (Adams and Kelley, 1998; Sutherland et al, 2009). These rocks were lithified, deformed, uplifted, eroded, and then buried underneath transgressive marine sediments prior to the late cretaceous that were deposited in mainly outer shelf environments. During this time subduction related deformation, including thrust faulting, is thought to have continued (Mazengarb and Speden, 2000).

By the Late Cretaceous as the New Zealand landmass began to separate from the supercontinent, large volumes of sediment to accumulate in a wedge on a continental shelf and trench slope off the east coast of the North Island forming a sequence of marine mudstones with subordinate siltstones and sandstones. The sequence is generally horizontal and only gently deformed suggesting there was a passive margin environment for the deposition period between the Late Paleogene and Late Cretaceous (Mazengarb and Speden, 2000). The wedge sediments earlier in the sequence were coarse grained however, as the eroding land mass wore down the sediment became finer-grained and the amount of calcium carbonate increased. To this day the sediments higher in the wedge become fine, including significant quantities of the swelling smectite clays (Mazengarb and Speden, 2000; Sutherland et al., 2009).

From Late Paleogene to Early Neogene, there was a significant change in the depositional environment as subduction processes were reactivated at the margin. The passive margin sediments began to be compressed by the subducting pacific plate causing them to thicken - a process which continues to occur to this day. The primary process behind this thickening is the production of low angle reverse faults. The rocks thrusted over the fault become brecciated and folded in the process. The reactivation of subduction at the plate margin is also believed to have led to the emplacement of the East Coast Allochthon thrust sheets which have been emplaced over the passive margin sediments, becoming intensely sheared and broken in the process. The thrust faults dip to the north to northeast signifying emplacement in a south west direction (Mazengarb and Speden, 2000; Sutherland et al., 2009).

The Neogene sequence overlies the allochthonous rocks in the eastern forearc and is thrusted against them in the west (Reyners and McGinty, 1999). They represent a range of marine shelf and trench slope depositional environments characterised by large thicknesses of terrigenous and volcaniclastic sediments consistent with the onset of the North Island shear zone and establishment of the subduction zone with a volcanic arc (Sutherland et al., 2009). There is a greater volume of these active margin sediments around the Tairawhiti area relative to the Hawkes Bay further south. This is attributed to the Tairawhiti being closer to the major sources of sediment, the Allochthon and the active volcanic arc.

Since the Late Miocene, following the initiation of oblique movement of the Pacific Plate, the Neogene sediments in the upper crust have been undergoing marginal-normal extension (Nicol

et al., 2007). This has been accommodated by normal faulting and folding that generally trend about NNE-SSW axes, subparallel to the modern plate boundary (Sutherland et al., 2009). In places these faults merge with decollement surfaces which are generally gently inclined toward the trench. Detachments accommodate dip-slip displacements, exceeding 2 km in places, and occur within Late Paleogene sediments characterised by high fluid pressures (Mazengarb, 1998). Onset by the establishment of these structural features, diapiric antiforms began to develop, containing cores of the Late Cretaceous to Late Paleogene passive margin sediments and melange (Mazengarb and Speden, 2000). The diapiric structures may be offset by late-stage normal faults. Widespread mud volcanism throughout the area is generally attributed to the presence of these diapiric structures where many remain active today (Reyners and McGinty, 1999).

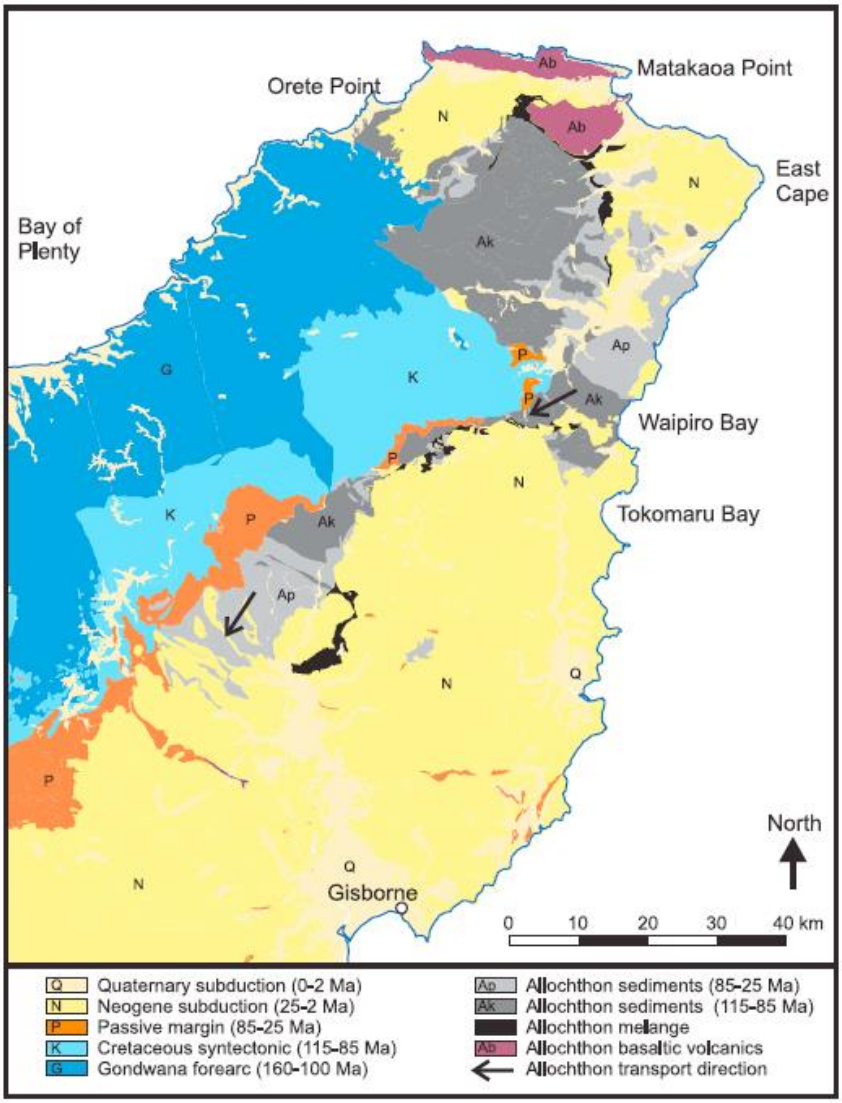

Figure 2.6: *Geology of onshore Raukumara Peninsula, separated by tectonic period (Sutherland, 2009).*

At present day, although though the region is regarded to be tectonically active there is a very few active faults in the area. Ongoing uplift of the Raukumara Ranges is considered to driven by the buoyancy of underplated sediment with a contribution of the thick oceanic crust of the Hikurangi Plateau rather than by way of uplift by faulting (Clark et al., 2010). Fig 2.6 shows the onshore geology of the Raukumara Peninsula based on the tectonic period in which the unit formed.

2.3.3 Stratigraphy

This section is based on the information from the 1:250,000 QMAP Series produced by the Institute of Geological Sciences which was compiled by Mazengarb and Speden (2000). This study uses the revised stratigraphic nomenclature for the eastern North Island which was proposed by Moore and others (1986). Older work such as Ridd (1964) that uses alternative nomenclature is referenced in this section, although it has been updated to use the more recent classification. The stratigraphy of the Raukumara area subdivided into five major units based mainly on their age and structural history, which has been summarised in the previous sections. These five major units from oldest to youngest include: Late Jurassic to Early Cretaceous basement rocks; in-place Late Cretaceous to Late Paleogene rocks; East Coast Allochthon (displaced Late Cretaceous to Late Paleogene rocks); Neogene rocks; and Quaternary sediments. In this section the units are briefly described and further classified into subgroups and formations. Only relevant formations to this study area are described in this section. Figure 2.7 shows a general stratigraphy of the major units and the associated tectonic setting.

The Late Jurassic to Early Cretaceous rocks formed are mapped as part of the Torlesse Supergroup which form the axial ranges and much of Southern Alps. The group comprises of well indurated quartzofeldspathic and lithic sandstone and mudstone, commonly known as ‘greywacke’ (Kamp, 1999; Mazengarb, 1993; Mazengarb and Speden, 2000).

The in-place Late Cretaceous rocks form a sedimentary sequence collectively known as the Matawai Group formed during the breakup of the Gondwana supercontinent. The Matawai Group comprises of moderately indurated sedimentary formations which outcrop along the south-eastern flanks of the Raukumara Range. The stratigraphy varies considerably across the peninsula (Mazengarb, 1993; Kamp, 1999; Mazengarb and Speden, 2000).

The Late Cretaceous to Paleogene rocks represent the passive margin sediments which includes the Tinui Group overlain by the Mangatu Group. The Tinui Group includes the Tahora, Owhena and Whangai Formations which generally grades for thick coarse-grained units to more calcareous fine-grained units. The Mangatu Group includes the Wanstead and Weber formations. The Eocene Wanstead (E) formation outcrops in the study area as a result of diapiric activity and fault displacement, and is inferred to be up to 200m thick (Mazengarb and Speden, 2000). They generally consist of smectite-rich calcareous mudstones with locally interbedded glauconitic sandstones, accumulated in deep ocean basins. Sediments within these units are commonly associated with mud volcanism. Landforms developed on these lithologies are typically unstable because of the clays, and outcrops are typically marked by slumps and earthflows (Moore et al., 1986; Moore, 1988; Mazengarb, 1993; Mazengarb and Speden, 2000).

The East Coast Allochthon (ECA) represents a large-scale displacement of Cretaceous to Late Paleogene rocks and are found outcropping in the north-eastern areas of the peninsula. They differ from the in-place rocks mainly by differences in structural style (Rait, 1992; Mazengarb and Speden, 2000).

Both the in-place and displaced Late Cretaceous to Late Paleogene rocks are unconformably overlain by a structurally simple sedimentary sequence of Neogene age that includes the Tolaga and Mangaheia Groups, covering most of the study area. The Tolaga Group (Mi) represents all sediment accumulated in the Miocene, further classified into early (e), middle (m) and late (l) sequences. The early sequences are terrigenous containing sequences of massive blue-grey mudstone and massive sandstone and are much thicker than the underlying pelagic groups (Mazengarb et al., 1991; Field et al., 1997; Mazengarb and Speden, 2000). The Middle to Late Miocene rocks are typically made up of conglomerate, sandstone, mudstone and limestone. Some of the Late Miocene sequences include abundant volcanic tuff derived from rhyolitic eruptions in the Coromandel Peninsula. On the peninsula the Tolaga Group is up to 1000m thick, though there is considerable local variation in both thickness and facies (Mazengarb et al., 1991; Field et al., 1997; Mazengarb and Speden, 2000).

The Latest Miocene to Pliocene Mangaheia Group (Pl) rocks are mainly sandstones, some of which are tuffaceous, and mudstone. The sequence is up to 2000m thick and outcrop from the northern Raukumara Peninsula to the Northern Hawkes Bay (Mazengarb and Speden, 2000).

Areas of severely crushed, mixed lithologies are mapped as melange (mel). Typically, fragments and blocks of Whangai Formation and Mangatu Group (passive margin) lithologies present in a smectitic mudstone matrix. The melange is associated with rocks of the East Coast Allochthon and is also present in the cores of diapiric structures bounded by Neogene rocks, i.e. it has apparently been formed by at least two different mechanisms in two main periods. The presence of melange is commonly indicated by areas of slumping (Mazengarb and Speden, 2000).

Quaternary sediments deposited in the Quaternary are present in onshore coastal plains, alluvial plains, swamps, alluvial fans and landslides.

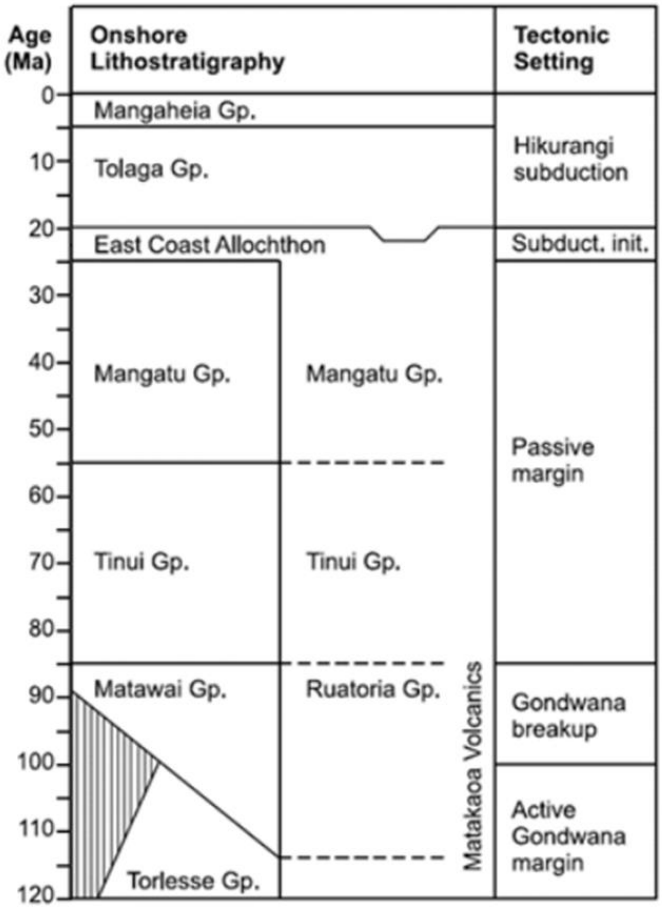

Figure 2.7: *General stratigraphy of Tairawhiti Region (modified from Sutherland et al., 2009).*

2.3.4 Local Geology

The most comprehensive study of the geology in the Waimata area was undertaken by Ridd (1964), published on behalf of BP Shell and Todd Petroleum Development. Ridd's (1964) work followed prior studies undertaken within the area, which received attention from oil companies in the first half of the 1900's because of its oil and gas seepages. The work of Ridd (1964) remains relevant, and is referenced as the principal data source in the 1:250,000 QMAP series referenced by Mazengarb and Speden (2000). The later revised Ridd's (1964) work to include the updated stratigraphy, geological and structural mapping. Figure 2.8 shows the geology surrounding the study area. The geological units are based on the 1:250,000 Geological Map of New Zealand QMAP series which are reference in the previous section (Section 2.3.3).

The study is area located within the central forearc basin at the southern end of the Raukumara Peninsula. Here, thick sequences of Neogene sediments (Mangaheia and Tolaga Groups) overlie passive margin sediments of the Paleogene (Mangatu Group), though there are surface exposures 'inliers' of Mangatu group as a result of diapirism or Mud Volcano activity (Neef and Bottrill, 1992). The Neogene sediments generally produce hilly terrain, whereas the Paleogene sediments produce low lying terrain characterised by slumps and earthflows (Ridd, 1964; Mazengarb and Speden, 2000).

The Waimata area mainly consists of a main valley with the Waimata River flowing through its centre. Several tributaries join the Waitamata River including the Mangaehu stream. At each extent of the valley are two major faults to the NW and SE that both trend in a NE-SW direction. To the NW is the Arakihi Fault which forms an area of steep topography underlain by sediments of the Mangaheia Group (Mazengarb and Speden, 2000). To the SE is the Horoweka Fault, forming an area of steep topography underlain by sediments of the Tologa Group (Neef and Bottrill, 1992). Both faults are mapped inactive normal faults with dominant downthrow in the SE direction. In between the two faults has formed the broad Waimata Syncline which is aligned in a similar direction.

Other dominant structural features include a group of rectilinear to gently arcuate faults also trending in a NE-SW direction within the valley. In Ridd (1964, 1970), two of these faults are named the Mangaehu and Waimata Faults, and they are understood to have developed in the late Neogene. Both faults were thought to have sinistral strike-slip sense of movement, though

more recent studies suggest that this is unlikely (Mazengarb and Speden, 2000). Both faults contain cross faults which intersect obliquely in a NW-SE direction. These cross faults generally form at the edge of the Paleogene inliers as a result of the diapiric folding, dipping steeply outward (Rait, 1992). These inliers are characterised by high rates of slumping and low-lying topography.

The site of the 2018 eruption is located at the margin of the mapped Mangatu Group exposure, also interpreted to be a NW-SE trending fault. The neighbouring Arakihi Road mud volcanoes on the Halls Farm follow the same fault alignment 500m to the NE.

In other areas of the Waimata Valley, outcrops of melange are exposed at the site of the Mangaehu Stream Mud Volcano which erupted explosively on four different occasions between 1901 and 1930. The melange originated from a diapiric core of Early Neogene sediments which punches through the overlying Late Neogene sediments (Ridd, 1970).

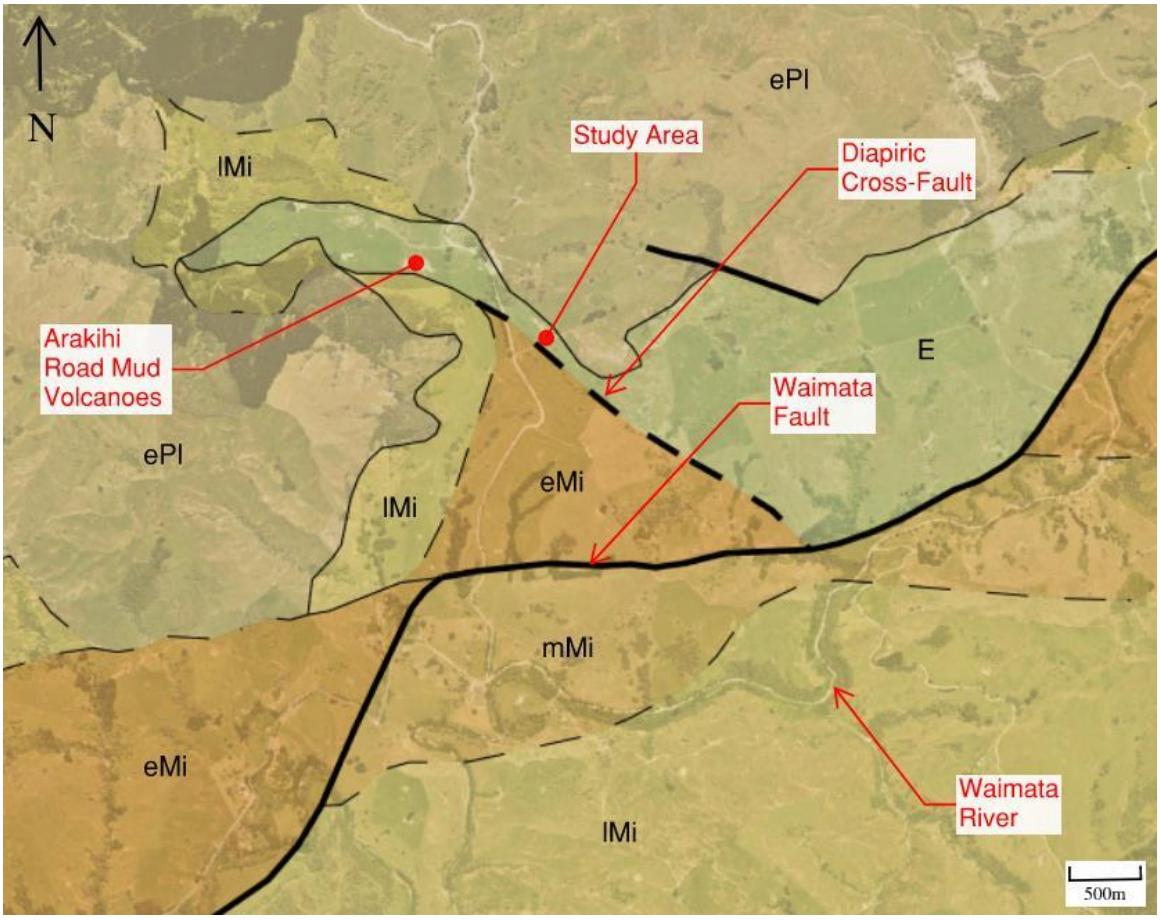

Figure 2.8**:** *Geology surrounding the study area, Waimata Valley, Tairawhiti (data from GNS QMAP 1:250,000 Geological Map of New Zealand. Key: E (Eocene), lMi (Late Miocene), mMi (Middle Miocene), eMI (Early Miocene), ePl (Early Pleistocene).*

CHAPTER THREE: METHODS

3.1 Site Investigation

To help characterise the mud volcano and associated material, it is necessary to investigate the site by utilising multiple different engineering geological techniques. These techniques included visual methods of engineering geological and geological mapping, geophysical methods including ground penetrating radar (GPR), and a variety of investigative methods to assess the subsurface conditions including drilling hand auger boreholes and undertaking in-situ shear vane and Scala penetrometer (Scala) testing. These in situ test methods are especially useful to characterise the properties of the materials before using the collected data to help make decisions regarding sampling of the material and to establish a schedule for further, more precise laboratory testing.

Geotechnical descriptions of the different encountered materials as the site were recorded in accordance with the New Zealand Geotechnical Guidelines '*Guidelines for the field classification and description of soil and rock for engineering purposes'* (NZGS, 2005). Following NZGS (2005), a field estimation of the grain size distribution, colour, strength, moisture, and plasticity are given for the different materials. The strength of the material is inferred by the various in situ test methods undertaken.

3.1.1 Engineering Geological Mapping

Engineering geological mapping assessments of the site were undertaken to identify surface features that are used to help characterise and determine the engineering behaviour of the mud volcano and the material. This included identifying geological and geomorphological features, as well as observing and describing the soils and rock fragments encountered at the site. The significant surface features are recorded on Figure 4.1 in the following chapter.

Images of the feature were taken from above using an Unmanned Aerial Vehicle (UAV) on 10 January 2019, three weeks after the eruption event. One of the images taken by the UAV is used as an image background for the mapping assessments. The observations and interpretations made are based on the photographs taken three weeks after the event, as well as during subsequent site visits in November 2019 and June 2020. This also allowed for interpretation of how the mud volcano evolved over-time following its initial eruption.

3.1.2 Ground Penetrating Radar

Ground penetrating radar (GPR) is an electromagnetic geophysical method for non-invasive and high-resolution imaging of subsurface structures and conditions (Assaad, 2004). The GPR data for this investigation was collected using a Mala GroundExplorer (GX) HDR using a 160 MHz antenna to identify structure within the shallow (10m) subsurface.

Collection of the GPR data involved tracing across the mud volcano in an approximate grid pattern, from one side of the feature to the other. Each line of the grid is called a transect, and where possible the transect was extended 1-2 m outside of the feature. Figure 3.1 shows some selected transects that were surveyed in the field. Four of these transects are presented in Chapter 4.

Figure 3.1: *Selected GPR transects across mud volcano. The highlighted transects correspond to GPR images produced for each respective number presented in the Chapter 4.0.*

3.1.3 In-situ Testing

In-situ testing was utilised as part of this research to characterise the engineering properties of the mud volcano material before further, more precise laboratory testing was undertaken. The in-situ tests serve as a quick and effective means to quickly test the material at various locations and depths across the site. The investigation locations where in-situ testing and sampling was undertaken is shown on Figure 3.2.

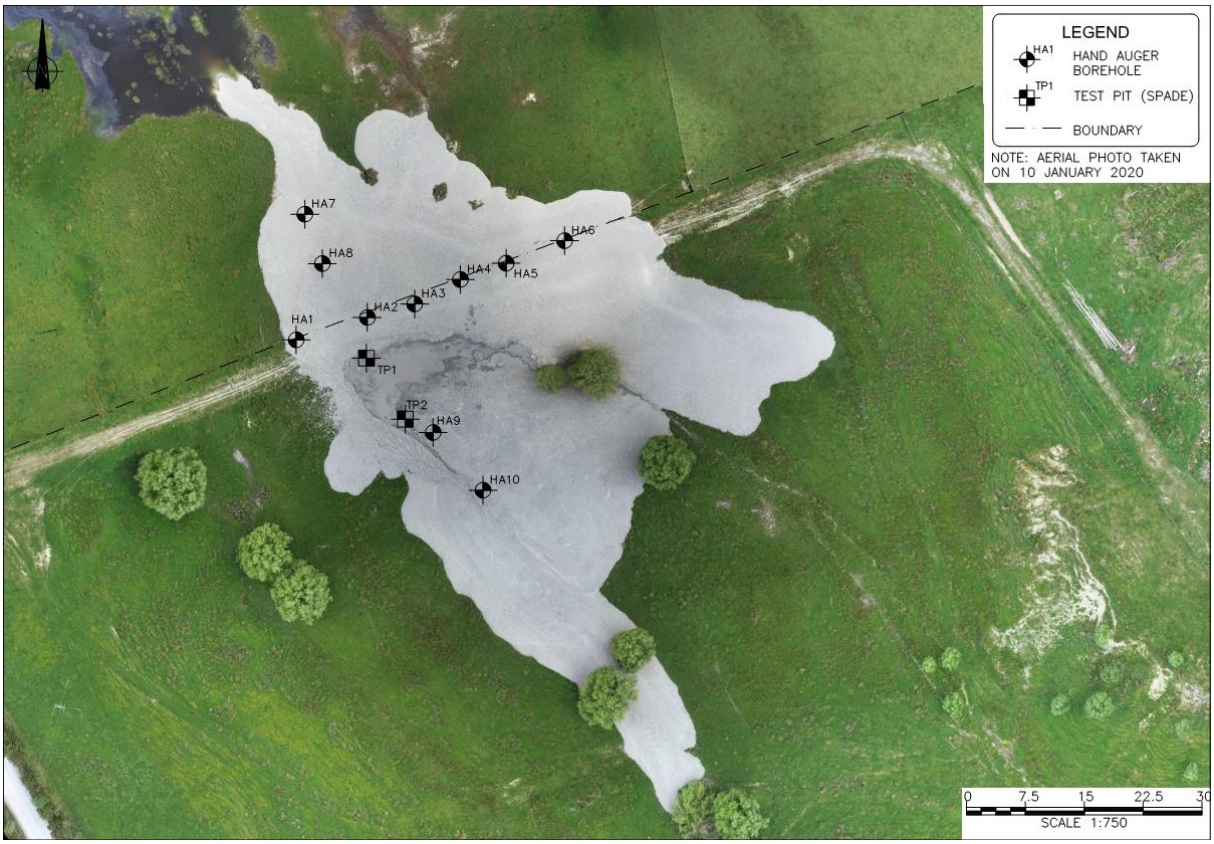

Figure 3.2: *Site investigation plan showing test and sample locations across the mud the volcano.*

3.1.3.1 Hand Auger Boreholes

Ten hand auger boreholes were drilled in a pattern of two intersecting lines, across and through the centre of the site. The purpose of these boreholes was to describe the mud volcano soil, determine its depth across the site, and to undertake a variety of soil strength tests at a range of depths within the soil. The boreholes were terminated when the mud volcano material was breached, and the underlying autochthonous soils were encountered.

3.1.3.2 Hand-held Shear Vane Tests

A handheld shear vane was used to obtain shear vane dial readings within the mud volcano soil. Testing was carried out in accordance with the NZGS Guideline for Handheld Shear vane Test (2001) which follows ASTM D 2573 (ASTM 2001). A 19 mm vane blade is pushed at least twice the length of the of the blade into the soil and torque is progressively added to the vane head until the soil shears and a maximum vane dial reading is recorded. The dial is then reset, and the vane and blade are rotated several times before a second reading is recorded.

The first reading taken is the peak undrained shear strength of the material. This is described as the ultimate state of stress that can be sustained by a material before its fails (Atkinson, 2007). The second reading gives the residual shear strength which is the strength of the material once it has failed (Atkinson, 2007). The difference between the peak and the residual shear strength indicates the sensitivity of the material to disturbance.

The tests were undertaken throughout each borehole at 0.25m to 0.5m intervals within the mud volcano material, until the autochthonous soils were encountered.

3.1.3.3 Scala Penetrometer Tests

The Scala Penetrometer Tests, also referred to as the Dynamic Cone Penetration Test (DCP), is a quick and inexpensive method of assessing the strength of shallow soil layers. The test is carried out using a 9 kg hammer and cone. It is useful for determining the relatively strength of different soil layers and finding the base of low strength soils. The number of drops of the hammer from a fixed height is recorded for every 50mm of cone penetration.

Adjacent to each hand auger borehole Scala Penetrometer tests were undertaken from the surface to the underlying autochthonous material.

3.1.4 Sampling

Samples of disturbed mud volcano material were collected for a variety of laboratory testing. The samples were taken from the test locations shown on Figure 3.2, including two additional test pits which were dug with a spade within the vent area. As previously mentioned, the sample locations were spaced around the site to determine any spatial variations within the material

relative to the vent area. Within each test location, samples were also taken a variety of depths, to determine any vertical variations of the material.

A few weeks following the eruption, a total of 50 fragments of rock expelled from the mud volcano were also collected from the surface for further analysis. The fragments were generally cobble (60 mm diameter) to boulder (50 mm diameter) sized and were collected from a variety of locations across the mud volcano site. This was undertaken to determine the lithological variety within the mud volcano material which can be used to understand how the material has migrated to the surface and the depths it may have come from, as well as understanding the level of mixing with deeper stratigraphic units that has occurred during the materials ascent.

3.2 Laboratory Methods

For this research, laboratory testing was used to help accurately infer the geological, index and geotechnical properties of the mud volcano materials. An understanding of these properties is prudent for interpreting the behaviour of the material which may help to understand how it came to manifest at the surface and how it may behave once it has erupted. The various laboratory methods utilised include: scanning electron microscopy, inductively couple plasma – mass spectrometry, and various geotechnical tests.

3.2.1 Particle Size Analysis

Particle Size Analysis (PSA) is a procedure used to determine the percentage of various grain sizes comprised within a soil known as the Particle Size Distribution (PSD) (Craig, 1974; Das 1985). The PSD is used to determine the textural classification of soils (i.e. gravel, sand, silt, clay etc.) which is important for assessment of a soils' engineering properties such as permeability and strength (Wentz et al., 2016). The results of a PSD are generally presented on a graph consisting of a logarithmic curve of the percentage finer than a certain particle size against effective particle diameter. This graph is known as a Particle Size Distribution Curve (Craig, 1974; Das, 1985; Atkinson, 2007).

Several laboratory methods are available for PSA, all of which require physical segregation of soil particles within a sample. Traditional methods of analysis include sieving and sedimentation, whilst more modern methods include laser diffraction (Das, 1985).

The traditional methods of analysis have limitations due to the difficulty in correctly analysing the size of irregularly shaped particles. The probability of a particle passing through a sieve depends on the nature of the particle, the number of particles of that size, and the properties of the sieve (Day, 1965; Das, 1985). Whilst sieving is readily and available, it is only suitable for sand and gravel-sized particles, therefore, sedimentation is typically used conjointly for the analysis of the finer particles. Sieving and sedimentation techniques are time consuming often required several days for analysis. Due to their laborious nature, only a few points on the PSD are usually measured and therefore may not capture the entire PSD of the sample (Ryzak and Bieganowski, 2011; Fisher et al., 2017).

PSA by laser diffraction works by passing a laser beam through the dispersed mud sample and measuring the angular variation in intensity of the scattered light (diffraction). Large particles scatter light at small angles relative to the laser beam and small particles scatter light at large angles. The pattern of scattered light is then analysed and used to calculate the particle size. It is reported as a volume equivalent sphere diameter (Ryzak and Bieganowski, 2011; Mori et al., 2012).

In comparison to the traditional methods, the modern method of laser diffraction is much faster requiring only minutes to complete a measurement, recording the entire PSD of the sample. The sample required to perform an analysis is also small which is advantageous when the available sample is limited. For these reasons, laser diffraction is also somewhat flawed as the small sample used for analysis may not be representative of the sample as a whole soil (Ryzak and Bieganowski, 2011; Miller and Schaetzl, 2012). Nevertheless, laser diffraction is widely accepted as the most accurate method for fine grained materials, and for the above reasons why it is the chosen method for PSA of this study.

For analysis, the mud volcano samples were taken from a selected range of test locations and depths across the site. Ten samples were tested in total, each from a different test location. Sample preparation involved placing approximately 10g of sample into a test tube with 20ml of 10% sodium hexametaphosphate (Calgon), a dispersant solution to help disaggregation and dispersion of the individual clay particles that may return false signals of coarser particles (Blott

et al., 2004). The test tubes were then placed in an ultrasonic bath for 5 minutes to further help the process and improve the accuracy of the tests.

Measurements of the samples was undertaken using a Mastersizer 3000 (Malvern Instruments, Malvern, UK) which uses a 52-detector array. The particle sizes were measured against a known refraction pattern for the range of grain sizes selected from the International scale for soil grain size classification, ISO 14688-1:2002 (ISO 14688-1), for all particles finer than 2 mm (coarse sand). For each sample, three different tests were completed, and the results are reported as a percent of the sample's particle volume. Particles >2mm were removed from the sample using a sieve to avoid damaging the Mastersizer. These particles were then measured as a percentage of the total mass of the sample to give an indication of their representation within the whole sample.

3.2.2 Atterberg Limits

The engineering properties of fine-grained cohesive soils depend largely on their moisture content. As moisture content changes, the soils can gradually transform from a semisolid state through a plastic state to a semiliquid state. The moisture content at which a soil behaves in each of these states is defined by the following parameters: the shrinkage limit (SL), plastic limit (PL) and liquid limit (LL). These parameters are collectively known as the Atterberg Limits (Terzaghi and Peck, 1948; Craig, 1974; Das, 1985; Atkinson, 2007). The LL, together with the PL, are the most important Atterberg Limits, which are essential in the classification of cohesive soils and their behaviour.

For this research, the LL and the PL were determined using the methods described in NZS 4402:1986, Methods of Testing Soils for Civil Engineering Purposes (NZS 4402), Tests 2.2 and 2.3, respectively. The tests were carried out for the material sampled from the vent area in TP1 and TP2. This was to allow correlation of the test results and due to the large absence of coarse-grained particles within the material.

3.2.2.1 Liquid Limit (LL)

The LL of a soil is defined as the moisture content at which the soil begins to behave in a liquid manner to a plastic manner (Craig, 1974; Atkinson, 2007). There are two commonly accepted

methods for determining the liquid limit (LL) of a material: the Casagrande Method and the Cone Penetrometer Method. As per the methods described in NZS 4402, the Casagrande Method is used for this study.

The sample is prepared by remoulding the soil on a plastic board and adding water until it becomes a semi-liquid state. The soil is then left for 24 hours at room temperature to allow the water to come to equilibrium with the clay. The soil is then placed into the Casagrande Cup and struck off level to the front of the cup. The soil in the cup is then carved using a Casagrande Tool forming a standard groove down its middle. The handle of the apparatus is then cranked causing the cup to rise and fall, striking the ground each rotation until the grove in the soil closes for a length of 13mm, then the total number of falls of the cup is recorded. The test method is then repeated for the soil at different moisture contents as more distilled water is added. The test was undertaken at five different moisture contents for each of the samples from TP1 and TP2. The moisture content of the soil then determined and plotted versus the number of falls of the cup on a semi-log graph.

3.2.2.2 Plastic Limit (PL)

The PL of a soil is defined as the moisture content at which the soil begins to behave in a plastic manner to a brittle manner (Atkinson, 2007). There is only one commonly accepted test to determine the plastic limit of a soil (Atkinson, 2007). This involves rolling the soil into a 3mm thread until it crumbles. The point at which the thread crumbles is the moisture content at which the soil stops behaving as plastic material and becomes a semi-solid.

From each TP location (TP1 and TP2), 30 grams of soil was dried until no longer sticky to touch. The samples were then worked by hand until cracks formed on the surface when rolled into a sphere. Each sphere was divided into two sub-samples. Within each sub-sample the soil is divided into approximately 4g portions to be tested by the same procedure. The portion is rolled in 3mm diameter threads and is worked and re-rolled until it breaks up before reaching the specified diameter. The moisture content of the portions is then determined and averaged for each sub-sample. The average of each of the samples is reported as the plastic limit for each test location. Due to the nature of the test, the results are influenced by the judgment of the person undertaking the test.

3.2.2.3 Plasticity Index (PI)

The Plasticity Index (PI) is another determined parameter that indicates the range of water content over which the soil behaves in a plastic state (Craig, 1974; Atkinson, 2007). Determination of the PI of a soil is derived from the difference between the LL and PL and is calculated using the following formula:

$$\boldsymbol{PI = LL - PL}$$

3.2.2.4 Liquidity Index (LI)

The liquidity index (LI) is the ratio between the difference of moisture content and the plastic limit to the plasticity index (Craig, 1974; Atkinson, 2007). The LI therefore puts the water content of a soil into the context of its plasticity, thus, giving an idea about the state of a soil for that water content. The LI is calculate using the following formula:

$$\boldsymbol{LI = \frac{(WC - PL)}{PI}\ x\ 100}$$

3.2.2.5 Activity

Another useful parameter related to the Atterberg Limits is the 'activity' (A). It is the relationship between the PI and the clay fraction (Das, 1985; Bell, 2006). This is a measure of the attractive forces in a sediment, based on the premise that surface area per mass increases with decreasing particle size, thus the amount of attracted water will be influenced by the amount of clay in the soil (Bell, 2006; Atkinson, 2007). It is used as an index for identifying the swelling potential of a clay soil (Das, 1985). The activity of a clay is calculated from the following formula derived by Skempton (1953):

$$\boldsymbol{A = \frac{PI}{\%\ of\ clay}}$$

3.2.3 Linear Shrinkage Tests

Also related to the Atterberg Limits, linear shrinkage tests are undertaken to determine the linear shrinkage of a disturbed soil sample. It is an effective test for determining the expansivity of a soil (Heidema, 1957; Cerato and Lutenegger, 2006). As part of this study these tests were undertaken in accordance with NZS 4402:1986 New Zealand Standard, Methods of testing soils for civil engineering purposes.

Three tested samples were taken from the vent area due to its consistent fine-grained nature, as well as the sample existing near its liquid limit. Firstly, the samples were tested to confirm whether they are near their liquid limit as per the procedures followed in Section 3.1.6.1 using the Casagrande cup. Once it was confirmed that the sample was within 15 to 25 blows, the sample was placed into a trough shaped shrinkage mould with a length of 140mm and a diameter of 25mm. The sample was then smoothed and placed into a 105˚ oven where it was left to dry for 24 hours.

After 24 hours the samples were removed from the oven and the longitudinal length of the sample is measured. The Linear Shrinkage (LS) of the sample is calculated as a percentage of the length of the mould:

$$\boldsymbol{LS}(\%) = \frac{\boldsymbol{Ls}}{\boldsymbol{L}} \boldsymbol{x\ 100}$$

Where Ls is the longitudinal length of the specimen (mm) and L is the length of the mould.

3.2.4 Crumb Test for Soil Dispersion

The presence of dispersive clays can cause significant engineering problems and their identification can be crucial (Knodel, 1991; Fell et al, 2015). The Emerson Crumb Test provides is a quick method for the identification of a dispersive clayey soil (Fell et al., 2015). It was developed by Emerson (1967) as a simple procedure to identify dispersive soil behaviour in the field, though it is now often used in the laboratory (Knodel, 1991). The method was later simplified by Sherard (1976) so that only four categories of soil dispersion are observed during the test (Fell et al, 2015). The crumb test gives a good indication of the potential erodibility of clay soils, however, it does have some limitations. A dispersive soil may in sometimes give a non-dispersive reaction in the crumb test. For example, some clay soils known to be dispersive

in the field such as Kaolinite, have shown non-dispersive reactions in the crumb test (Knodel, 1991; Fell et al, 2015). Generally, if the crumb test indicates dispersion, the soil is probably dispersive. Crumb tests are typically run in-conjunction with other tests such as a pinhole test and double hydrometer test to accurately determine the presence of dispersive clays within a soil and its erodibility (Fell et al, 2015).

The crumb test is undertaken as part of this study to identify the likely presence of dispersive clay soils within the expelled mud material. This can be used to infer the erodibility of the mud which may influence how long the feature is existent in its present state. Dispersive soils are also likely to contribute to an already large sediment supply within the Waimata Valley catchment (Carter et al., 2010).

A sample from the vent (TP1) and a mud flow (HA8) were each tested in accordance with ASTM D6572-20, Standard Test Methods for Determining Dispersive Characteristics of Clayey Soils by the Crumb Test. The test consists of placing a cubicle sample or 'crumb' of about 15 mm at its natural water content into 250 mL of distilled water. As the vent sample is very wet in its natural state, it was air-dried to near its plastic limit (PL) before undertaking the test. The crumb is left in the water undisturbed for two hours. At the end of the waiting period, the crumb and water are observed and the presence of any colloidal cloud in the water is evaluated visually by its size. A second observation is made after 24 hours.

3.2.5 Ring Shear Tests

The ring shear test is a method used to determine the residual strength of a soil using a remoulded sample. The ring shear test measures the shear strength at any degree of strain, providing the shear strength parameters of cohesion (c') and friction angle (Φ) for one sample. As the mud volcano material has essentially failed leading to its deposition, it is the chosen method used in this study to determine its strength properties. The samples used for the test were collected from TP1 due to its consistent fine-grained nature. HA3 is also tested as it contains the highest clay content out of all the samples. This is to assess whether there is an apparent relationship between the clay content and residual shear strength of the soil.

The apparatus used to undertake the ring shear tests is the Wyhekam Farrance Annular Ring Shear Machine and is conducted in accordance with the methods described in ASTM D7608-18, Standard Test Method for Torsional Ring Shear Test to Measure Drained Fully Softened Shear Strength and Stress Dependent Strength Envelope of Fine Grained Soils.

The sample is manipulated to bring it near its plastic limit, then moulded into the base of the ring shear annular device, containing an inner diameter of 70mm, and an outer diameter of 100mm. The top of the sample is then smoothed off with a smooth-edged scraper and the remaining parts are the apparatus is assembled. Each sample was consolidated in increments of 5 kg up to be 15 kg, which correspond to normal pressures ranging from 218 kPa to 654 kPa.

3.2.6 Scanning Electron Microscopy (SEM)

The overall structure and texture of soil has a strong influence on the behaviour of a soil. In clay rich soils, the structure and texture that primarily influences physical properties is microscopic (Grabowska-Olszewska et al., 1984; Selby 1993). Scanning electron microscopy (SEM) is a technique that is ideally suited to analysing the configuration, texture, and fabric of fine-grained soil samples. (Bohor and Hughes, 1971). It is used in this study to detail how the various clay and silt size particles contact each other (edge-to-edge, edge-to-face, or face-to-face), and the shape and distribution of pore spaces within the sample.

Samples for the SEM were selected from two test locations at the site (HA3 and HA10). These two locations were chosen to account for spatial variability across the site. From each test location four samples of 10g were collected and air dried at 40.5˚C for 24 hours. The samples were then carefully broken to expose the soil fabric and placed on a stainless-steel mount using epoxy resin. The samples were subsequently placed in a Polaron SC 7640 sputter coater and coated with platinum. Next, the samples were coated for 450 seconds at 5-10 mA and 1.1kV. A FEI Quanta 200F Environmental Scanning Electron Microscope. The chamber pressure, beam spot size and voltage are noted on each image. A magnification factor ranging from 50× to 50,000× was used to analyse the microstructure of the soil.

3.2.7 Laser Ablation Inductively Coupled Plasma Mass Spectrometry

Laser Ablation Inductively Couple Plasma Mass Spectrometry (LA-ICP-MS) is a rapid, highly sensitive instrument capable of analysing multi-element suites, including major and trace elements (Liu et al., 2013). LA-ICP-MS was used as part of this analysis to compare the collected data to that of two other mud volcanoes within the Waimata Valley, the Mangaehu Stream Mud Volcano, and the Arakihi Road Volcano (Stanley, 2019). Two samples were prepared from each of the TP samples within the vent of the mud volcano (TP1 and TP2) for LA-ICP-MS analysis. These samples were chosen due to their fine-grained nature and absence of coarser material.

Using a centrifuge, fine-grained sediments (predominantly clay) were retained and concentrated in solution following the standard method prescribed for preparation of slides for XRD analysis. The concentrated solution was pipetted onto a 1" circular glass disc or rectangular glass disc, sufficient to deposit a >100 μm layer of fine sediment and left for 48 hours to dry (Figure 3.3).

For each sample, three-line ablations were performed with the settings summarised in Table 3.1 (below) and results integrated. A cleaning ablation was performed before each line ablation in order to remove any contamination that may be present on the surface of the sediment, followed by a 60 second wait period in order to eliminate disturbance within the test environment.

Table 3.1: *LA-ICP-MS Settings*

Spot Size	80 μm
Speed	0.04 mm s^{-1}
Repetitions s^{-1}	5 Hz
Energy density	4.5 J cm^{-2}
Scan line length	3 mm

The ICP-MS was calibrated against NIST610, NIST612, BCR, and BVH0 standard for the following 38 isotopes: Na, Mg, Al, Si, P, K, Ca, Ti, V, Cr, MN, Fe, Co, Ni, Cu^{63}, Cu^{65}, Zn, Sr, Y, Zr, Mo, Cd, Cs, Ba, La, Ce, Nd, Sm, Eu, Tb, Dy, Yb, Pb and U. Isotope were chosen to give a spread of the major trace elements, trace elements and rare earth elements which are common to the geology in the area while avoiding isotopes with masses which could be misinterpreted as other isotopic combinations, most notably Ar40 and Cl35 is often counted as As75.

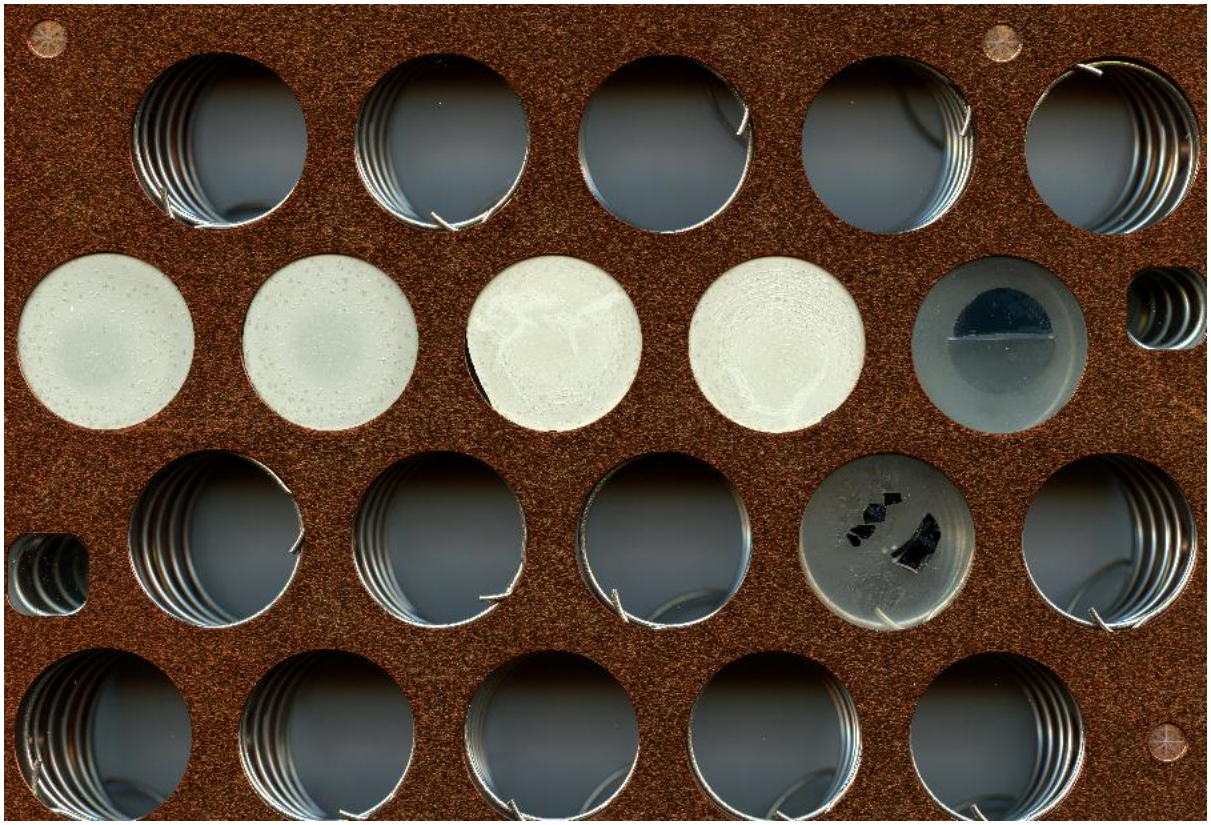

Figure 3.3**:** *Image of glass slides with dried clay sediment prior to Laser Ablation. The glass standard discs are also shown.*

CHAPTER FOUR: SITE CHARACTERISATION AND MATERIAL PROPERTIES

4.1 Site Characterisation

4.1.1 Mapping and Site Observations

The characteristic features of the mud volcano are shown on the engineering geological map below (Fig 4.1). The mud volcano is characterised by a slightly elevated vent area in the western central portions of the site, with three distinct mud flows or 'fingers' propagating from the vent to the north, east and south. These flows appear to be constrained by the topography, concentrating in previous gullies and depressions. These flows would have also been assisted by the domed shape of the site that had formed by uplift resulting from earthquake activity prior to the eruptive event. Compared to the mud volcano morphologies described by Mazzini and Etiope (2017), this mud volcano is similar to the pie-shaped morphology described as a smooth dome-like structure. There is a lack of mud material extending west from the vent area, rather, an elevated cone edifice has formed approximately 1.5 m above the vent. Due to the topography, it is likely that a mud flow was unable to form in this area and instead formed a cone structure.

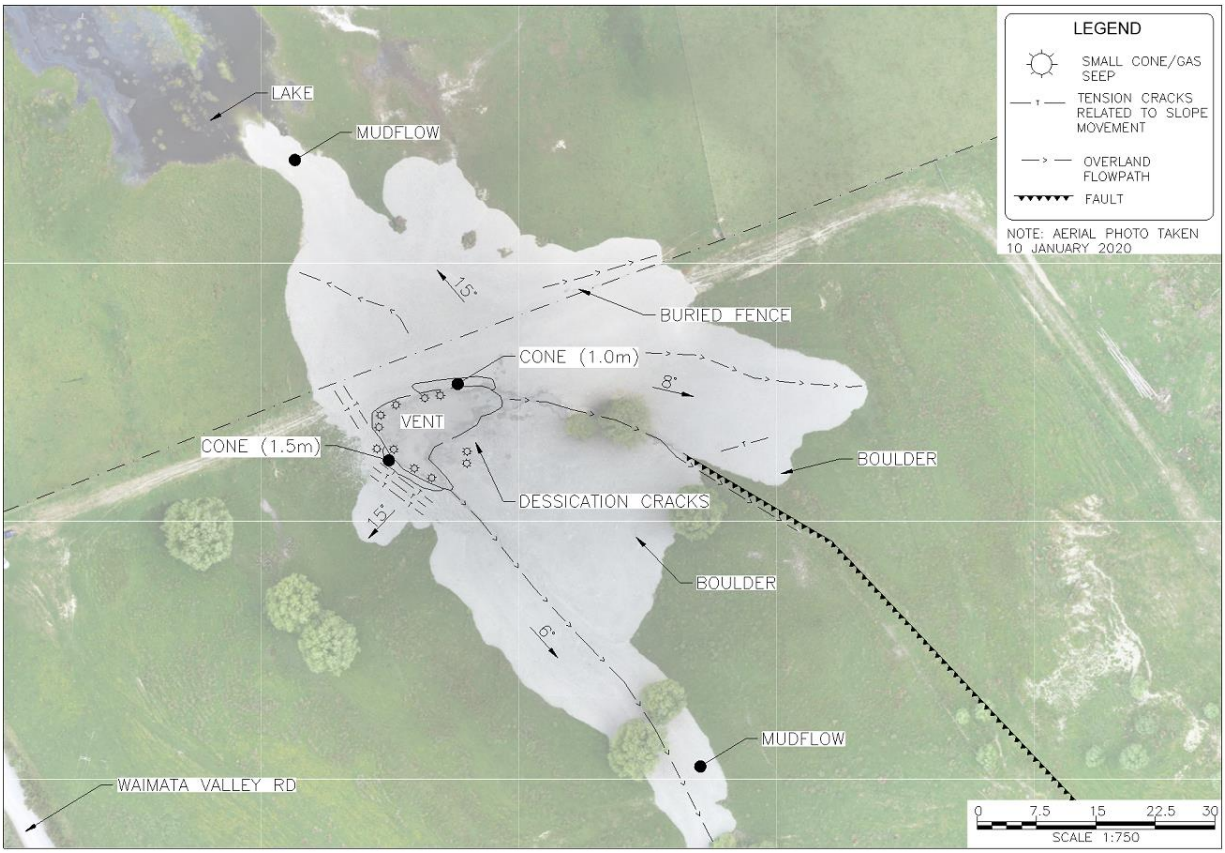

***Figure 4.1**: Engineering geological map of mud volcano site at boundary of Hall and Utting farms.*

The flow to the north reached approximately 40m upstream before terminating. The angle of the flow is approximately 15˚ highlighting the significance of the uplift prior to the eruption. This flow has consequentially dammed the stream that previously flowed through the site resulting in the formation of a lake. Mud volcanoes are commonly documented to block flowing water bodies such as the Brookby Farm (Pettinga, 2003) and Mangaehu Stream (Ridd, 1970; Mazengarb, 1997) mud volcanoes. Dammed water bodies with significant water flows can be hazardous if they are breached, which happened at the previously mentioned sites following eruption. The southern flow extends the furthest from the vent at angle of 6˚ for an approximate distance of 100 m. This flow propagated downstream along the now-dried stream channel, enveloping several large trees in its path.

The vent is characterised by an elevated area of highly cohesive yet fluid mud. Within the vent material there is lack of granular material relative to the material outside of the vent. This is attributed to the continued low-energy activity of the vent following the eruption, expelling fine grained silts and clays within saline fluid and gas. The larger fragments of rock are interpreted to have been brought to the surface during the early high-energy stages of the eruption within the expelled mud and carried further from the vent. Methane gas and saline fluid continues to escape from vent via several minor vents, with gas venting or 'burping' occurring every 10-30 seconds. There are also several minor vents noted outside of the major vent area. Adjacent to the vent area is an area of fine-grained mud characterised by the formation of desiccation cracks as it dries. These desiccation cracks highlight the clayey nature of the material.

Several preferential surface flow paths have formed across the mud volcano. The flow paths carry rainwater as well as fluid expelled from the vent out to the edge of the feature. The flow paths have formed significant depressions in the volcano only months after the initial eruption highlighting the erodibility of the mud and the potentially dispersive nature of the clay matrix. Slump scarps and tension cracks were noted directly west of the vent, on slopes with a gradient of approximately 15˚. These features signify that the mud has remobilised following its deposition at the surface. In relation to other slopes in the region these are relatively flat, and this movement highlights the vulnerability of the material to slope failure once it has erupted. To the southeast of the site, the trace of a small fault was located trending to the northwest and southeast. This fault is inferred to follow a similar orientation underneath the mud volcano and is interpreted to be the line source for the expelled mud. The Arakihi Road mud volcano field

also exists along the same fault line northwest of this site. This fault is interpreted to have formed as a result of diapiric activity and intersects the Waimata Valley fault line further south (Ridd, 1970; Neef and Bottrill, 1992).

4.1.2 Ground Penetrating Radar (GPR)

A GPR signal consists of three major components: the air wave, the ground wave, and the primary reflectors. Several features of the subsurface can interfere with this signal producing a distorted image. These features commonly include: the water table, clay soils, and discontinuous surfaces such as faults. As observed during investigations, this site contains saturated soils with high clay contents, therefore, it necessary to apply a select set of processes to the collected data to help reduce the impact of these features, helping to produce a clearer image of the subsurface (Assad, 2004; Daniels, 2004).

A total of 88 transects across the mud volcano site were measured using the GPR. The data collected from these scans was interpreted using the GPR processing software RadExplorer and used to produce a GPR profile of selected transects. The processes that were applied included: DC Removal, Time-Zero Adjustment, Migration, Background Removal, Bandpass Filtering and Topography Correction. Four GPR profiles are selected that represent the observations frequently made of the subsurface across the site (Figs 4.2 and 4.3).

It is clear from Figures 4.2 and 4.3 that the GPR signal becomes very distorted below a depth of approximately 4m across the site. This is due to the shallow soils containing a high clay and water content which causes attenuation of the EM wave resulting in a loss of signal. Several interferences to the signal are also recorded at the surface. This is represented by the concave structures observed on the GPR profiles. The majority of these interferences are interpreted to be the trees within the site which correlate with their positioning along the transect.

Specific areas of interest have been highlighted on the selected GPR profiles and are shown in Figure 4.4. In all the images (A-E) there are clear discontinuities in the GPR signals represented by an offset in the horizontal lineation's. These discontinuities are interpreted to be either ruptures or faults within the subsurface. The positioning of these discontinuities on the GPR

profile generally matches the rupture pattern observed at the site following the Te Araroa earthquake prior to the mud volcano eruption (Refer Section 2.2, Fig 2.4).

The conductivity of the soils makes it difficult to observe the potential source of the mud at depth, however, Image B shows an interesting reflection configuration at approximately 4m depth which may represent upwelling material and correlates with the centre of the vent. The use of GPR at this site is useful for determining structure within the surficial soils (<4m depth), however it highlights the challenges of using the equipment in highly conductive, saturated soils. To determine the deeper subsurface structure of the site more precisely, other geophysical methods may be more beneficial. The subsurface of a mud volcano field in the Mangapakea Valley, New Zealand was effectively profiled through the use 3D electrical resistivity survey highlighting its subsurface structure to a depth of approximately 30m (Zeyen, 2011). This method may be useful for further characterisation at the Waimata Valley site.

Figure 4.2: *Selected GPR profiles of transects No. 365 and No. 380. Square boxes correlate to specific areas of interest shown in Fig 4.4.*

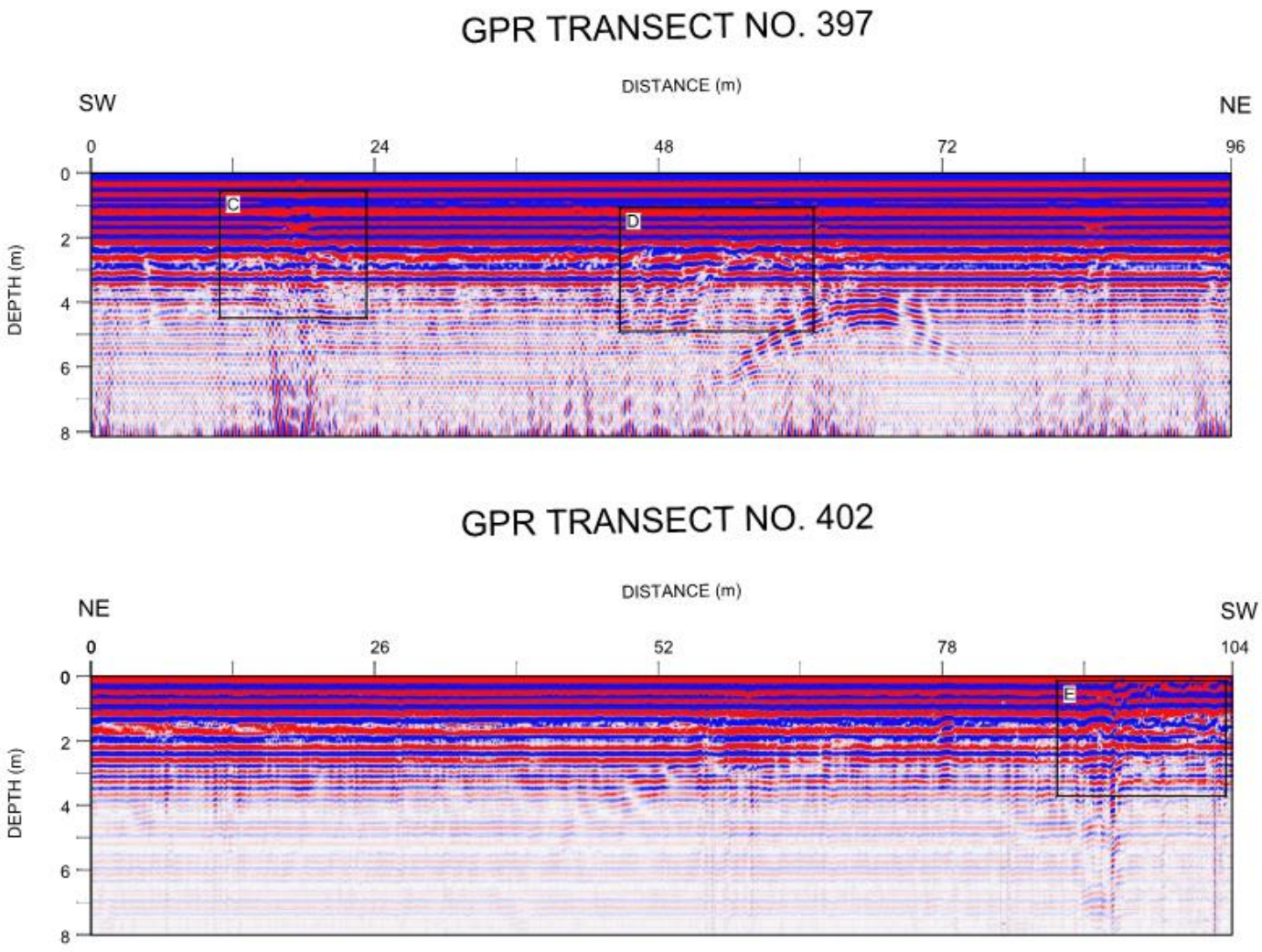

Figure 4.3: *Selected GPR profiles of transects No.397 and No. 402. Square boxes correlate to specific areas of interest shown in Fig 4.4.*

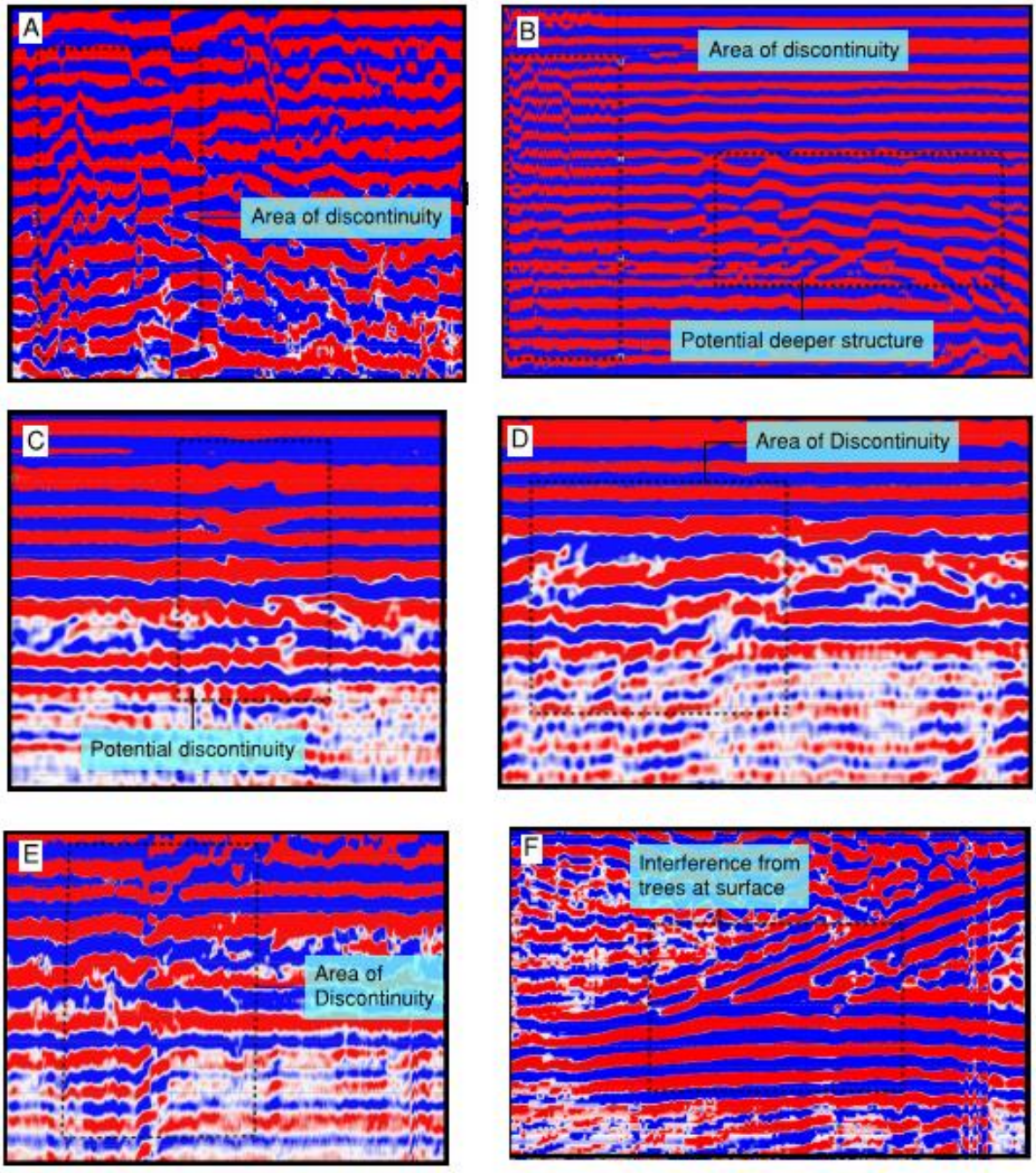

Figure 4.4: *Specific areas of interest highlighted from GPR profiles shown in Fig 4.2 and 4.3. A) Area of discontinuity represent a potential fault/rupture within mud volcano. B) Area of discontinuity represent a potential fault/rupture within mud volcano. A potential deeper structure within mud volcano highlighted by the abnormal layers, possible change in subsurface material. C), D) and E) Areas of discontinuities shown by offset of horizontal lineation's, indicating a possible fault or surface rupture. F) Interference of signal by trees at surface creating a convex shape in lineation's.*

4.1.3 In-Situ Testing

From the 10 hand augers drilled across the site, a subsurface profile was able to be inferred and interpreted. A cross section through the middle of the site has been drawn based on these interpretations as shown on Figure 4.5. The general interpreted subsurface profile across the mud volcano site is described in Table 4.1, as well as further explained as follows.

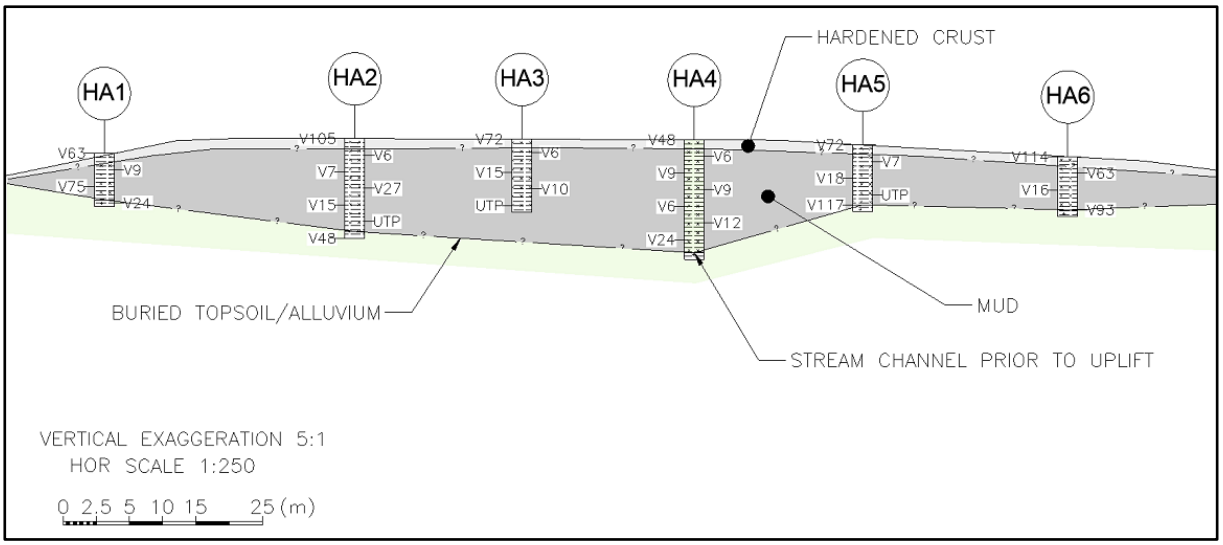

Figure 4.5: *Cross Section of mud volcano showing subsurface conditions through middle of site.*

Table 4.1: *Interpreted Subsurface Profile*

Depth to base of layer (m BGL)	Soil Description	Interpretation
0.1 to 0.2	Silty CLAY, some gravel; whitish grey. Stiff, dry, slightly plastic; gravel, fine to medium, mudstone	Hardened crustal layer formed across site due to drying of expelled mud
0.3 to 2.8	Silty CLAY, trace gravel; grey. Very soft, moist to wet, highly plastic; gravel, fine, mudstone	Expelled mud existing at natural moisture content
>2.8	CLAY, minor silt, minor organics; greyish brown. Firm, moist to wet, moderately plastic; organics, fibrous and amorphous	Underlying buried topsoil and alluvium

Across the site a distinct whitish grey dried crust had formed. The crust comprised of a very fine matrix of sit and clay with occasional clasts ranging from sand to boulder sized. This crust had been formed due to the drying of the extruded mud at the surface. The crust was

significantly stiffer than the underlying mud and vent material. The dried crust was easily traversed by foot whereas the highly fluid vent material was unable to be traversed without sinking or getting stuck. All hand augers indicated the depth of the crust to be between 0.1 m to 0.2 m across the site.

Underlying the dried crust is the mud material of similar description though having a darker grey appearance. The mud was very sticky to touch with a significantly greater moisture content compared to the overlying crust, demonstrating highly plastic behaviour. This is because as the material is buried beneath the crust, the moisture of the material is retained. The wet mud is inferred to be close to its natural water content, similar to that of when it was first erupted. The thickness of mud was greatest surrounding the vent area and decreased with increasing radial distance from the vent. This was indicated by the hand augers surrounding the vent area (HA2, HA3, and HA9), encountering a depth of mud at a maximum of 2.8 m near the vent, and between 0.2 m to 0.4 m at the periphery of the mud volcano indicated by hand augers HA1, HA6 and HA7. The depth of these materials was also confirmed by the Scala penetrometer tests. This trend of depths across the site confirms the mud volcanoes pie shaped morphology highlighted in Section 4.1.1.

Beneath the expelled mud materials are brown clays with minor fibrous and organic materials. These clays are interpreted to be the autochthonous materials that represent the ground surface prior to the eruption. The organic nature of the soils indicate that the materials are likely to be buried topsoil or alluvium, deposited by the stream channel that used to flow through the site. All hand augers encountered these materials below the overlying mud though their total thickness is unknown.

The hand-held shear vane was used as a diagnostic test during the field investigations to determine the in-situ shear strength of the material in its current conditions. The tests were undertaken within each borehole at approximately 0.5m depth intervals. The peak and residual strengths at each depth interval are presented in Table 4.2, including the soil description and interpretation. Occasionally large rock fragments within the mud were encountered within the borehole and influenced test results. Where these fragments were encountered, the test was undertaken at a lower depth to get a representation of the mud matrix, rather than the rock fragment.

Table 4.2**:** *In-situ Peak and Residual Strength of materials encountered within Mud Volcano.*

Interpretation	Peak Shear Strength Range (kPa)	Average Peak Shear Strength (kPa)	Residual Shear Strength Range (kPa)	Average Residual Shear Strength (kPa)
Dried Crust	45-168	84	8-17	12
Mud	3-25	10	2-7	6
Buried Topsoil/Alluvium	45-109	81	11-33	25

The shear-vane results show that the dried crust of the mud volcano is of 'stiff' consistency (50 kPa to 100 kPa) on average. The hardened crust material is determined to be sensitive based on the difference between the peak and residual shear strengths. The wet mud material forming most of the mud volcano is of 'very soft' consistency (<12 kPa), and is 'insensitive'. Although the hardened crust and underlying mud are inferred to contain a very similar material make-up, there is a large variance in their strengths. This is attributed to the difference in moisture condition of the materials. This is an uncommon relationship observed in clays, as generally, sensitive clays possess high moisture contents. A under consolidated clay would be expected to be of high sensitivity (Bell, 2006). The abnormal sensitivity results of the material may be due to the erupted material existing in an already remoulded state.

The Scala Penetrometer Test (Scala) is principally designed for use in cohesionless sands and fine gravels to provide an indicative relative density of the soil. The test is often determined to be inappropriate for use in cohesive soils as it cuts through the clay material, and changes in moisture contents greatly influence the results (Stockwell, 1977). No cohesionless soils were encountered at this site however, the tests were still undertaken to determine the depth of the mud material, as well as provide a diagnostic assessment of the allowable bearing capacity of the material. The results of the test show that the material is penetrated approximately 400mm per single blow of the hammer (See Appendix C). Although care should be taken where inferring any Scala data correlation within cohesive soils, the results highlight the very low strength of the mud material and an indicative allowable bearing pressure of less than 35 kPa is assumed in its current state (Stockwell, 1977).

4.1.4 Surface Sampling

The following observations have been made from the surface sample at the site. The correlations of the stratigraphic units are based only on visual observations and further compositional testing is necessary to be accurately determined. The largest proportion (33%) of the sampled rock was the sheared sandstone containing quartz and calcite veins interpreted to be from the Torlesse Supergroup (Fig 4.6). These calcite veins likely indicate the presence of fluid prior to the ascent of the mud, responsible for the hydraulic fracturing of the source rocks (Mazengarb and Speden, 2000; Deville, 2009). The second largest proportion is the thinly interbedded sandstones and mudstones inferred to be sourced from the Mangatu Group. Also likely to part of Mangatu Group is the greensand (13%), which is representative of the thick glauconitic sandstone of the Wanstead formation (Ridd, 1964; Neef and Bottrill, 1992; Mazengarb, 2000). An interesting lithology sampled was the grey siltstone and sandstone that was noted to be discharging gas interpreted to be methane (9%). These rocks are inferred to be sourced from either hydrocarbon rich Tinui Group, or the underlying Matawai group also known for its hydrocarbon generation (Lewis and Marshall, 1996; Mazengarb, 1997).

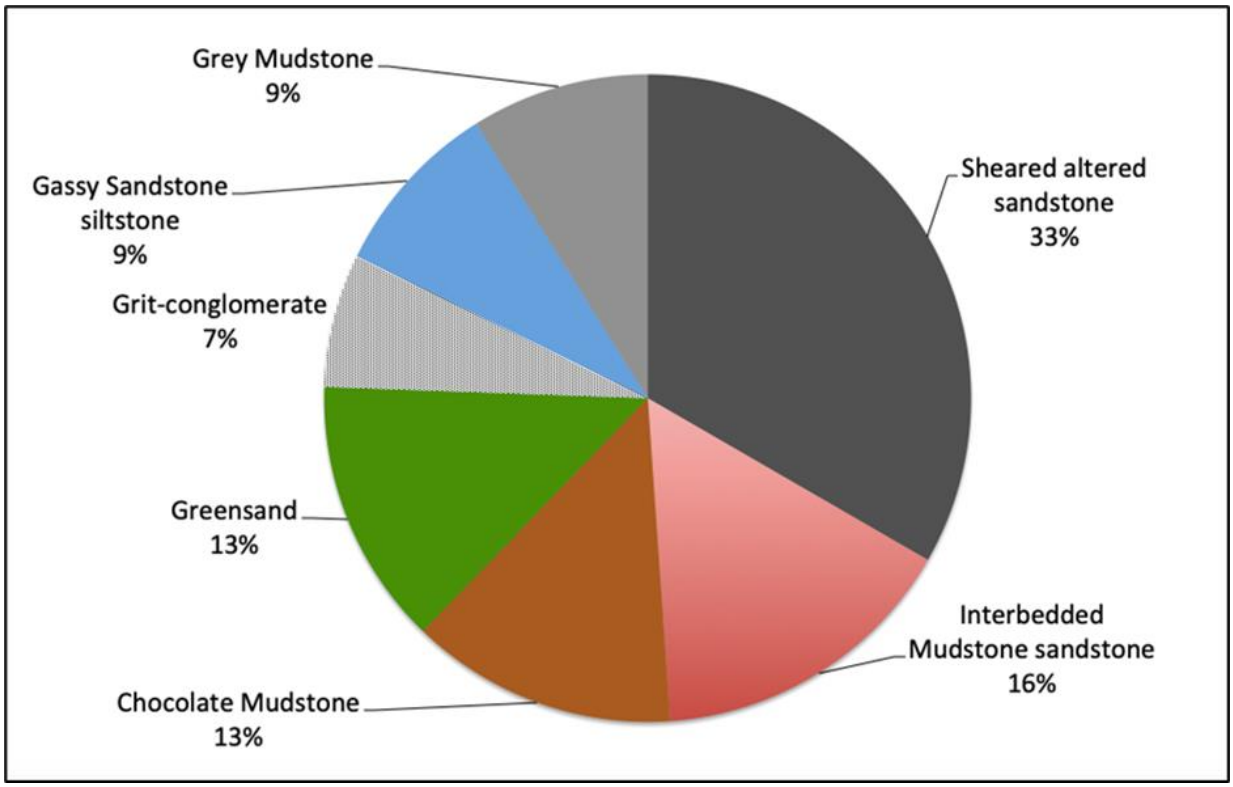

Figure 4.6: *Proportion of fragments of rock expelled from mud volcano based on their lithology.*

The chocolate mudstone (13%) is also inferred to be sourced from the Tinui Group, and the grit-conglomerate from the Matawai Group. The homogenous grey mudstone (9%) may be from one of several groups, including the Mangahei Group, Tolaga Group, Mangatu Group or Tinui Group. The Torlesse Supergroup and Matawai Group are older than the assumed age of the source material that contributes most of the material expelled at the surface. This is not surprising considering the extensive faulting in the area.

4.2 Geological Properties

4.2.1 Scanning Electron Microscopy (SEM)

The SEM images presented in Figure 4.7 show most of the mud matrix comprises of platy clay minerals inferred to be smectite-type which is the dominant clay within the stratigraphic source of the mud. A more comprehensive collection of the SEM images is also presented in Appendix B with identification of the various minerals. This smectite clay is derived from the degradation of Paleogene mudstone strata characteristic of the highly sheared scaly clays forming the thrust-generated melange zones and diapiric structures of the eastern North Island (Mazengarb, 1997; Pettinga, 2003). The clays appear to be distributed in a random orientation with no preferential structure. This is attributed remobilisation of the clay and lack of consolidation (Bell, 2006). Other clay minerals such as illite and kaolinite are likely to be present within the matrix which may form as a result of diagenesis of the source material, or due to assimilation within the intrusive domains as the mud ascends to the surface. Similar platy minerals are also observed within the matrix which are likely to be either micas and/or chlorite (See Appendix B). These are common assemblages within material associated with mud volcanism (Deville, 2009; Blouin, 2019). Silt to sand-sized particles (60μm to 200μm) within the matrix are likely to predominantly be quartz, albite, and calcite, indicated by their angular shapes. To confirm the mineralogy of the clays and crystals techniques such as X-ray Diffraction (XRD) or energy-dispersive X-ray spectroscopy should be utilised.

The images also show relatively large amounts of pore spaces even though the sediment is dominated by clay and silt sized particles. The pore spaces are likely related to fluid and gas escaping from within the mud as it is expelled at the surface and continues to dry out. Large, elongated cavities interpreted to be desiccation cracks highlight this drying out process. As the material has not consolidated the pore spaces remain prominent.

Observations correlating to the images shown in Figure 4.7 are described below. These images were chosen to best represent the observations made across the analysed samples.

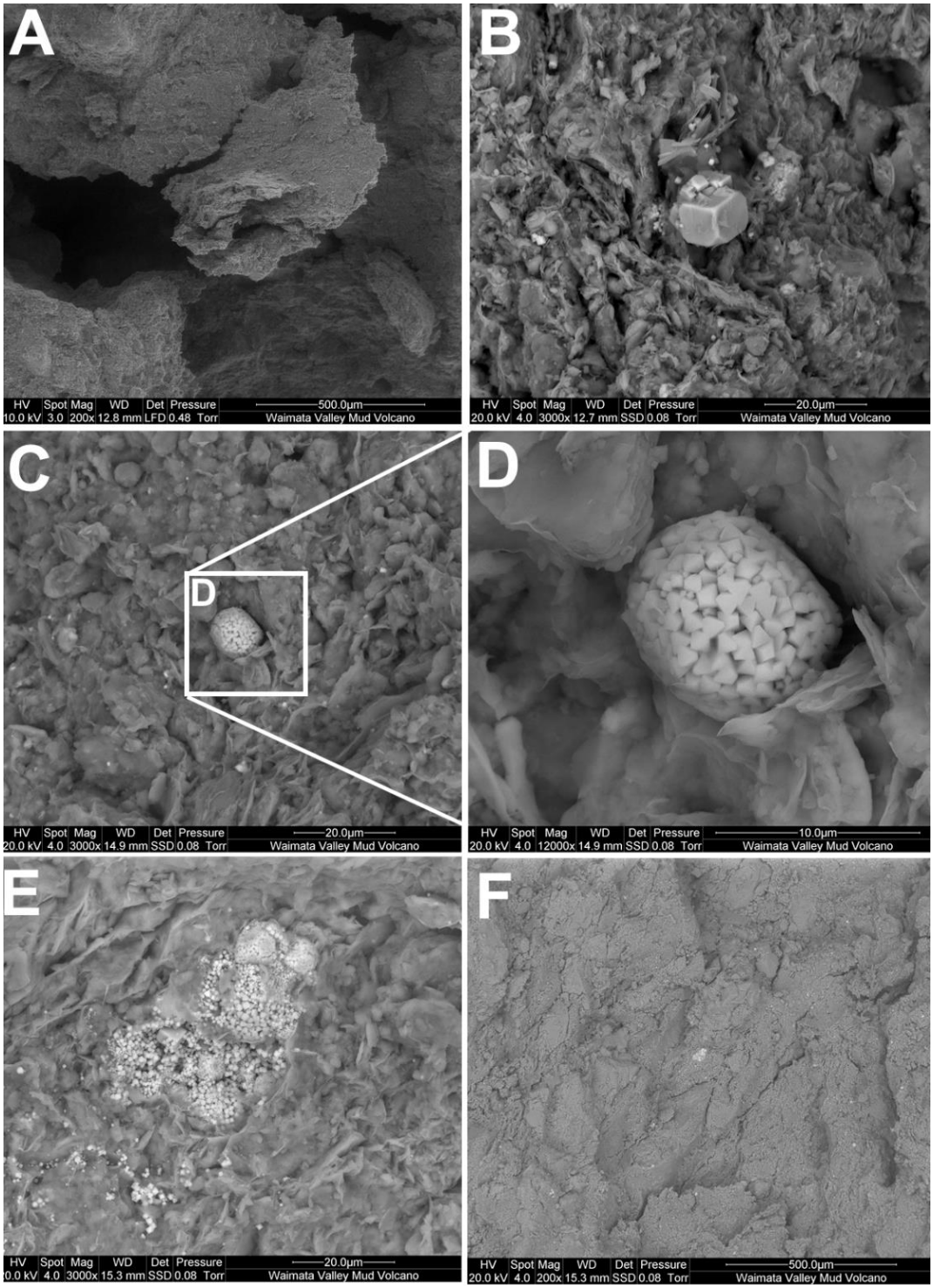

Figure 4.7*: A) Desiccation cracks in clayey soil, due to post-eruption shrinkage and drying (HA3_013); B) halite crystal growing in void from dewatering of marine water (HA3_046); C) & D) pyrite growth (light coloured so is charging) within smectite clay mineral plates (HA10_030 & HA10_31); E) sodium chloride growth within cavities due to dewatering of seawater (HA10_021); (F) more cracking due to desiccation and shrinkage of clays post-deposition of mud volcano (HA10_01).*

Figure 4.7 (A) and (F) highlights the large, elongated cavities formed within the structure. These are indicative of desiccation cracks that form due to shrinkage of the clayey soil as it dries out at the surface once it has erupted. These desiccation cracks were also observed on a larger scale across the mud volcano structure as highlighted by the site mapping and characterisation. Large pore spaces are also left because of the fluid and gas phases escaping form the structure once it has erupted at the surface.

Figure 4.7 (B) and (E) shows a halite (NaCl) salt crystal formed with a cavity. The halite would have been originally precipitated when the material was originally deposited in a marine environment. The salt crystals would have then grown as the sediment matured and eventually remobilised. This therefore shows that some of the original fabric and microstructure of the sediment is preserved, even when it has erupted at the surface.

Figure 4.7 (C) and (D) show a light-coloured aggregate of octahedral crystals within clay mineral plates. The light colour likely indicates that the crystal is charging resulting from the SEM. This occurs if the mineral is conductive and absorbs the electron current. The crystals are likely to be pyrite which is commonly found in marine sediments (Deville, 2009). The aggregate of pyrite crystals within spherical shape as shown is known as a framboid (Chen et al., 2015). At high magnification factors such as x12,000 shown in Fig 4.7 (D), the platy nature of the clay minerals is observed suggesting is smetitic composition.

4.2.2 Inductively Coupled Plasma – Mass Spectrometry (ICP-MS)

The data collected from the ICP-MS is plotted on Figures 4.8, 4.9 and 4.10. Each figure represents the major, trace and rare earth element concentrations in each sample. The recent Waimata Valley mud volcano (WV-MV) tested as part of this study is shown on each figure as an average of all laser ablation scans. The other plots shown on the figures were collected from the Arakihi Road (AR-MV) and Mangaehu Stream (MS-MV1 and MSMV-2) mud volcanoes as a part of another study undertaken by Stanley (2019). Without the plots from the other mud volcanoes the data would be somewhat meaningless, however, by comparing each of the plots similarities in their chemical fingerprints are observed.

Each figure shows a broadly similar fingerprint across each mud volcano highlighting their similar composition, and therefore a likely similar source of material. Furthermore, the Arakihi

Road mud volcano (AR-MV) and recent Waimata Valley mud volcano (WV-MV) show very similar chemical fingerprints signalling they likely come from the same mud reservoir. The two Mangaehu Stream mud volcanoes likely come from a similar deeper source following a different migratory path to the surface. This is also evident by the distance that separates the different mud volcanoes, as well as the differing geology.

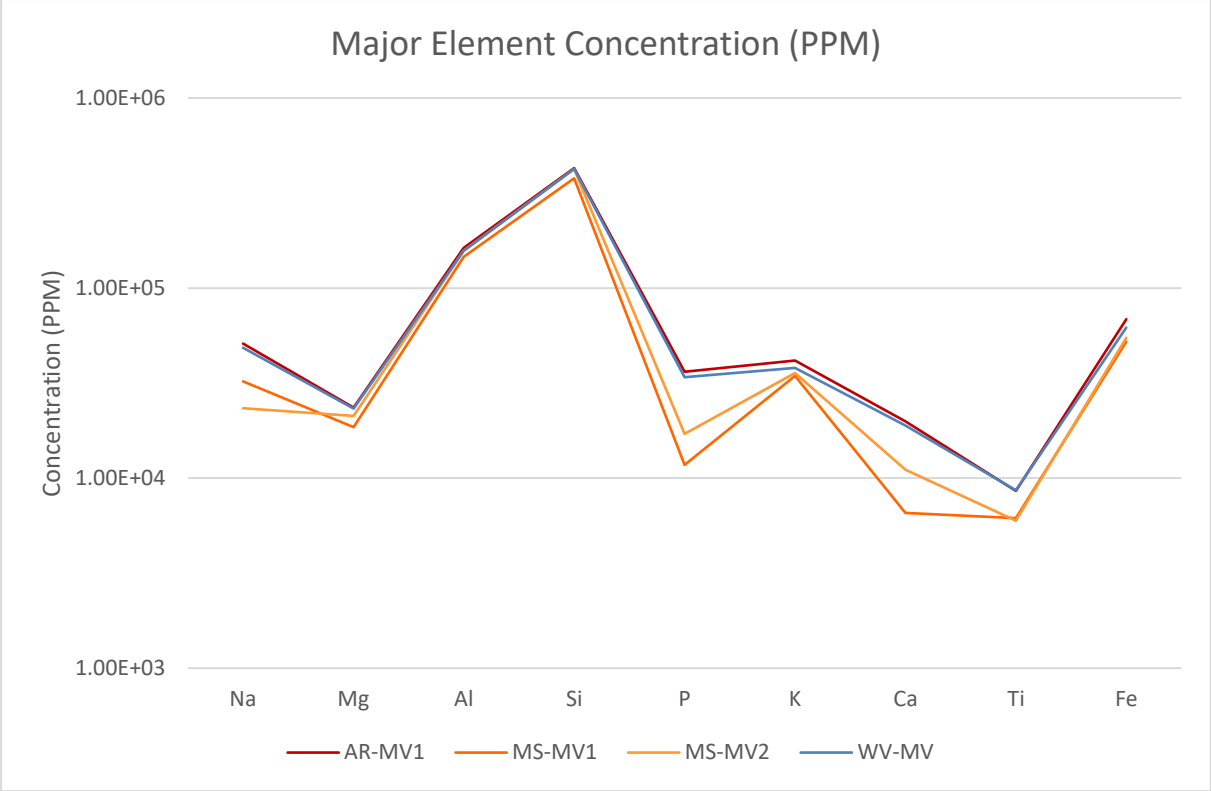

Figure 4.8: *Major element concentrations of sediments from various Waimata Valley mud volcanoes.*

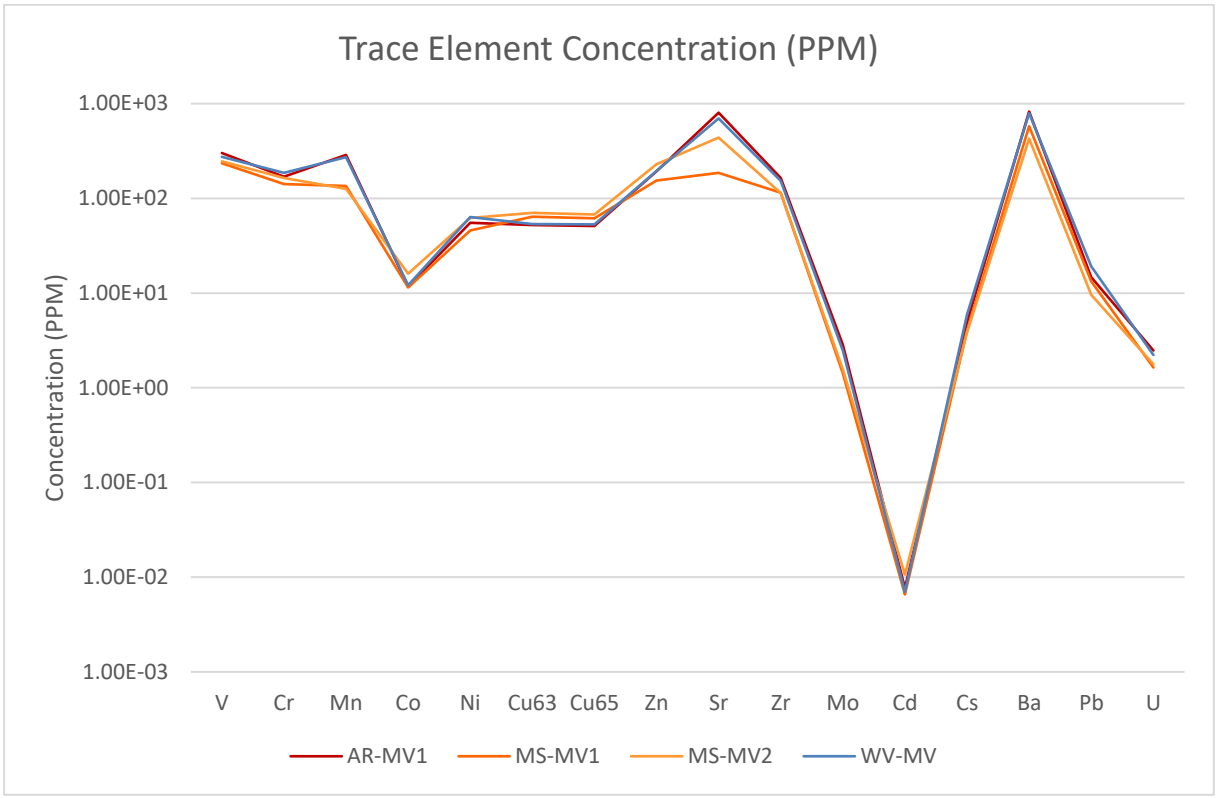

Figure 4.9: *Trace element concentrations of sediments from various Waimata Valley mud volcanoes.*

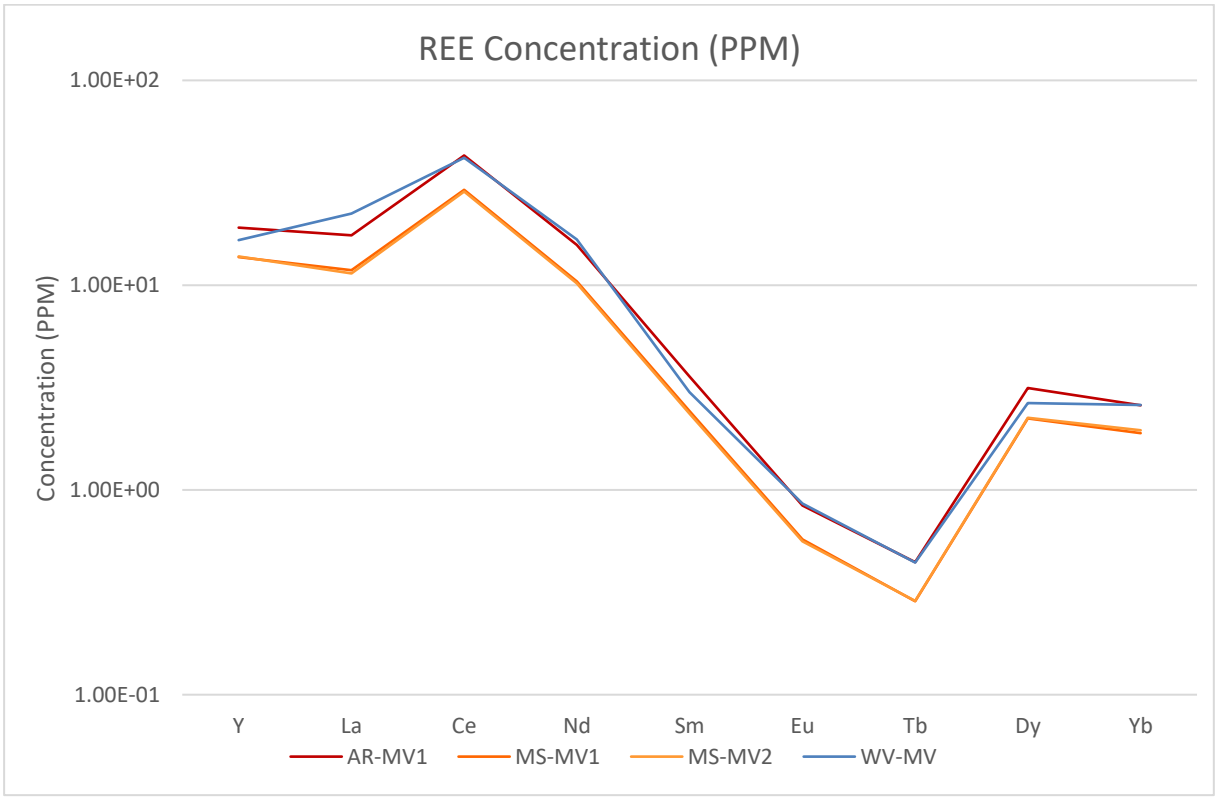

Figure 4.10: *Rare earth element concentrations of sediments from Various Waimata Valley mud volcanoes.*

4.3 Index Properties

4.3.1 Particle Size Distribution

The PSD of the mud volcano samples can give some indication of the geological origin of the extruded material, as well as highlighting the level of assimilation within the intrusive and extrusive domains (Yassir, 1989). It also influences the permeability of a material which is an important factor in explaining how deeply buried sediments become overpressured leading to mobilisation and potentially mud volcanism (Kopf et al., 1998; Kopf et al., 2005).

The results from the particle size analysis (PSA) are presented on the PSD graph (Fig 4.11). Each tested sample is represented by a different coloured plot and symbol, to distinguish between the samples and to highlight their variability. Each sample was tested three times using the Malvern Mastersizer and the average of each test is what is presented. The entire dataset used to create this graph is shown in Appendix C. To avoid damaging the measuring instrument, particles greater than 2mm were removed from the sample were removed using a sieve (Fig 4.12). As per ISO 14688-1, this represents all particles larger than a coarse sand (gravels). The proportion of gravels >2mm within each sample was determined by their combined mass relative to the mass of the entire sample. For all the tested samples, the proportion of the gravels removed ranged from 1% to 3% and were measured within the fine gravel bandwidth (2mm to 6mm). The predominant composition of the gravels were quartz, mudstone, and rounded greywacke.

There is a general consistency shown across the plots with the majority containing greater than 80% fines (clay and silt sized particles). The PSD of HA5 at a depth of 1.0 m, shows a relatively larger absence of clay and fine to medium silt within sample, containing a larger proportion of coarse silt and fine sand. This may highlight the particle size variance with depth across the site. There appears to be no relationship with spatial variance.

It is somewhat surprising that the dominant fraction size across all samples is within the silt bandwidth (0.002 mm to 0.06 mm) when compared to the images produced by the SEM. From the images, it appeared that there is a larger proportion of clay than what has been determined by PSA. The behaviour of the material from field observations, as well as the laboratory tests (Section 4.3.2), clearly show that it is influenced by clay. There are a couple of factors that could have contributed to a lower proportion of clays than what is truly representative of the

material. Firstly, although a deflocculant agent was used during the sample preparation, there is still a likelihood that not all the clay particles were segregated into individual grains. Though, as the clays are interpreted to be predominantly smectite which contain weak attractive forces between the individual particles, the deflocculant is likely to be effective (Das, 1985). Another factor may be that the instrument used for the PSA measures the PSD of the sample as a proportion of its volume rather than its mass. Smectite clays are generally the finest of the clays (Das, 1985; Nadeau, 1985). This may disproportionately represent the sample relative to the theoretical PSD derived by the samples mass. Nevertheless, the SEM images also evidently show a large presence of silt particles within the soil matrix.

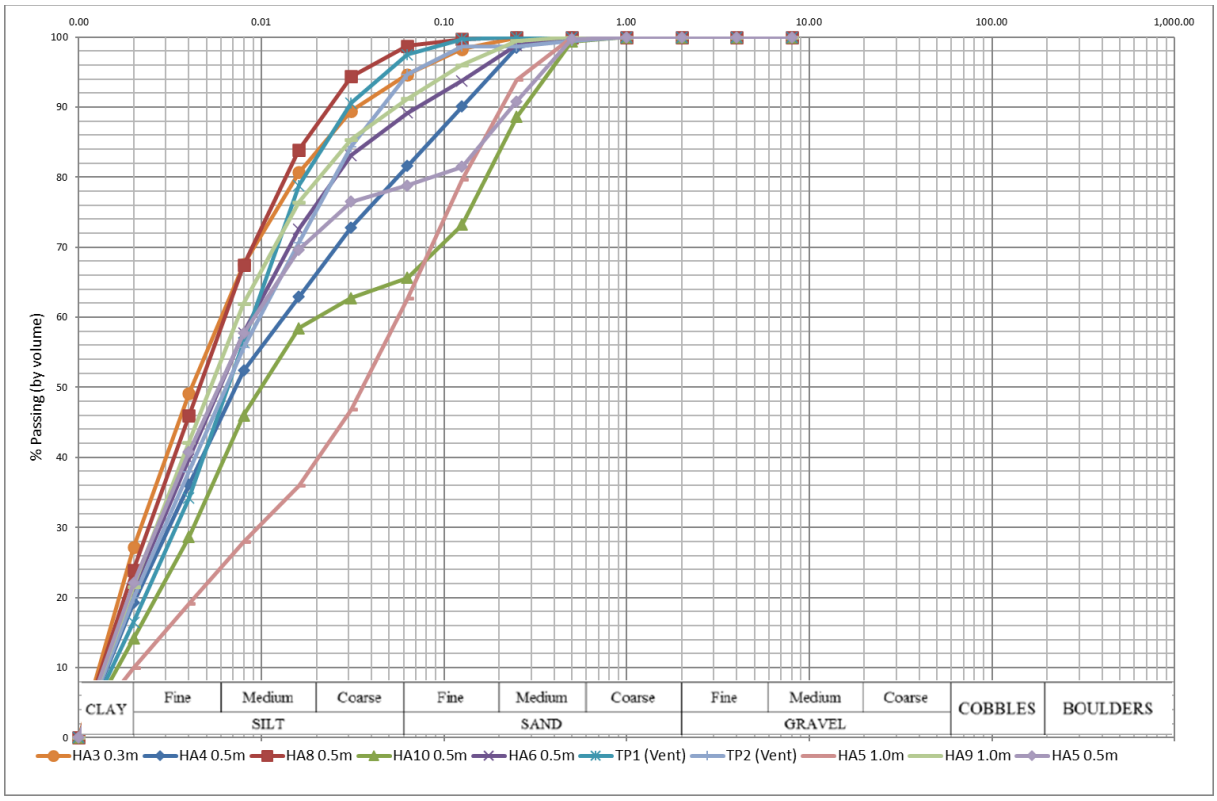

Figure 4.11**:** *PSD distribution curves of mud volcano samples. The data shows percentage passing curves for all sample tests.*

The particle size distribution data obtained shown in Figure 4.11 was used to create a grain size percentage graph for each sample (Fig 4.13). These particle size bands were based on the same international scale (ISO 14688-1) used in the PSA. The graph highlights the clear dominant silt-sized proportion within each portion, and their fine-grained nature overall. The range of grain size proportion for all samples is shown in Table 4.3.

When compared to other PSD curves produced for material associated with mud volcanism around the world (c.f. Yassir, 1989, Blouin, 2019), the curves produced are broadly similar showing a predominant clay and silt composition. It is inferred that the mud volcano samples with these grain-size distributions would be of very low permeability, which is considered an important controlling factor is mud mobilisation and mud volcano formation (Yassir, 1989; Kopf et al., 1998; Kopf et al, 2005).

Figure 4.12: *Fine gravels removed from sample prior to PSA using the Malvern Master Sizer 3000. Predominant composition of gravels is quartz, mudstone, and greywacke.*

Table 4.3: *Range of grain size proportion within all mud volcano samples tested for PSA.*

Grain Size (mm)	**Range of grain size proportion (%)**
Clay (<0.002)	10.0 to 27.2
Silt (0.002 to 0.063)	51.5 to 81.0
Fine Sand (0.063 to 0.2)	1.2 to 31.2
Medium Sand (0.2 to 0.63)	0 to 11.4
Coarse Sand (0.63 to 2.0)	0

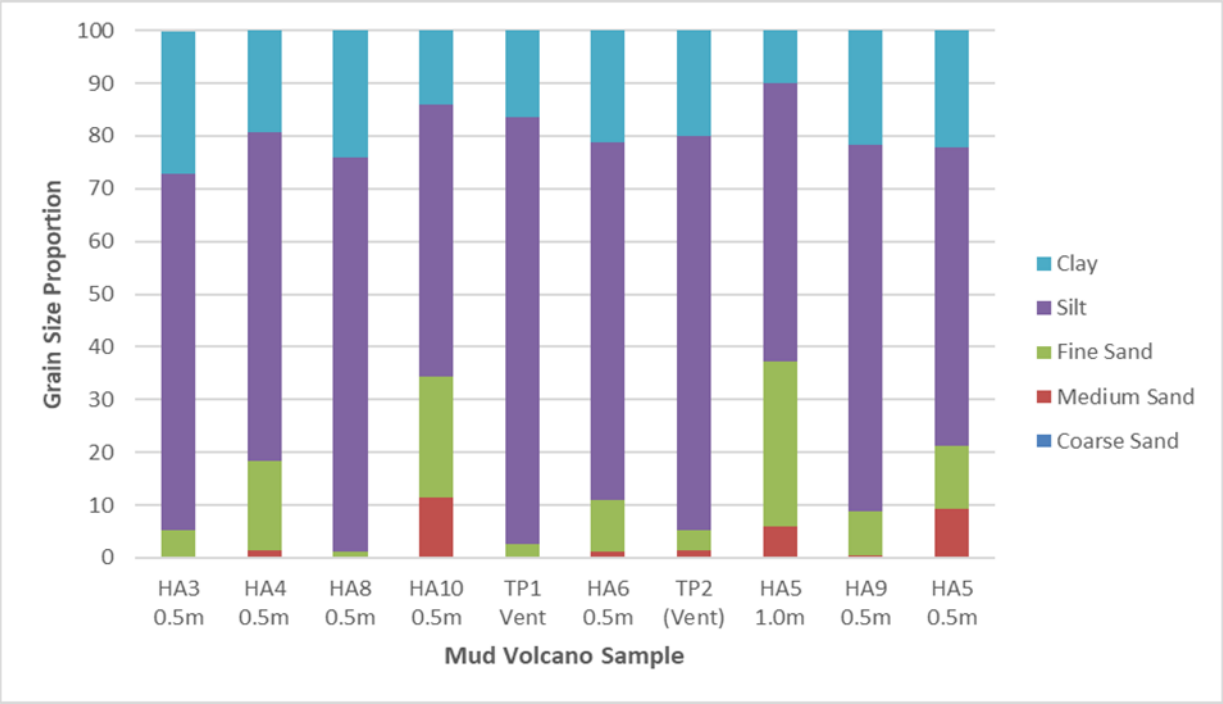

Figure 4.13: *Grain size proportion graph showing the grain sizes present in each sample at the mud volcano site. The samples here directly correlate to the particle-size distribution curves in Fig. 4.11.*

4.3.2 Atterberg Limits

The determined Atterberg limits and associated parameters for the mud volcano samples are presented in Table 4.4. The liquid and plastic limits derived for all samples were generally consistent, showing a range of 10.2% and 2.5% respectively.

Table 4.4*: Index properties of Mud Volcano samples.*

Sample	LL (%)	PL (%)	PI (%)	WC (%)	LI (%)	Clay Content (%)	Activity
TP1	56.0	22.8	33.2	82.4	178.1	16.5	2.1
TP2	57.7	24.1	33.6	77.7	157.9	19.9	1.9
HA3	65.7	24.3	41.4	54.4	72.4	27.20	1.9
HA4	55.1	25.3	29.8	56.6	105.1	19.3	1.9
HA8	63.2	24.0	39.2	48.2	62.3	24.0	1.9
HA10	55.5	24.0	31.5	51.9	89.4	14.2	2.0

4.3.2.1 Plasticity Index (PI)

The PI of the mud volcano samples ranges from 29.8% (HA4) to 41.4% (HA4). The Plasticity Chart developed by Casagrande (Das, 1985; Atkinson 2007) classifies the soils based on their PI and LL. The plasticity chart below (Fig 4.14), classifies all the tested samples to be highly plastic or "fat" clays as they all plot above the A-line which represents the difference between inorganic silts and inorganic clays (Das, 1985). This comes as no surprise as the PI is significantly influenced the presence of the smectite clay minerals. A general positive trend between increasing clay content and increasing PI is shown. There is no obvious spatial trend in the PI data, with results varying across the site.

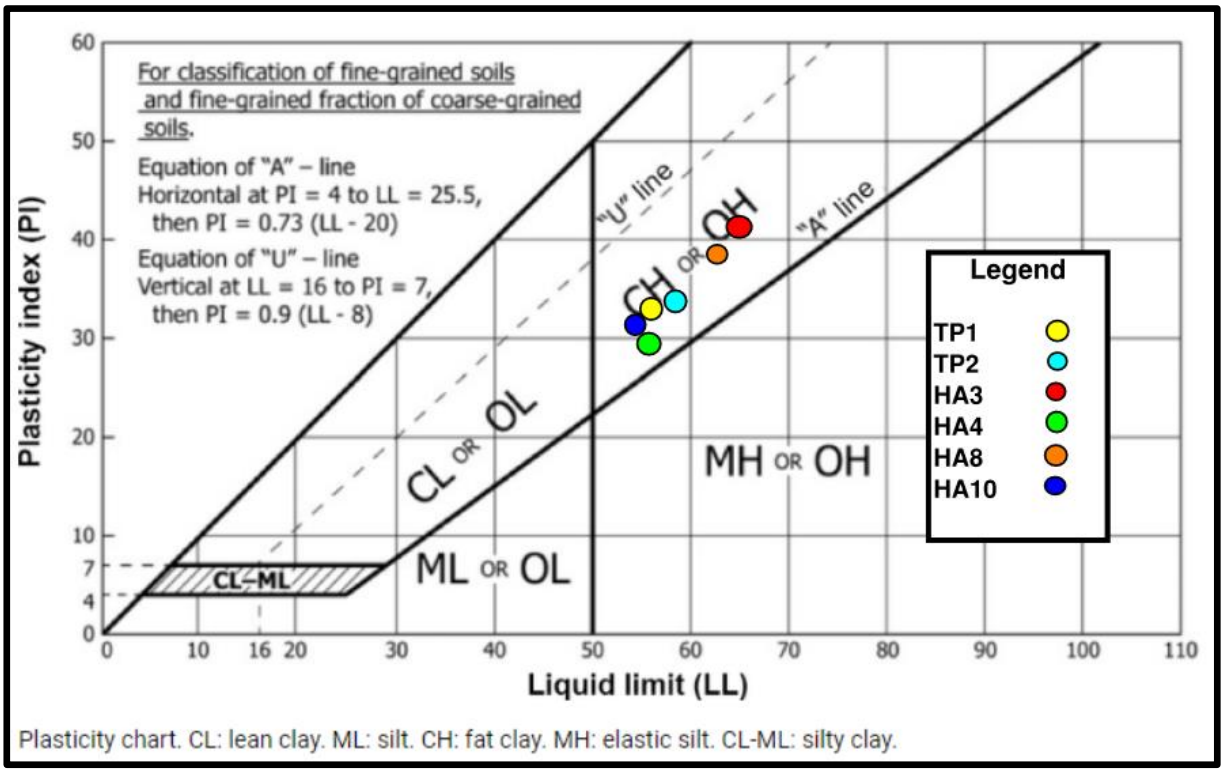

Figure 4.14: *Plasticity chart showing the relationship between the plasticity index and liquid limit. Points plotting below the "A" line have the characteristics of silt soils. Points plotting above the "A" line have the characteristics of clay soils (Modified from Atkinson, 2007).*

4.3.2.2 Liquidity Index (LI)

The LI values varied greatly across the site ranging from 62.3% (HA8) to 178.1% (TP1). There is a general trend shown that the samples taken from within the vent have a greater LI that the samples taken from surrounding the vent. This is attributed to the vent area being at the source of fluid which is continuously expelled from the mud volcano. This causes the mud within the

vent to contain a high-water content leading the material to behave as a liquid. The fluid expelled from the vent area is less likely to reach the outer flanks of the mud volcano where the LI values are lower leading the material to behave plasticly. Closer to the surface, the mud become brittle as moisture is removed due to evaporation. The properties of these materials were not assessed in their natural state though it is expected the LI values would be 0.0%.

4.3.2.3 Activity

The activity of the mud volcano samples ranges from 1.9 to 2.1 which are typical values of soils containing high quantities of smectite (Das 1985; Bell, 2006). These values are plotted on the Actvity Chart modified by Bell (2006) on Figure 4.15. These soils are measured to be active, with a high swelling potential due to their high-water holding capacity and high cation exchange capacity (Bell, 2006).

Similar active behaviour is expected to be shown within the parent material. Marine clays predominantly comprised of smectite typically have an activity of greater than 1 (Yassir, 1989). At depth, a highly active clay is likely to contain significant amounts of porewater, and due to the low permeability of the material, the porewater is unable to escape the sediment leading to the development of overpressure (Deville, 2009). As discussed in Chapter 1, this is a prerequisite factor of sediment remobilisation leading to mud volcano eruption. The activity results of the samples may suggest there is only minor assimilation of the mud matrix with the intrusive domain materials during its ascent to the surface.

4.3.3 Linear Shrinkage

The results of the linear shrinkage tests show the average to shrinkage to be 17% over the three vent samples. As the vent sample contains a linear shrinkage of greater than 15%, as well as a liquid limit of greater than 50%, it is classified as an expansive soil in accordance with NZS 3604:1999, Timber Framed Buildings.

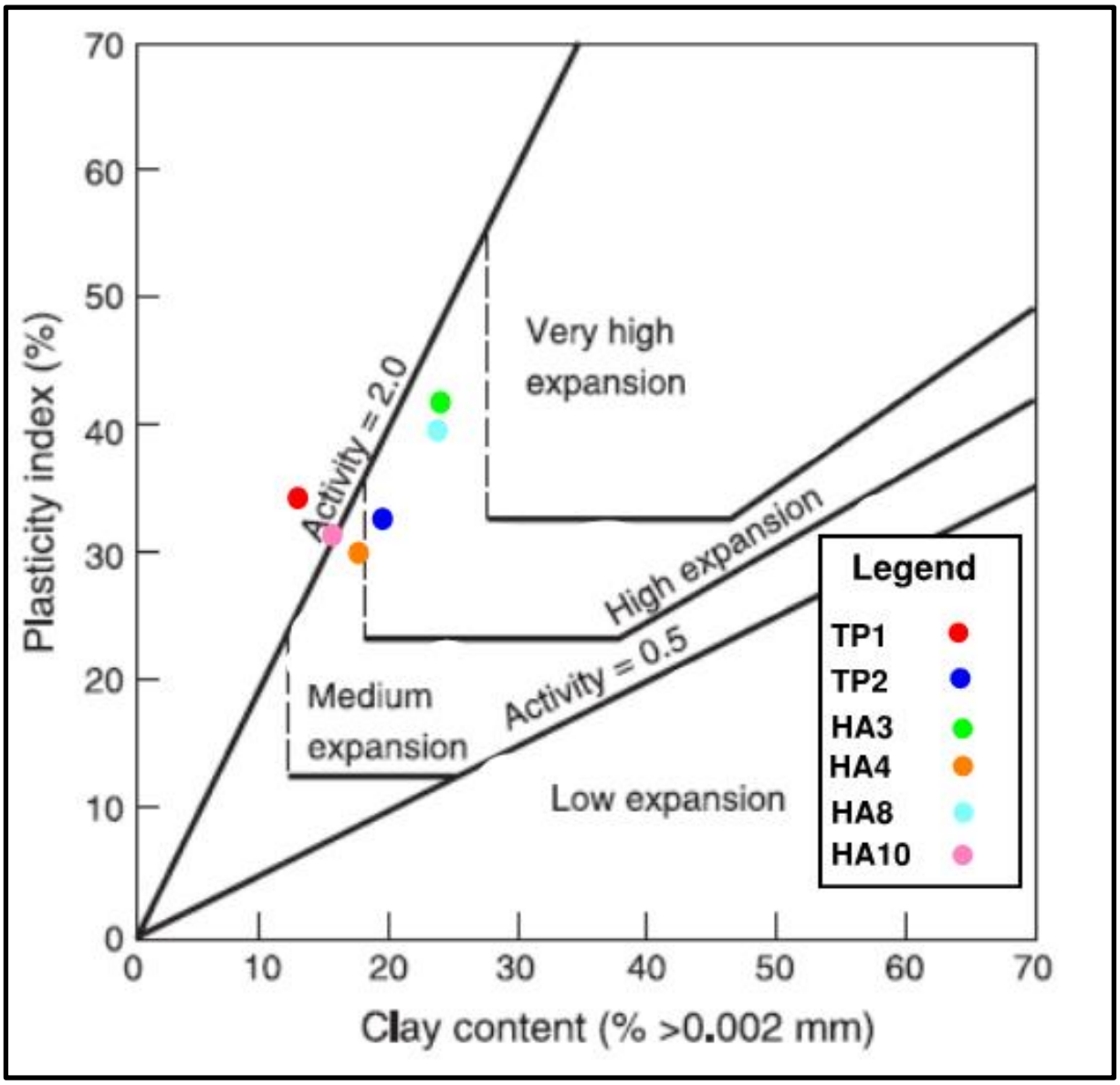

Figure 4.15: *Activity chart of common clay soils. Activity of tested mud volcano samples is shown on chart. Smectite activity line generally recorded between 1.0 and 7.0 (Bell, 2006).*

4.4 Geotechnical Properties

4.4.1 Ring Shear Tests

The results of the ring shear tests are presented in Figure 4.16. The strength parameters are determined by the relationship between the Shear Stress and the Normal Stress, defined by the following equation (Terzaghi, 1948):

$$\boldsymbol{\tau = c + \sigma tan\phi}$$

The cohesion (c') of the material is determined to be 0 kPa for both samples. Although the material contains significant proportions of silt and clay this is not a surprising result due to the predetermined unconsolidated nature of the material. The friction angle (Φ) of the material is determined to be 13.5˚ for TP1 and 11.3˚ for HA3. The likely reason for the friction angle of HA3 measuring lower than TP1 is due to the higher clay content within the sample. To give context to these determined parameter values, pure smectite clays have been measured to have residual friction angles between approximately 6˚ and 8˚ (Moore, 1991; Kopf et al., 1998; Kopf et al, 2005).

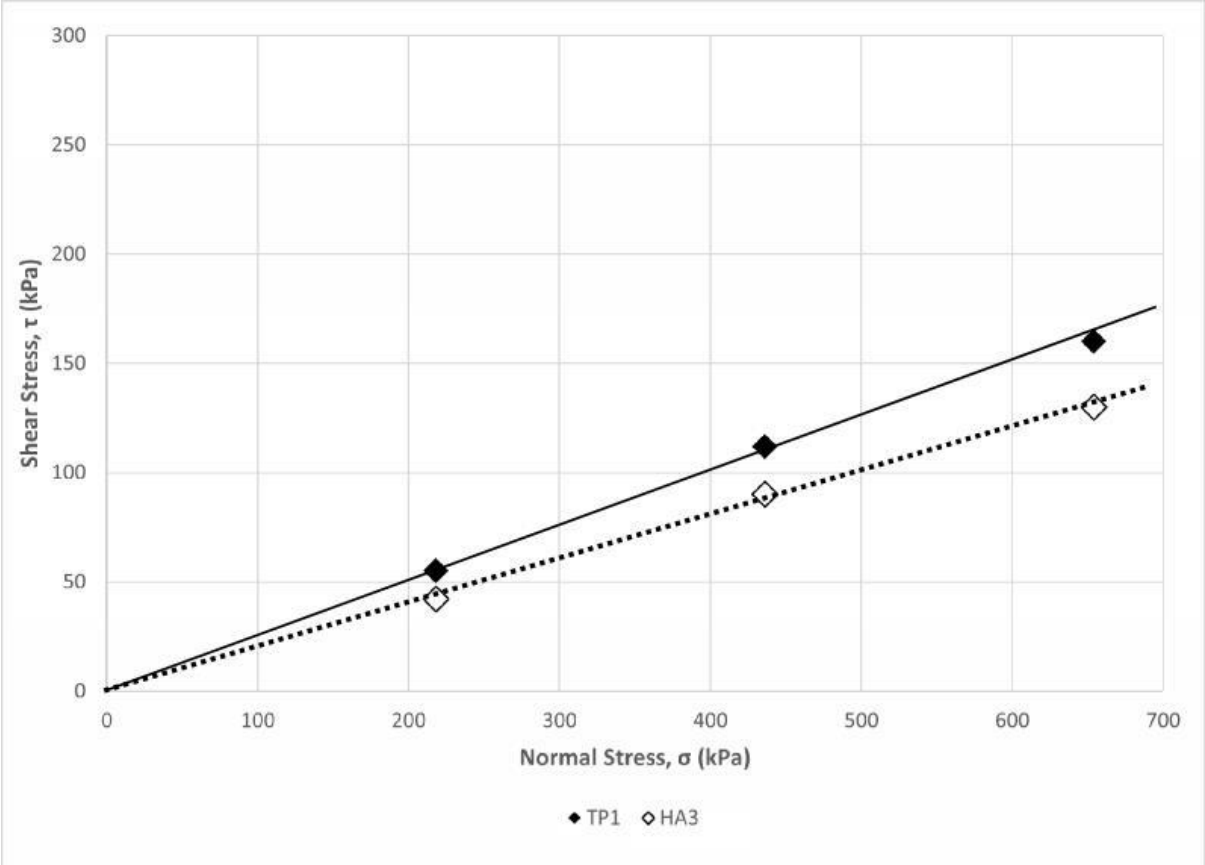

Figure 4.16: *Ring shear test results for mud volcano samples collected from TP1 and TP4.*

4.4.2 Crumb Test for Soil Dispersion

A grade is given to each of the samples (TP1 and HA8) based on the appearance of the water using the following criteria (Knodel, 1991):

- Grade 1 – No colloidal cloud develops. Even though the crumb may slake and spread away from the original crumb because of this slaking activity, no trace of a colloidal cloud is observed in the water.
- Grade 2 - A colloidal cloud is observable, but only immediately surrounding the original crumb. The has not spread any appreciable distance from the crumb.
- Grade 3 - A colloidal cloud emanates an appreciable distance from the crumb. However, the cloud does not cover the bottom the glass, and it does not meet on the opposite side of the glass bottom from the crumb.
- Grade 4 – The colloidal cloud spreads completely around the circumference of the glass. The cloud may not completely obscure the bottom of the glass, but the cloud does completely cover circumference of the glass. In extreme cases, the entire bottom of the glass is covered by the colloidal cloud.

Based on the criteria above, both samples are given a Grade 1 as there was no colloidal cloud developed (Fig 4.17). Both samples, however, did begin to slake almost instantly after being placed in the distilled water. This is clearly observed in the images taken one hour (centre) and twenty-four hours (right) below.

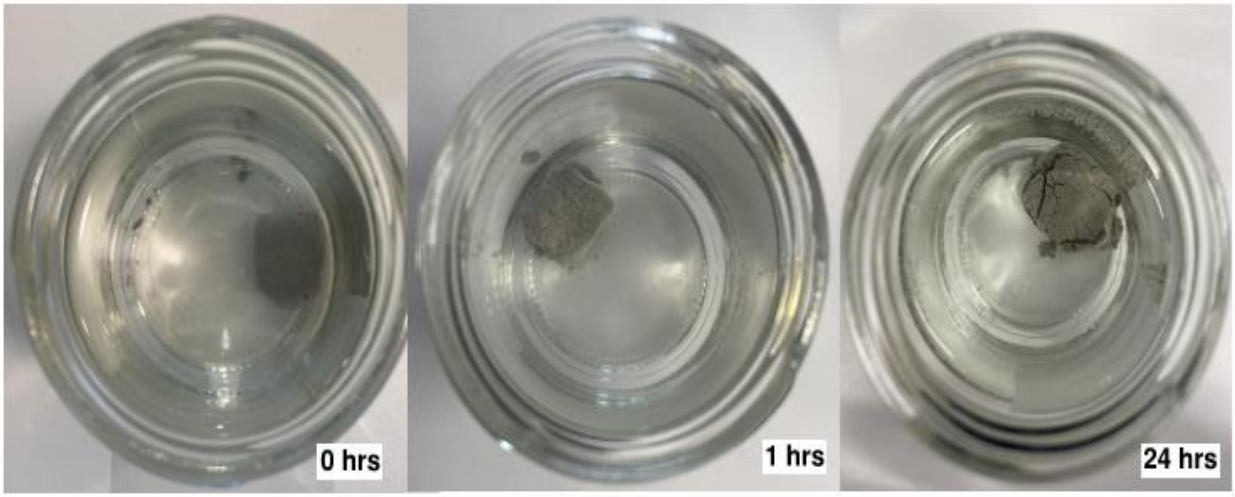

Figure 4.17*: *Crumb test performed on TP1 sample over 24 hours.

Applying the results to the flow chart shown in Figure 4.18, an Emerson class number is assigned to the soil sample, which can be used to confirm the type of clay minerals present. The Emerson class number given to tested samples (TP1 and HA8) is either Class 4 or Class 5. It is difficult to distinguish between these two classes as the presence of carbonates and gypsum is

unconfirmed. The present clay minerals based on these class numbers is therefore most likely Ca/Mg montmorillonite (smectite) and illite. These results are consistent with the index properties (Atterberg limits, activity) determined for the mud volcano material in this study, identifying highly active, swelling clays.

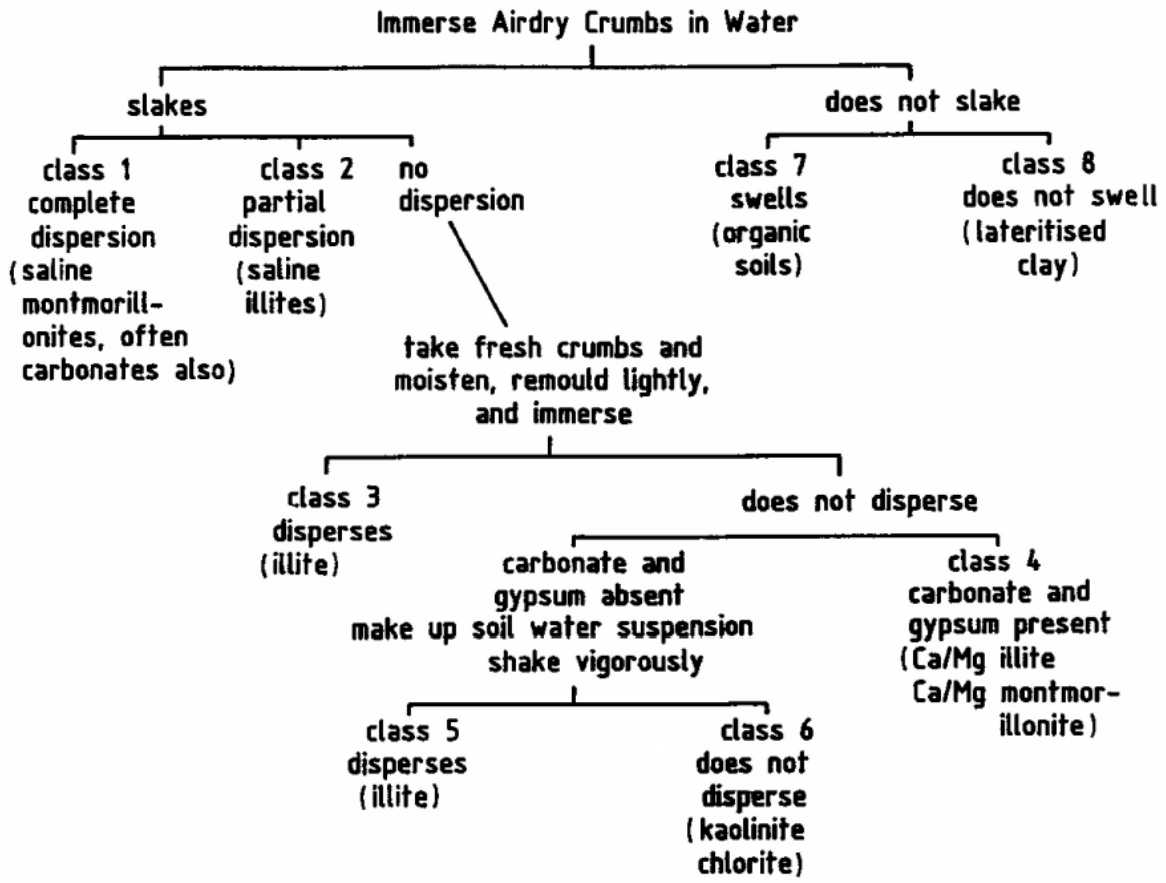

Figure 4.18: *Determination of the Emerson class number of a soil (Ingles and Metcalf, 1972)*

CHAPTER FIVE: DISCUSSION

5.1 Development of Mud Volcano

This study has used an engineering geological investigation to characterise the recently formed Waimata Valley mud volcano and the associated materials. The information gathered, as well as reference of the local and regional geological history, is used to help establish a model of the formation and subsequent development of the mud volcano. It is challenging to accurately infer the mechanisms occurring at depth without comprehensive subsurface and geochemical data, however, over the past few decades there have numerous overseas studies undertaken on the occurrence and development of various mud volcanoes, which are used to compare and contrast the occurrence of the recent Waimata Valley mud volcano as part of this study. The formation of the Waimata Valley mud volcano is broken into four different phases of development which includes: diapir initiation, formation of a mud reservoir, formation of mud volcano, and the re-establishment of reservoir equilibrium (Fig 5.1).

5.1.1 Diapir Initiation

It is commonly reported that the mud material associated with mud volcanism along the North Island's East Coast is derived from deeply buried, overpressured sediments accumulated at a passive-margin setting in the Paleogene (Ridd, 1970; Mazengarb, 1998; Mazengarb and Speden, 2000; Pettinga, 2003). Sediments of a similar geological period are also the predominant source of mud volcanoes from overseas examples (Kopf, 2002; Mazzini and Etiope, 2017). These sediments within the Tairawhiti region are typically part of the Mangatu Group and in particular the Wanstead Formation, typically comprising of smectic mudstones (Mazengarb and Speden, 2000). The investigation of the mud volcano materials at the Waimata Valley mud volcano showed its highly smetitic composition, which is reported similar to other mud volcanoes within the region (Ridd; 1970, Mazengarb and Speden, 2000; Pettinga, 2003).

Following the deposition of these clay-bearing sediments, tectonic activity reactivated along the Hikurangi Margin, and the passive-margin sediments were rapidly buried under a thick sequence of Miocene sediments (i.e. Tolaga Group) (Mazengarb, 1998; Mazengarb and Speden, 2000). The rapid burial of these passive-margin sediments is inferred to have created low-density sequences as the porewater was unable to escape from within its structure due to their

inherent low permeability, leading to gravitative instability within the strata. This causes the low-density layers to become buoyant in the surrounding units. It is widely recognised that this gravitative instability is a main driving engine in diapir initiation (Kopf, 2002; Deville, 2009; Mazzini and Etiope, 2017). These material properties were confirmed during the investigation of these materials.

Another contributing factor to the diapir initiation is the development of overpressure within these sediments formed by the trapped pore-water and a likely capping impermeable layer. The overpressure within diapirs is also likely to enhanced by volumetric expansion due to the generation of hydrocarbons from kerogens, or additional cracking of heavy hydrocarbons into lighter ones. Additionally, dehydrations reactions (i.e. illitization of clay minerals) is likely to contribute to the fluid overpressures (Mazzini and Etiope, 2017). The variable clay fraction observed in the Waimata valley mud volcano materials highlighted the likelihood of these reactions occurring. There is an obvious influence of hydrocarbons within the formation of the mud volcano indicated by the gas expelled at the surface during and following the eruption. Although the composition of this gas was not confirmed as part of this study, based on numerous other mud volcano studies, the gas is interpreted to be methane (Kopf, 2002; Deville, 2009; Mazzini and Etiope, 2017). The principle source of methane gas within the region is through to predominantly originate from the underlying formations of the Tinui Group which contain significant organic material (Lewis and Marshall, 1996; Mazengarb and Speden, 2000, Pettinga, 2003; Barnes et al, 2010). Another source of the methane may also be derived from the fault networks themselves due to the evolution of organic material (Maison et al, 2018). The buoyant, overpressured sediments cause hydrofracturing of the overlying impermeable layers allowing for migration of the sediments toward the surface along structural highs and fault networks (Deville, 2009; Mazzini and Etiope, 2017).

The formation of the major fault networks along the Raukumara Peninsula is considered to have formed as the Neogene strata partially detached and slid along a decollement surface in a SE direction under the influence of gravity in response to late-Miocene uplift and seaward tilting of the forearc. During the process of sliding, the major anticline and synclines along the Raukumara Peninsula would have formed (i.e. Waimata syncline). The sliding Neogene block has broken into smaller parts are normal faults (i.e. Arakihi Fault) that have propagated through the sequence connecting with the decollement surface (Mazengarb, 1997; Barnes et al., 2010;

Scherwath et al, 2010). The formation of these faults and structural highs (anticline axis) allows for permeable pathway overpressured sediments leading to the upwelling of the sediments and the formation of diapirs from the source layer.

The diapir continues to develop, migrating toward the surface along the present fault zones. The process is accelerated and sustained to the shallow depth of the earth (<100m), as the diapir meets pressurised fluids in reservoirs and fractures, contributing to an increasing overpressure. During the ascent of the diapir, hydrofracturing leads to the brecciation of the surrounding units (Kopf, 2002; Deville, 2009; Mazzini and Etiope, 2017). This brecciation is observed in the lithological variation of the clasts expelled at the surface of the Waimata Valley mud volcano. By surface sampling, it was clear there was a large range of lithologies native to various formations. This also reinforces the notion that the mud has likely migrated a large distance during its ascent.

5.1.2 Formation of Mud Reservoir at Shallow Depth

It is undetermined how far the rising diapir ascends toward the surface and further investigation is required to confirm these details. It is considered likely that as the rising diapir approaches the surface, an additional fracture network is established at the crest of the anticlinal structure, forming alternative pathways for fluids to escape to the surface (Rait, 1992; Mazengarb, 1998; Deville, 2003; Dupuis et al, 2019). These fractures manifest at the surface as a series of faults, observed within the Waimata Valley, propagating from the Waimata Fault through the recent and Arakihi Road mud volcano sites. The escape of these fluids causes an equilibrium within the diapir and surrounding sediments to be reached, slowing, or completely stopping its ascent leading to the formation of a mud reservoir at a shallow depth. The mud reservoir continues to be recharged from the fluid sources at depth, whilst at the top of the reservoir, fluids continue to escape at the surface (Deville, 2003; Pettinga, 2003). The mud reservoir therefore remains in a semi-fluid state and the lack of overburden pressure assures the mud remains under-consolidated. The consistency of the material observed at the surface immediately following the eruption of the recent mud volcano is interpreted to be similar to that of the mud reservoir.

The escaping fluids is observed at the surface as numerous permanent seeps, leading to the formation of a low-lying saline marsh-like area, such as the Arakihi Road mud volcano field in the Waimata Valley.

It is considered likely that the mud reservoir may migrate laterally within the subsurface forming sills as the mud diverges from the chamber (Deville, 2003). Often the formation of these sills may cause inflation of the overlying sediments manifesting as uplift at the surface (Niu et al., 2019).

5.1.3 Mud Volcano Formation

Due to their presence along the same fault network, and observations of their recent concordant activity, the recent Waimata Valley mud volcano eruption is interpreted to be part of the same subsurface architecture as the Arakihi Road mud volcanoes. The results of the ICP-MS analysis also suggest that the materials extruded at each site are of very similar elemental composition and therefore likely to be from the same reservoir. Prior to the recent eruption, an equilibrium between the mud reservoir and the discharging/recharging fluids had been established, however, the large extrusion of mud on 18 December 2018 is evidence on how the equilibrium can become de-established.

During the Te Araroa earthquake, uplift occurred at the site, forming alternative subsurface conduits, as well as likely changing the pressures with the mud reservoir ultimately disrupting its equilibrium. This did not result in an immediate expulsion of the migrating mud, rather it formed a shallow pocket where gas and fluidised mud became trapped. Eventually, the pressure formed by the fluids became sufficient to remove the clay plug within the fault-zone and cause an eruption at the surface. From the aerial mapping and subsurface investigations, it is estimated 11,200 m^3 of the fluidised mud had expelled at the surface, likely significantly reducing the size of the mud reservoir.

Based on the documented timing of the eruption, it is interpreted that most of the mud volcano was formed by a single eruptive event. Due to the relatively flat topography of the surrounding land, several mud flows formed simultaneously during the eruption and propagated radially from the vent. This ultimately formed the sub-circular pie-shaped edifice, though, a couple

mudflows have extended further than the average circumference of the feature as they concentrated in topographical depression formed by stream channels. The morphology of the feature differs to the Arakihi Road mud volcanoes. This shows that the behaviour of mud volcanoes can differ even if though there arise from the same source.

5.1.4 Re-establishment of Reservoir Equilibrium and Future Activity (?)

Following the recent eruption of the Waimata Valley Mud Volcano it is likely that the shallow mud reservoir has been significantly depleted and the overpressure has been reduced. Due to the depletion of the reservoir, subsidence often manifests at the surface following mud volcano eruptions as cavities in the subsurface are formed (Dupuis et al, 2019; Odonne et al, 2020). There has been no evidence of reservoir collapse at the Waimata Valley site following the eruption though this may take time to manifest. GPS monitoring of the ground surface may be useful in determining ground subsidence following mud volcano formation.

The presence of permanent gas seeps in the Waimata Valley, as well as the numerous other seeps in the eastern North Island, indicates that the reservoirs are semi-closed systems, with most leakage being accommodated by more permeable zones or conduits (Kopf, 2002; Pettinga, 2003; Mazzini and Etiope, 2017). In the case of the recent eruption, the conduit is formed along the NW-SE trending cross fault formed at the edge of the rising diapiric core of Neogene sediments. The increased activity of the permanent gas seeps at the neighbouring Arakihi Road mud volcanoes prior to the eruption is indicative of these fluid migration paths trying to relieve the critical state pressures in the gas/fluid reservoir. Two years following the recent eruption, a permanent gas seep at the site appears to have been established as activity continues, and activity at Arakihi Road has reduced to a normal level. Throughout the Tairawhiti region, several mud volcanoes have re-erupted after significant quiescent periods. Given the continued activity of the recent mud volcano site, as well as the neighbouring Arakihi Road mud volcano, future eruptive events should not be discounted.

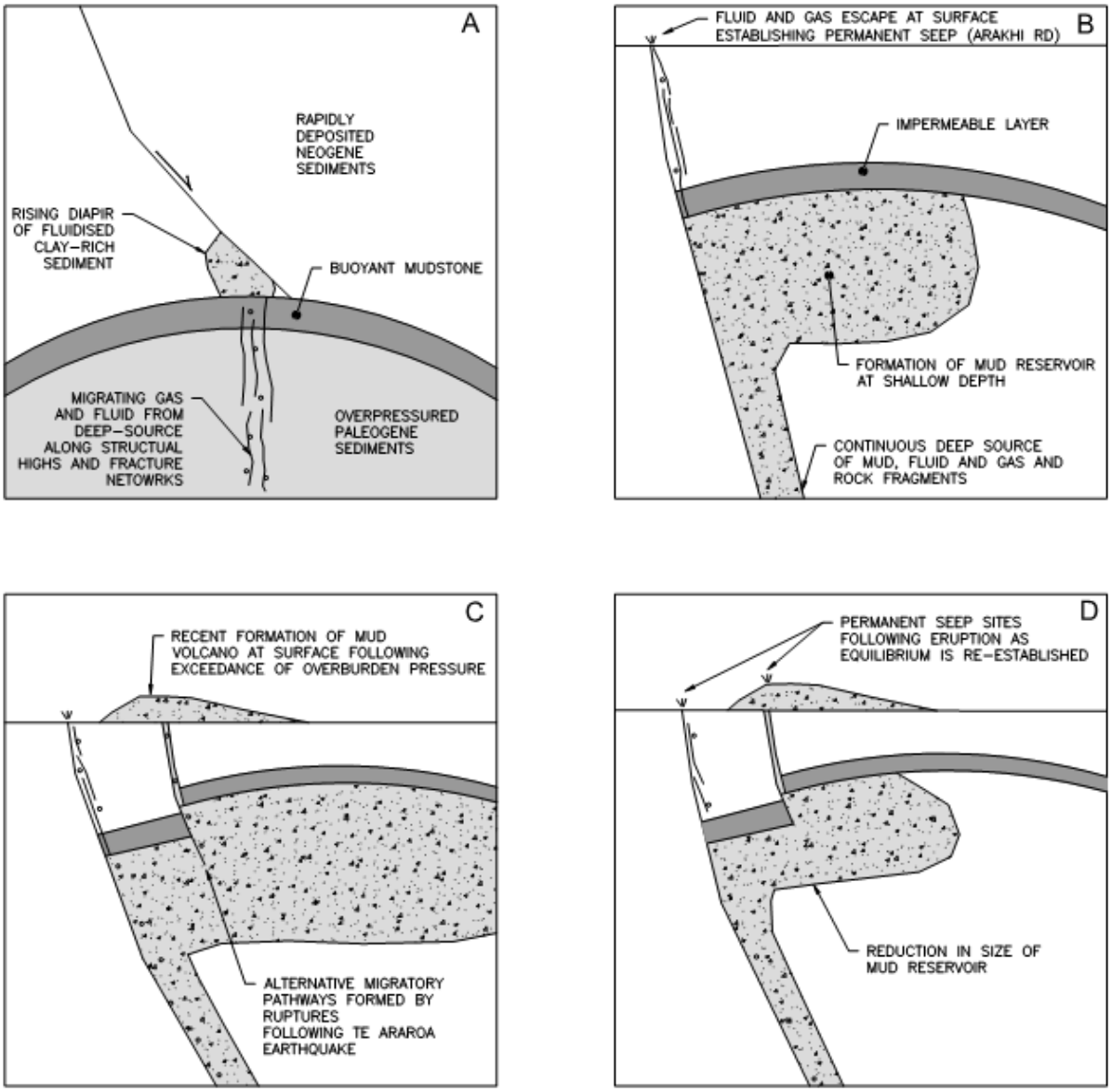

Figure 5.1: *Schematic diagram of recent Waimata Valley mud volcano eruption as described in Sections 5.1.1 to 5.1.4. A – Diapir Initiation, B – Formation of Mud Reservoir at Shallow Depth, C – Mud Volcano Formation, D – Re-establishment of Reservoir Equilibrium and Future Activity. Diagrams not to scale.*

5.2 Comparison to Pettinga (2003) Model

Prior to this study, the documentation of the mud volcano eruption at the Brookby gas seep, Hawkes Bay (Pettinga, 2003), was the most recent and comprehensive study of a mud volcano eruption within the East Coast Basin of New Zealand's North Island. Based on his study, Pettinga (2003) developed a model for the formation of the mud volcano (Fig 5.2).

The similarities of the geological settings allow for comparisons of the eruptive event documented by Pettinga (2003), to the recent Waimata Valley eruption. An understanding of

these events may also be able to be applied to other/future eruptions within the region. Whilst the Pettinga (2003) interpretation was formulated based on visual observations, this study had the benefit of various site investigative and laboratory techniques, particularly regarding the erupted materials' properties to help devise a new model for the recent Waimata Valley mud volcano (Fig 5.1).

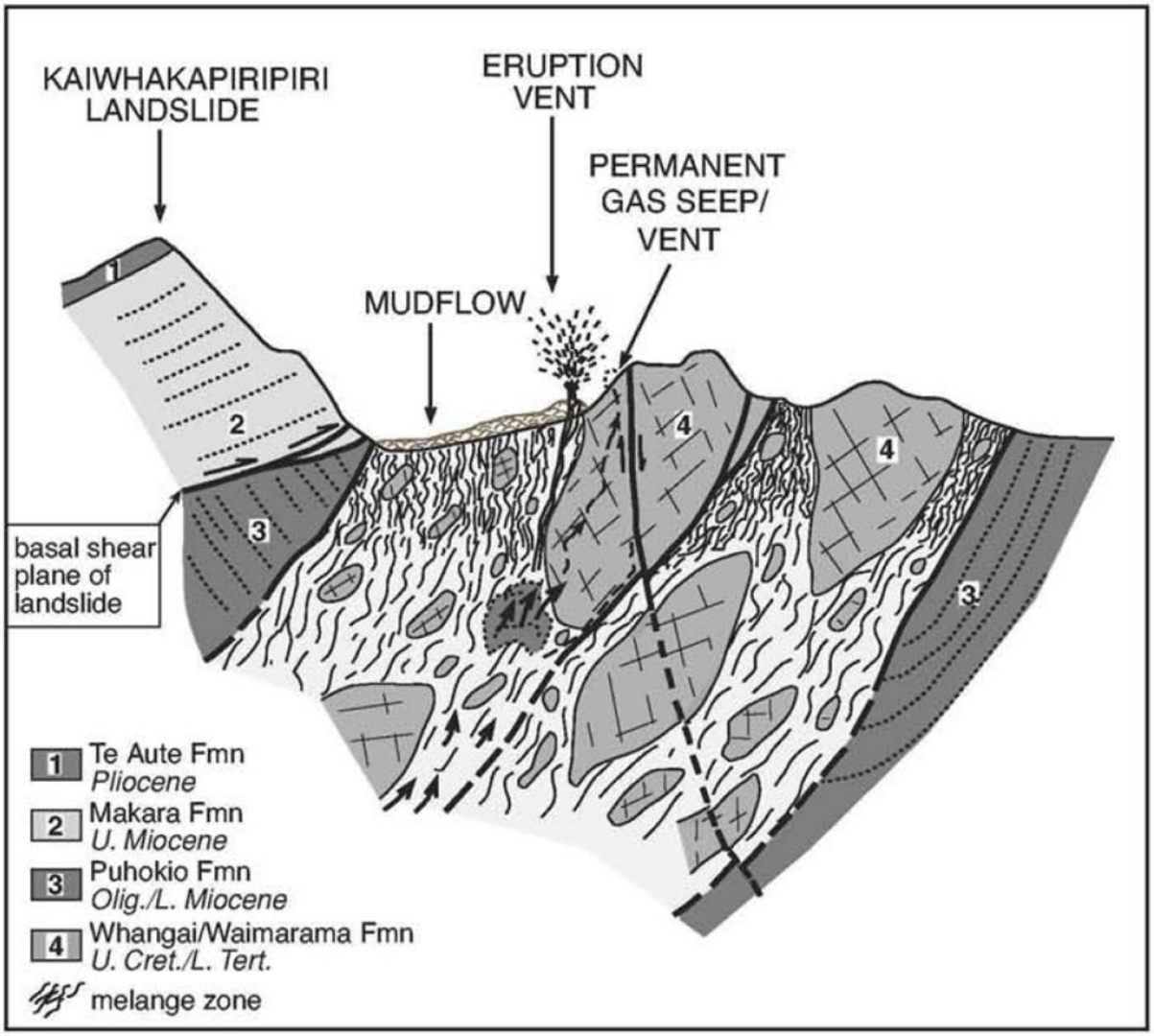

Figure 5.2: *Diagrammatic cross-section of the geological setting and controls on the eruption mechanism for the Brookby gas seep and 1994 mud volcano eruption (Pettinga, 2003).*

5.2.1 Similarities with Pettinga (2003) Model

Pettinga (2003) associated the eruption with significant fluid movement within scaly fabric dominated fault zones along the accretionary margin of the North Island's east coast. The eruption is interpreted to have been formed by a mobilised mud with extremely high fluid content, triggered by the rapid venting of fluids. The fluids comprising of mainly methane gas

accumulated in a pocket at shallow depth and depressurise episodically by rapid venting. The extruded mud mainly comprised of highly cohesive plastic clay that had plugged the fault conduit. Following the expulsion of the clayey mud, a dome began to form at the surface, which was then followed by gas venting and a mud blast. The mud component of the blast is interpreted to largely represent the fluidised clay from within the shallow gas pocket and the residual clay within the conduit following the removal of the plug. Other mud and exotic rocks were also assimilated from the conduit walls during the blast as the gas reached the surface.

Based on these observations, it is inferred that the materials are similar to those of the Waimata Valley mud volcano eruption. Laboratory testing confirmed the highly plastic nature of the material, and field sampling highlighted the significant mixing that has occurred during the muds ascent along the fault system by the large variance in the lithologies of the clasts within the extruded mud.

Further geochemical and geophysical testing is required to confirm the size depth the fluid reservoir and mud chamber at the Waimata Valley site, however, similarly to the Brookby Farm site, it is inferred to be accumulating at a shallow depth (<100m), and an establishment of critical pressures within the reservoir led to the extrusion of the mud material.

Another similarity of the events is the presence of a neighbouring permanent seep that showed increased activity prior to the mud extrusion, highlighting the semi-closed reservoir system. Following both eruptions, the neighbouring seep, as well as the eruptions sites, showed a reduction in activity to normal levels.

5.2.2 Contrasts with Pettinga (2003) model

The Brookby Farm mud volcano and surrounding permanent gas seeps occur within an area characterised by complex deformation. These deformation styles include tight recumbent and isoclinal folding, and reverse and/or thrust faulting (Pettinga, 2003). The thrust faulting is often accompanied by narrow zones of tectonic melange comprising of fragments and blocks of Whangai and Mangatu lithofacies within a sheared, smetitic clay matrix (Mazengarb and Speden, 2000; Pettinga, 2003). The permanent gas seep at the site occurs within a large floater block within the melange zone, whilst the mud which formed the eruption and mud flow

migrated upward along the contact between the floater block and the surrounding melange. The source of fluids for both the permanent seep and mud eruption is inferred to have migrated along a thrust fault containing scaly clay fabric (Pettinga, 2003).

In comparison, the conduit of the recent Waimata Valley eruption is formed by fault systems associated with a rising diapiric core of overpressured Neogene sediments, rather than tectonic melange formed by thrust faulting. Whilst there was a clear influence of seismic activity on the fluid reservoir and conduit system at the Waimata Valley site, there was no such association at the Brookby Farm.

Also, in contrast to the Brookby Farm eruption, there was no evidence of explosive activity across the mud volcano. Pettinga reported impact craters and pock marks on the surface of the mud flows, as well as rock fragments lying outside of the mud volcano edifice. These craters are formed by the impact of rock fragments on the soft mud (Dimitrov, 2002; Odonne et al, 2020). This explosively activity was reportedly preceded by the formation of a mud dome whereas at the Waimata Valley mud volcano, there was no evidence of these features suggesting a more effusive style eruption. This contrast in explosive activity may be explained by the difference in properties of the mud reservoir materials allowing for a larger overpressure within the mud to be established.

5.3 Geotechnical Aspects

Based on the laboratory tests undertaken, the mud materials are highly plastic with high natural water contents ranging from 48.2% to 82.4%. If subjected to additional loading, it is very likely that these under consolidated materials would result is significant amounts of settlement. This has been widely experienced at other mud volcano sites around the world. For example, at the Lusi mud volcano in East Java, up to 3m of settlement has been experienced across the expelled mud materials, even as far away as 1.5km from the vent (Rahardjo, 2015). Mud volcanoes also commonly experience large ground deformations following an eruption resulting from the collapse of the mud chamber area as the materials are removed and expelled at the surface. This would also likely manifest as large deformations at the surface (Deville, 2009; Roberts, 2011; Dupuis et al., 2019; Odonne et al., 2020).

The measured strength properties of the material (S_u and ϕ_r) are very low, therefore, a very low bearing capacity of the soil is expected. This would mean that the mud is an unsuitable founding material for any buildings and structures. The unsuitability of the mud is also substantiated by the expansive properties of the material. This was validated by the laboratory tests such as the Atterberg limits and linear shrinkage tests. The mud material would not pass as 'good ground' based on the New Zealand Standard NZS 3604:2011 Timber-framed buildings. Although it is unlikely that the subject site will be developed in the future, as previously highlighted materials associated with mud volcanoes is remarkably similar in New Zealand and around the world (Kopf, 2002; Mazzini and Etiope, 2017). The behaviours of the material shown at the subject site can therefore be reasonably applied to other sites where development is proposed, such as Wheatstone Road on the fringes of Gisborne city.

The presence of gas is also known to degrade the geotechnical properties of the material. The degradation can perturb the foundations and may induce landslides (Etiope, 2015). Small amounts of gas bubbles within the material, as well as gas dissolved in porewater, affect the response to loading and unloading, rendering the soil compressible, and enhancing local shearing and pore pressure build-up (Sobkowicz and Morgenstern, 1984; Etiope, 2015). This effect also increases the potential for flow or cyclic liquefaction (Etiope, 2015). Even though the solid fraction being emitted from a mud volcano may be intermittent, gas seeps often remain permanent contributing to the degradation of the materials such as at Arakihi Road, Brookby Farm, and Wheatstone Road (Ridd, 1970; Pettinga, 2003; Speden, 2004). Two years after the recent eruption in the Waimata Valley, gas continues to be emitted from the mud volcano and is likely to remain permanent as highlighted in Section 5.1 and 5.2.

The measured properties of the mud material are also interpreted to have an important influence on the mud volcano formation. Based on the grain-size distributions of the materials, and the presence of highly active clays, the mud is inferred to have a very low permeability. This low permeability, as well as the low strength of the material, have two important geological implications leading to mud mobilisation at depth, and its subsequent extrusion at the surface. Firstly, these properties allow pore pressures to build at depth, especially within fault zones and mud reservoirs (Yassir, 1989, Kopf et al., 2005; Tanikawa et al., 2010). Fault movement is facilitated by the low intrinsic strength and reduced effective stress of the material in fault zones, whilst the low viscosity and high internal pressure promotes mud mobilisation (Kopf et

al., 1998; Kopf et al., 2005). The low permeabilities of the mud, together with the grain-size variation, are also considered to have a secondary effect on the periodicity in mud volcano activity resulting from the blocking of the conduits allowing for the accumulation of fluids within the mud chamber (Kopf, 1998; Tanikawa et al., 2010).

Seismic activity is likely to cause stress state perturbations along fault zones and within mud reservoirs, which in turn may induced excess pore pressure transients in the low permeable sediments leading to mud ascent and extrusion (Yassir, 1989; Kopf et al., 2005; Manga et al., 2009). In the case of the Waimata Valley mud volcano, the Te Araroa earthquake that preceded the eruption is likely to have altered the stress state within the mud reservoir and along the present fault systems.

5.4 Hazards

Geohazards are geological situations and or/features that can present critical conditions resulting in damage or risk. The recent Waimata Valley mud volcano represents geohazards for the possibility of future eruptions, as well as the behaviour of the erupted sediments exposed at the surface. These geohazards are discussed in the following sections with reference to other mud volcanoes within New Zealand and around the world. An understanding of the geohazards posed by mud volcanoes and the associated risks is essential for future planning and risk management within the region.

5.4.1 Eruption Hazards

Although it is inferred that the eruption of the Waimata Valley mud volcano was more effusive in style, several accounts of explosive eruptions have been documented in New Zealand and worldwide (Ridd, 1970; Kopf, 2002, Pettinga, 2003; Deville, 2009; Mazzini and Etiope, 2017). The nearby Mangaehu Stream mud volcano has been documented on multiple occasions to have erupted explosively throwing boulder-sized rocks tens- to hundreds of metres from the vent (Ridd, 1970). Such activity would be extremely hazardous for humans, wildlife, and infrastructure, particularly for mud volcanoes near developed areas such as Wheatstone Road on the fringes of Gisborne. As highlighted in the previous section (Section 5.2), future explosive activity at the subject or neighbouring Arakihi Road roads should not be discounted. Even

though the mud volcano is rural, an explosive eruption would present risk to traffic along the adjacent Waitemata Valley Road and the farm dwellings.

Explosive eruptions have also been known to produce fire from the emitted self-igniting methane (Etiope, 2015, Mazzini and Etiope, 2017). This is thought to be related to the high velocity of gas that may reach supersonic speed and thus self-combust causing a fiery eruption. Such eruptions have been documented around the world. In 2014 an explosive eruption of the Macalube Mud Volcano in Sicily caused the death of two children aged 7 and 9 (Mazzini and Etiope, 2017; Sciarra et al., 2019).

The most significant hazard produced by the Waimata Valley mud volcano was the formation of mud flows during the eruption. Even on relatively flat land these flows extended further than 100m from the vent completely covering anything in its path.

5.4.2 Geotechnical Hazards

As the activity of a mud volcano reduces, there are still several hazards that can arise. At the Waimata Valley site the mud volcano is up to 3m deep in some areas. The mud material, particularly surrounding the vent, behaves like quicksand and can be a lethal trap. As previously highlighted in Section 2.2, this was observed only hours after the eruption as curious stock became stuck in the mud and had to be rescued. Following the eruption, the mud volcano attracted media attention which raised the curiosity of the public and attracted many visitors. Even though the mud volcano is on private land, it easily visible and accessible from the public Waimata Valley Road. Many of the visitors were at risk of becoming trapped within the feature. Appropriate mitigation measures were implemented in the weeks following by forming a new boundary fence, adding padlocks to the gates, posting signage, and removing stock from the paddock. Such measures should be considered for all mud volcano features.

The laboratory testing undertaken showed the material to be of very low strength ($\phi_r = 13^\circ$) meaning it is vulnerable to remobilising, even on gentle slopes. An infinite slope analysis for the fully saturated mud material shows that minimum slope angle of only 6˚ is required for a Factor of Safety (FoS) of less than 1.0, meaning the slope will fail ultimately leading to remobilisation of the mud (Appendix C). Geomorphic assessments at the site showed evidence

of remobilisation of some of the mud flows at the steeper slopes at the western edge though it could not travel far due to topographical constraints. A remobilised mud creates an inundation hazard for anything downslope of the feature. The remobilised mud or mud flows also have the potential to block stream/river channels forming a dam. This was observed at the subject site where one mud flow following the eruption blocked a flowing stream which led to the formation of a new lake. The blocked stream has a low flow capacity therefore a breach of the dam is less hazardous, however, this is not the case for many other mud volcanoes. Mud flows formed by the Mangaehu and Hangaroa mud volcanoes formed dams within streams/rivers of significant flows and resulted in large flooding events once they had breached (Ridd, 1970). A remobilised mud flow at the Brookby Farm also resulted in the damming of a stream channel (Pettinga, 2003).

5.4.3 Ecological Hazards

The Waimata River drains the hill-country catchment north of Gisborne city, with the river joining the Turanganui River in the Gisborne CBD before discharging into the Poverty Bay. Due to the highly erodible and unstable formations within the catchment, the river is characterised by a high sediment influx (Kettner et al., 2007; Marden et al., 2008; Cater et al., 2010). The material emitted from mud volcanoes is highly unstable and erodible, therefore, there is the potential for these features to contribute to the already high sediment volumes within the Waimata River. Directly below the site is the dried stream channel which flows into Waimata River. During high rainfall events it is very likely that surface runoff will carry the mud volcano material into stream and eventually the Waimata River.

Mud volcanos are also commonly associated with oil seeps (Kopf, 2002; Mazzini and Etiope, 2017). The emitted oil comprises polycyclic aromatic hydrocarbons which are highly toxic to humans and the environment (Starodub, 2005) and may induce hypoxia within waterways reducing its biodiversity (Etiope, 2015; Abbasov and Baloglanov, 2018).

A famous global case of the negative environmental effects of mud volcanoes is the Lusi eruption in East Java, Indonesia. The erupted first initiated in 2006 and continues to emit mud today. At its peak the mud volcano emitted up to 180,000 cubic metres of material a day (Mazzini et al., 2007; Istadi, 2009; Jennerjahn, 2013). The emitted mud from the mud volcano

is channelled into the Porong River which is affected by intensive land use and hydrological alterations in a densely populated catchment (Jennerjahn et al., 2013). The mud volcano has more than doubled the suspended matter and particulate organic carbon load of the river (Istadi, 2009; Jannerjahn, 2013). The decomposition of this organic matter is contributing to oxygen depletion in the river and adjacent coastal waters, severely affecting the well-being of aquatic environments (Mazzini et al., 2007; Istadi, 2009; Jennerjahn, 2013). The mud volcano is a prime example of the potential adverse effects on the ecology and biogeochemistry of aquatic systems that can arise.

5.4.4 Greenhouse Gas Emissions

Mud volcanoes are one of the five categories (including gas-oil seeps, microseepage, submarine seepage and geothermal-volcanic manifestations) of geological sources of methane that are currently considered a major contributor of atmospheric methane volumes (Kopf, 2002; Mazzini and Etiope, 2017). The emission from geological sources account for approximately 10% of total methane emissions from anthropogenic and natural sources (Mazzini and Etiope, 2017). The Waimata Valley mud volcano is likely to continue to emit gas for many years to come.

5.5 Precursors and Evacuation

As mud volcano eruptions are often paroxysmal and commonly occur in remote areas, it is difficult to determine the precursory signals to an eruption. Fortuitously, due to the uplift activity at the Waimata Valley site following the Te Araroa earthquake, the site had been closely monitored leading up to the event, though there had been no visual sighting of the eruption occurring. The following section highlights the precursors that were observed leading up to the eruption at the subject site, as well as other common precursors to mud volcano eruptions from other New Zealand and overseas examples. These typically include seismic activity, gas venting and geomorphic changes.

5.5.1 Seismicity

It is widely accepted that gas migration, seepages, and mud volcano eruptions can be triggered by earthquakes, and may act as a precursor for eruptive events. This occurs by the passage of

seismic waves or by co-post-seismic changes in crustal stress and permeability (Kopf, 2002; Bonini, 2009; Manga et al., 2009; Mazzini and Etiope, 2017). Seismicity also induces liquefaction of weak sediments, affecting fluidisation and loss of strength, as well as fracture opening, all of which are important controls in mud volcano genesis (Kopf, 2002; Bonini, 2009; Mazzini and Etiope, 2017). Many mud volcanoes in New Zealand and around the world have been associated with earthquakes. In New Zealand two mud volcanoes have been documented to have erupted following the Hawkes Bay earthquake in 1931. This included the Hangaroa mud volcano which occurred immediately following the earthquake (Ridd, 1970; Mazengarb, 1997), as well as the Sponge Bay mud volcano which uplifted the shore platform by 2.1m occurring two weeks after the same earthquake. Although being one of the most extensively studied mud volcanoes in the world, the trigger of the Lusi volcano is still debated. One of the commonly hypotheses accepted hypotheses is that strike-slip faulting caused the release of overpressured fluids through already present diapiric structures (Mazzini et al., 2007).

As previously highlighted in this study (Section 2), the Waimata Valley mud volcano eruption occurred at a site where there were significant surface deformations and uplift that had occurred following the Te Araroa earthquake two years prior. Other mud volcanoes in the Waimata Valley including at Arakihi Road and Mangaehu Stream, as well as the Hangaroa River further south, were also reported to exhibit increased activity following the same earthquake event. Many other mud volcanoes in the region remained quiescent following the earthquake which potentially highlights the variable circumstances in which these mud volcanoes form, and how many may be interconnected within the subsurface. In the case of the Waimata Valley mud volcano, it is obvious that the Te Araroa earthquake has had an influence in its occurrence, effecting the pressure balance within the mud reservoir and forming an alternative pathway for the fluidised mud to migrate to the surface. There were no major earthquakes recorded in the months leading up to the eruption occurring.

5.5.2 Gas Venting

At sites where a permanent gas seep has been established, increased activity by way of rapid gas venting is generally demonstrated at a mud volcano site prior to an eruption (Pettinga, 2003; Mazzini and Etiope, 2017), though it does not necessarily indicate that an eruption is going to occur. It is accepted that the increased activity is a result of the permanent fluid migration paths

attempting to relieve critical state pressures in the mud chamber. Essentially, the increased gas venting is the difference between the fluids migrating into the reservoir, relative to the fluids migrating out (Pettinga, 2003). Prior to the Waimata Valley eruption, there had been no prior gas venting as the permanent seep had not been established. Rather, gas from what is interpreted to be a similar source, escaped at the Arakihi Road mud volcano field. Two years after the recent eruption, the gas continues to bubble to the surface at both mud volcano sites.

5.5.3 Geomorphic Changes

The raised dome feature formed prior to the eruption at the Waimata Valley mud volcano site was clear evidence of an upwelling body at a shallow depth. This feature was also suggested by the GPR surveys undertaken across the site following the eruption. The upwelling body caused surface deformations in an arcuate shape. Reports from overseas mud volcano eruptions also commonly report ground deformations occurring anywhere from hours to months before the event (Mazzini et al., 2007; Madonia et al., 2011). Hours before a mud volcano eruption in Sicily on 11 August 2008, an articulated fracture network developed in the areas immediately surrounding the vent, as well as extending up to 1km from the vent (Madonia et al., 2011). This preceded a large mud extrusion with many morphologically analogous features to the eruption at the subject site. These examples clearly show that the surface deformations can be a precursor to a mud volcano eruption.

5.6 Monitoring and Further Investigation

To comprehensively understand how a mud volcano develops, as well as the hazards they pose, it is necessary to monitor their activity and growth. As mud volcanoes are usually in a dormant stage due to the typically short duration of eruptions, the use of long-term monitoring is fundamental to determine episodic processes and transient changes (Mazzini et al, 2009; Menapace et al., 2017). In recent history, there has been limited mud volcanoes in New Zealand that have been monitored surrounding their eruptive phase. This following section highlights some available monitoring techniques that could be applied to developing a greater understanding of the Waimata Valley mud volcano, as well as others in the region. These techniques include a variety of geospatial, geochemical, geophysical, and geotechnical instrumentation. The combination of techniques is generally a powerful tool to developing a more comprehensive understanding of a complete mud volcano system.

5.6.1 Geospatial

Geospatial techniques are commonly used to monitor the ground deformations at the surface and subsurface of a site. For this reason, they are widely applied to the monitoring of landslides (Gunn et al, 2013; Uhlemann et al, 2016), as well as for observing volcano deformations and interpreting magmas supply dynamics (Niu et al, 2019), though they have sparingly been used to monitor mud volcanoes. Interferometric Synthetic Aperture Radar (InSAR) combines two or more SAR images of the same area acquired at different times to map surface deformations between the time interval spanned by the images (Mazzini and Etiope, 2017). InSAR observations of mud volcanoes play a useful role in documenting eruptive activity and forecasting associated hazards (Niu et al, 2019). It can be used to characterise ground deformation before, during and after an eruptive event. InSAR has been used for monitoring significant mud volcanoes around the world including in Indonesia (Istadi et al, 2012), Azerbaijan (Antonielli et al, 2014) and Canada (Niu et al, 2019). Other spatial techniques used to monitor the surface deformations of mud volcanoes is the use of global positioning systems (GPS) (Hochstein and Sudarman, 2010; Kadirov et al., 2013), or LiDAR change detection. LiDAR imagery has been produced for the Waimata Valley mud volcano both prior and immediately following the eruption. This would be a powerful tool to determine how the mud volcano developed at the surface. These techniques could also be used to assess the relationship of the mud volcano activity with seismic activity.

5.6.2 Geochemical

The dormant phase of a mud volcano typically characterised by vigorous seepage of water, gas and petroleum (Menapace et al, 2017). These seepages often demonstrate pulsating behaviour interpreted as the continuous inflation and deflation of the conduit system once a sufficient overpressure is reached and fluids burst out (Etiope et al., 2009, Mazzini and Etiope, 2017). Therefore, monitoring the changes in the volume and geochemistry of gas, water and mud emitted is important to understanding the origins and development of a mud volcano, as well as acting as a precursory signal for future eruptive activity. The emitted constituents are generally collected at the site and then analysed in the laboratory. The changes in the flux of gas and water can be monitored onsite with various instrumentation such as fluxmeters (Mazzini et al, 2009).

5.6.3 Geophysical

There is a wide variety of geophysical techniques that are useful in determining the subsurface architecture of a Mud Volcano. As seen as part of this study, GPR was used to profile the shallow (5m to 15m) subsurface structure beneath the mud volcano though it had limitations. Other techniques that are commonly used to profile the shallow subsurface include 3D electrical resistivity imaging (Zeyen et al., 2011; Odonne et al., 2020). The technique can be used to also shown temporal changes introducing another dimensionality to the data (Gunn et al., 2013). This technique has successfully been used in a study of a mud-volcano field in the Wairarapa region, New Zealand. The mud exhibits very low resistivity (high conductivity) and allows for conduits to be profiled linking the surface vents to a deeper mud chamber (Zeyen et al., 2011). Similar properties were observed during the GPR studies at the subject site.

For deeper subsurface profiling of the intrusive and potentially the source domains, techniques such as 3D seismic survey or gravimetric survey can be used (Istadi et al, 2009; Kirkham, 2015; Dupuis et al., 2019; Odonne et al., 2020). These techniques help to delineate structural controls at depth, as well as potential sources of the mud material (Odonne et al., 2020)

5.6.4 Geotechnical

Other geotechnical techniques that are useful in characterising the subsurface of a mud volcano are deep boreholes, as well as cone penetration tests (CPTs) (Kopf et al, 2009; Istadi et al, 2012; Dupuis et al., 2020). Deep boreholes can be used to confirm the source geology of the expelled mud, as well as helping to correlate geophysical data (Dupuis et al., 2019). Deep boreholes can be coupled with instruments such as piezometers to monitor pore-water pressures of a certain depth range (Uhlemann et al., 2013). CPTs with pore pressure measurement helps to determine how the material behaves in the subsurface which can lead to ascertaining how it may migrate to the surface (Kopf et al, 2009). These techniques are only suitable during the dormant phase of a mud volcano due to their intrusive nature and the risks associated.

5.7 Planning Implications

The paroxysmal nature of mud volcano eruptions, as well as the broad range of hazards that can arise, highlight the importance of identifying and mapping mud volcanoes throughout the East

Coast region to allow the risks to be managed appropriately. The recent eruption at the Waimata Valley shows that mud volcano eruptions can occur without much warning. Fortunately, the eruption occurred in a remote area where the consequences are reduced relative to more developed areas. Nevertheless, there are many examples from overseas eruptions that highlight the potential disastrous consequences that can result, most famously the Lusi eruption in 2006 that led to the displacement of 40,000 residents in East Java, Indonesia (Mazzini et al, 2007). A way of potentially reducing the risk of mud volcano eruptions is to help delineate the precursory signals to an eruption (Section 5.5). This should be incorporated into planning decisions throughout the region after detailed assessments of the mud volcanoes occurrence has been undertaken including large scale mapping and monitoring efforts.

Another way to help reduce the risk of mud volcano eruptions would be to develop a Trigger Action Response Plan (TARP) based on the information collected. The triggers could be set by the precursory signals of a mud volcano eruption to allow for an appropriate risk management response.

5.8 Summary of Discussion

By undertaking an engineering geological investigation of the recently erupted Waimata Valley mud volcano and its associated materials, a greater understanding of how the expelled material manifests at the surface is achieved. A new model for the development of the mud volcano has been formulated based on this investigation and could be applied to other mud volcanoes within the region. This model contains both similarities and differences to other models previously developed for the formation of mud volcanoes within region and highlights the variable circumstances in which they form.

By developing this greater understanding of the mud volcano, it is possible to identify the potential geohazards that may arise for future events that will inevitably continue to occur throughout the region. This includes hazards that arise both during and following a mud volcano eruption.

The mud volcano of this study highlights how these events can occur at sites with no previous association of mud volcano activity, as well as little warning leading to the expulsion of the material. It is therefore important to delineate the potential precursory signals to such events.

In this case, seismic activity, ground deformations and increased activity of nearby gas seeps were identified precursors to the event. Further monitoring and investigation of the site is necessary to gain a more comprehensive understanding of how these mud volcanoes occur and to predict the likelihood of future eruptions.

CHAPTER SIX: CONCLUSIONS

6.1 Summary of Research

The formation of the recent Waimata Valley mud volcano on 15 December 2018 has provided a rare and valuable opportunity to gain a better understanding of the processes and mechanisms that cause deeply buried sediments to mobilise and manifest at the surface. This was primarily achieved through an engineering geological investigation of the site and the associated materials. An understanding of these aspects helps to determine the behaviour of the material at the surface and any potential hazards that may arise. Whilst this study was focused on a single event, the findings may be relevant for understanding mud volcano systems within the Tairawhiti Region and elsewhere. The main conclusions of this study are broken down into different aspects regarding the development of the mud volcano, the mud properties, and the associated geohazards.

6.1.1 Mud Volcano Development

Insights into the development of the recent Waimata Valley mud volcano has led to the following main conclusions:

- Observations of the site prior to the mud volcano formation highlighted the influence of seismic activity. Immediately following the Te Araroa earthquake on 2 September 2016, significant ground deformations were recorded at the site which subsequently formed a conduit for the new mud volcano.
- The mud volcano is interpreted to have erupted effusively and lasted no more than three hours.
- The eruption formed a series mud flows that propagated radially from the vent where one blocked a small stream resulting in the formation of a lake. It is estimated that 11,200m^3 of mud has been expelled at the surface, measuring up to 3m deep surrounding the vent area.
- The mud volcano is interpreted to be associated with diapiric activity caused by gravitative instability from overpressured deeply buried sediments. These sediments mobilise and migrate toward the surface along structural highs and fault networks.
- It is interpreted that the mud accumulates within a shallow reservoir where pressures resulting from an influx of fluid may result in an extrusion at the surface.

- The difference in morphologies of the recently formed Waimata Valley mud volcano and the neighbouring Arakihi Road mud volcanoes highlights the variable properties of these features even within the same mud volcano system.

6.1.2 Mud Properties

An engineering geological investigation, including subsequent laboratory testing of the mud volcano materials, has led to the following conclusions regarding its engineering properties:

- The mud matrix comprises predominately of silt and clay with occasional fragments of rock. The lithological variety of the rock fragments suggests the mud has migrated a large distance. SEM confirmed the significant clay content of the mud matrix, as well as its pelagic origins.
- The highly plastic and active behaviour of the clay suggests it is predominantly smectite though diagenetic reactions and stratigraphic mixing has also led to other clay minerals such as illite and kaolinite within the fraction.
- The clay contains a very similar chemical fingerprint to the Arakihi Road mud volcano suggesting that they originate from the same mud reservoir at a shallow depth. This fingerprint varies slightly from other mud volcanoes within the Waimata Valley though the similarities suggest a similar deep source.
- The mud is of very low strength with a measured friction angle of 11.3˚. The unconsolidated nature of the material suggest it innately exists at residual strength.
- The intrinsic low permeability and strength of the material are interpreted to strongly influence the mobilisation of deeply buried sediment leading to its extrusion at the surface.
- The engineering properties of materials associated with mud volcanism has seldom been researched within New Zealand, and around the world for that matter. Due to the similarities of the materials associated with mud volcanism, the properties learnt from this study can be applied to other mud volcanoes throughout the region.

6.1.3 Geohazards

Interpretations of the mud volcano event, as well as the engineering properties has led to the following main conclusions regarding the geohazard associated with mud volcanism:

- This eruption is a prime example into the paroxysmal nature of mud volcanoes and how they can erupt with little warning.
- Seismic activity, ground deformations, and increased gas venting of nearby seeps highlighted the precursory signals to the eruptive event.
- By delineating the precursory signals leading to the formation of the mud volcano it may be possible to predict future events.
- Evidence from the formation of this mud volcano, as well as other examples highlight the potential geo-hazards that may arise both during and following an eruption.
- A significant hazard highlighted from this event is the formation of highly mobile mud flows. These flows may extend large distances even on gentle slopes and create an inundation hazard for anything in its path.
- The mud volcano is now considered dormant, however, the establishment of a permanent gas seep following the eruption highlights that future activity should not be discounted.
- The formation of this mud volcano highlights the need to understand the hazards, occurrence, and geotechnical implications of mud volcano activity as events will inevitably continue to occur within a rapid growly region. These findings should be incorporated into future planning decisions within the region.

6.2 Limitations and Future Research

Mud volcanoes represent a complex field of research due to the complexity and diversity of these structures and their geological background. Whilst this study has benefited from the rare opportunity of documenting an eruption both prior and immediately following the event, there are limitations particularly regarding the processes and mechanisms occurring within the source and intrusive domains, as well as subsurface architecture of these mud volcano systems.

This research is based on surface observations and limited subsurface information regarding the areas complex geology and structure which are fundamental to fully understanding the occurrence of mud volcanoes. The increased activity of only some mud volcanoes following the Te Araroa earthquake suggests there is a structural relationship between the mud volcano systems on a regional scale. Further work should be undertaken to understand the complex geology of the Waimata Valley, as well as the East Coast region of New Zealand's North Island.

This could include a combination of direct and geophysical investigation methods such as comprehensive geological and structural mapping, deep bore holes and 3D seismic surveys.

A greater understanding of the geochemistry of the mud volcano materials is necessary to determine their composition and origins. ICP-MS was useful in comparing the origins of different mud volcano systems; however, further testing should be undertaken to confirm their stratigraphic source. This would include isotope analysis and the gas and fluid, as well as confirming the mineralogy of the clay minerals by XRD.

The engineering geological investigation was useful in characterising the mud volcano at the extrusive domain as well as the materials engineering properties, however, an understanding of the how the mud accumulates in the shallow subsurface is undetermined. The use of GPR was useful in delineating structure at the surface though it was limited by the highly conductive nature of the soils. Other shallow geophysical methods such as 3D electrical resistivity surveys have proved useful in characterising the shallow mud reservoir of other mud volcano systems and would likely be beneficial if utilised at the subject site.

Although the site had been observed prior and shortly after the eruption, the paroxysmal nature of the event meant that it was not directly observed. Through the use of techniques such as InSAR or LiDAR change detection it may be possible to observe how the deformed immediately prior to the eruptions leading to a greater understanding of how the mud is extruded at the surface.

Many of these suggestions are far beyond the scope of this thesis and there are many time and budget constraints due to the complexity of these systems. Notwithstanding, these would all lead to a more comprehensive understanding of mud volcano systems as a whole. The reward of such studies should be an improved understanding of the processes and mechanisms that led to mud volcanism, as well as their associated geohazards.

REFERENCES

Abbasov, O. R., Baloglanov, E. E. (2018). Mud volcanoes of the world: Classifications, activities and environmental hazard (informational-analytical review). *European Journal of Natural History,* 5, pp.12-25.

Adams, C. J., Kelley, S. Provenance of Permian-Triassic and Ordovician metagraywacke terranes in New Zealand: Evidence from $^{40}Ar/^{39}Ar$ dating of detrital micas. *GSA Bulletin*, 110(4), pp.422–432.

ASTM International. *Standard Test Methods for Determining Dispersive Characteristics of Clayey Soils by the Crumb Test (ASTM D6572-20).* West Conshohocken, Pennsylvania: ASTM International.

ASTM International. *Standard Test Method for Torsional Ring Shear Test to Measure Fully Softened Shear Strength and Stress Dependent Strength Envelope of Fine-Grained Soils (ASTM D7608-18).* West Conshohocken, Pennsylvania: ASTM International.

Antonielli, B., Monserrat, O., Bonini, M., Righini, G., Sani, F., Luzi, G., Feyzullayev, A. A., Aliyev, C. S. 2014. Pre-eruptive ground deformation of Azerbaijan mud volcanoes detected through satellite radar interferometry (DInSAR). *Tectonophysics,* 637, pp.163-177.

Assaad, F. A., 2004. *Field Methods for Geologists and Hydrogeologists*. Springer, Berlin.

Atkinson, J. H., 2007. *The Mechanics of Soils and Foundations* (2nd ed). Taylor & Francis, London & New York.

Ballance, P. F. (1975). Evolution of the Upper Cenozoic Magmatic Arc and plate boundary in northern New Zealand. *Earth and Planetary Science Letters*, *28*(3), pp.356-370.

Barnes, P. M., Lamarche, G., Bialas, J., Henrys, S., Pecher, I., Netzeband, G. L., Greinert, J., Mountjoy, J. J., Pedley, K., Crutchley, G. (2010). Tectonic and geological framework for gas hydrates and cold seeps on the Hikurangi subduction margin, New Zealand. *Marine Geology*. 272, pp.26-48.

Bell, F, G. (2006). *Engineering Geology*. (2nd Ed). Elsevier Science and Technology, Amsterdam.

Blott, S. J., Croft. D. J., Pye. K., Saye, S. E., Wilson. H. E. (2004). Particle size analysis by laser diffraction. *Geological Society Special Publication,* 232, pp. 63-73

Blouin, A. (2019). *Mud generation from stratified sediments in a context of mud volcanism: the role of gas*. PhD Thesis. Earth Sciences. University of Pau and the Adour Region.

Bohor, B. F., Hughes, R, E. (1971). Scanning Electron Microscopy of Clays and Clay Minerals. *Clays and Clay Minerals*, 19, pp. 49-54

Bonini, M. (2009). Mud volcano eruptions and earthquakes in the Northern Apennines and Sicily, Italy. *Tectonophysics*. 474, pp.723-735.

Brown, K. M. (1990). The nature and hydrogeologic significance of mud diapirs and diatremes for accretionary systems. *Journal of Geophysical Research*, *95*(B6), pp.8969–8982.

Carter, L., Oprin, A. R., Kuehl, S. A. (2010) From mountain source to ocean sink – the passage of sediment across an active margin, Waipaoa Sedimentary System, New Zealand. *Marine Geology*. 270 (1-4), pp.1-10.

Cave, M. (2017). The Mud Volcanoes of The Tairawhiti. *Geoscience Society of New Zealand annual conference 2017 (Abstracts).* 19.

Cerato, B. A., Lutenegger, J. A. (2006). Shrinkage of Clays. *Proceedings of the 4th International Conference on Unsaturated Soils,* Carefree, AZ, April 2-6, ASCE, Reston VA, pp. 1097-1108.

Chen, H., Wang, S., Chen, Z., Yan, W., Li, G. (2015). Geochemical and magnetic signals for the mud volcano-induced methane seepage in the core sediments of Shenhu area, northern South China Sea. *Environmental Earth Sciences*, *73*(10), pp. 6365–6378.

Clark, K., Berryman, K., Litchfield, N., Cochran, U., Little, T. (2010). Evaluating the coastal deformation mechanisms of the Raukumara Peninsula, northern Hikurangi subduction margin, New Zealand and insights into forearc uplift processes. *New Zealand Journal of Geology and Geophysics*, *53*(4), pp.341–358.

Craig, R. F. (1974*). Soil Mechanics* (6th ed.). Chapman & Hall, London, 8-10.

Daniels, D. J. (2004). *Ground Penetrating Radar (2nd Edition).* ESA Publications.

Das, B, M. (1985). Principles of Geotechnical Engineering (1st ed.). PWS Publishers. Boston, Massachusetts.

Day, P.R. 1965. 'Particle fractionation and particle size-analysis', in C.A. Black et al., (eds). *Methods of Soil Analysis.* Agronomy No. 9 Part 1. American Society of Agronomy, Madison, WI, pp. 545-567.

Deville, E., Battani, A., Griboulard, R., Guerlais, S., Herbin, J. P., Houzay, J. P., Muller, C., Prinzhofer, A. (2003). The origin and processes of mud volcanism: new insights from Trinidad. *Geological Society, London, Special Publications*, 216(1), pp. 475-490.

Deville, É. (2009). 'Mud volcano systems', in Lewis, N., and Moretti, A. (eds). *Volcanoes: Formation, Eruptions and Modelling*. Nova Science Publishing, pp.95-126.

Dimitrov, L. I. (2002). Mud volcanoes-the most important pathway for degassing deeply buried sediments. *Earth-Science Reviews*, *59*(1–4), pp.49–76.

Dupuis, M., Imbert, P., Odonne, F., Vendeville, B. (2019). Mud volcanism by repeated roof collapse: 3D architecture and evolution of a mud volcano cluster offshore Nigeria. *Marine and Petroleum Geology,* 110, pp.368-387.

Emerson, M, M. (1967). A classification of soil aggregates based on their coherence in water. *Australian Journal of Soil Research, 5(1),* pp 47-57.

Etiope, G., Feyzullayev, A., Baciu, C. L. (2009). Terrestrial methane seeps and mud volcanoes: A global perspective of gas origin. *Marine and Petroleum Geology*, *26*(3), pp.333-344.

Etiope, G. (2015). *Natural Gas Seepage*. Springer International Publishing, Switzerland.

Fell, R., MacGregor, P., Stapledon, D., Bell, G., Foster, M. (2015). Geotechnical Engineering of Dams. London: CRC Press.

Field, B. D., Uruski C. I., Beu, A. G., Browne, G. H., Crampton, J. S., Funnell, R., Killops, S., Laird, M. G., Mazengarb, C., Morgans, H. E. G., Rail, G. J., Smale, D., Strong, C. P.

(1997). Cretaceous-Cenozoic geology and petroleum systems of the East Coast Region, New Zealand. *Institute of Geological and Nuclear Sciences monograph 19*. Lower Hutt. Institute of Geological and Nuclear Sciences Ltd. Wellington, New Zealand.

Fisher, P., Aumann, C., Chia, K., O'Halloran, N., Chandra, S. (2017). Adequacy of laser diffraction for soil particle size analysis. *Public Library of Science, 12*(5), pp.1–20.

Grabowska-Olsezewska, B., Osipov, V., Sokolov, V. (1984). *Atlas of the Microstructure of Clay Soils.* University of Warsaw, Warsaw.

Gunn, D. A., Chambers, J. E., Hobbs, P. R. N., Ford, J. R., Wilkinson, P. B., Jenkins, G. O., Merritt, A. (2013). Rapid observations to guide the design of systems for long-term monitoring of a complex landslide in the Upper Lias clays of North Yorkshire, UK. *Quarterly Journal of Engineering Geology and Hydrogeology, 46,* pp. 323-336.

Heidema, P. B. (1957). The Bar-Shrinkage Test and the Practical Importance of Bar-Linear Shrinkage as an Identifier of Soils. *Proceedings of the 4th International Conference on Soil Mechanics and Foundation Engineering*, Vol 1, pp. 44-48.

Hochstein, M. P., Sudarman, S. (2010). Monitoring of LUSI mud-volcano-a geo-pressured system, Java, Indonesia. *Proceedings World Geothermal Congress,* pp. 25-29.

Ingles, O. G., Metcalf, J.B. (1972). *Soil Stabilisation.* Butterworths.

Istadi B. P., Pramono, G. H., Sumintadireja, P. Syamsu, A. (2009). Modeling study of growth and potential geohazard for LUSI mud volcano: East Java, Indonesia. *Marine and Petroleum Geology,* 26, pp.1724-1739.

Istadi, B. P., Wibowo, H. T., Sunardi, E., Hadi, S., Sawolo, N. (2012). Mud Volcano and Its Evolution. *Earth Sciences Publication,* 17, pp.375-434.

Jennerjahn, T. C., Janen, I., Propp, C., Adi, S., Nugroho, S. P. (2013). Environmental impact of mud volcano inputs on the anthropogenically altered Porong River and Madura Strait coastal waters, Java, Indonesia. *Estuarine, Coastal and Shelf Science,* 130, pp.152-160.

Kadirov, F, A., Guliyev, I. S., Feyzullayev, A. A., Safarov, R. T., Mammadov, S. K., Babayev, G. R., Rashidov, T. M. (2014). GPS-Based Crustal Deformations in Azerbaijan and

Their Influence on Seismicity and Mud Volcanism. *Physics of the Solid Earth*. 6, pp.99-107.

Kamp, P, J, J. (1999). Tracking crustal processes by FT thermochronology in a forearc high (Hikurangi Margin, New Zealand) involving Cretaceous subduction termination and mid-Cenozoic subduction initiation. *Tectonophysics,* 307, pp.313-343

Kettner, A. J., Gomez, B., Syvitski, J. P. M. (2007). Modelling suspended sediment discharge from the Waipaoa River System. *Water Resources Research*, 43, W07411.

Kirkham, C. B. (2015). A 3D seismic interpretation of mud volcanoes within the western slope of the Nile Cone. *Unpublished PhD Thesis*. Cardiff University, Wales.

Knodel, P. C. (1991). Characteristics and Problems of Dispersive Clay Soils. *Technical Report R-91-09.* United States Bureau of Reclamation, Denver, CO.

Kopf, A., Clennell, M. B., Camerlenghi, A. (1998). Variations in sediment physical properties and permeability of mud-volcano deposits from Napoli dome and adjacent mud volcanoes. *Proceedings of the Ocean Drilling Program: Scientific Results*, *160*(September), pp.625–644.

Kopf, A. J. (2002). 'Significant of Mud Volcanism'. *Review of Geophysics,* 40(2). 1005.

Kopf, A. J., Clennell, B., Brown, K. M. (2005). 'Physical Properties of Muds Extruded from Mud Volcanoes: Implications for Episodicity of Eruptions and Relationship to Seismicity, in Martinelli, G. and Panahi, B (eds), *Mud Volcanoes, Geodynamics, and Seismicity.* Springer, Netherlands, pp.263-283.

Kopf, A., Stegmann, S., Delisle, G., Panahi, B., Aliyev, C, S., Guliyev, I. (2009). In situ cone penetration tests at the active Dashgil mud volcano Azerbaijan: Evidence for excess fluid pressure, updoming, and possible future violent eruption. *Marine and Petroleum Geology,* 26, pp.1716-1723.

Lewis, K. B., Marshall, B. A. (1996). Seep faunas and other indicators of methane-rich dewatering on New Zealand convergent margins. *New Zealand Journal of Geology and Geophysics*, *39*(2), pp. 181–200.

Litchfield, N., Ellis, S., Berryman, K., Nicol, A. (2007). Insights into subduction-related uplift along the Hikurangi Margin, New Zealand, using numerical modeling. *Journal of Geophysical Research: Earth Surface*, *112*(2), pp.1–17.

Liu, Y. S., Hu, Z. C., Li, M., Gao, S. (2013). Applications of LA-ICP-MS in the elemental analyses of geological samples. *Chinese Science Bulletin*, 58(32), pp.3863-3878.

Madonia, P., Grassa, F., Cangemi, M., Musumeci, C. (2011). Geomorphological and geochemical characterisation of the 11 August 2008 mud volcano eruption at S. Barbara village (Sicily, Italy) and its possible relationship with seismic activity. *Natural Hazards and Earth System Sciences*, 11, pp. 1545-1557.

Manga, M., Brumm, M., Rudolph, M. (2009). Earthquake triggering of mud volcanoes. *Marine and Petroleum Geology*, 26, pp. 1785-1798.

Marden, M., Mazengarb, C., Palmer, A., Berryman, K., Rowan, D. (2008). Last glacial aggradation and postglacial sediment production from the non-glacial Waipaoa and Waimata catchments, Hikurangi Margin, North Island, New Zealand. *Geomorphology*, 99, pp.404-419.

Maison, T., Potel, S., Malie, P., Mahlmann, R, F., Chanier, F., Mahieux, G, Bailleul, J. (2018). Low-grade evolution of clay minerals and organic matter in fault zones of the Hikurangi prism (New Zealand). *Clay Minerals*, 53, pp.579-602.

Mazengarb, C., Francis, D. A., Moore, P. R. (1991). *Sheet Y16 – Tauwhareparae. Geological Map of New Zealand 1:50,000*. Department of Scientific & Industrial Research. Wellington, New Zealand.

Mazengarb, C. (1993). Cretaceous stratigraphy of Raukumara Peninsula. *Institute of Geological and Nuclear Sciences, science report 93120.* Institute of Geological and Nuclear Sciences Ltd. Lower Hutt.

Mazengarb. C. (1997*). Slope instability and mud volcano hazard assessment, Gisborne District Council.* Client Report. Ref: 1997/44692D.13. Institute of Geological and Nuclear Sciences Ltd. Lower Hutt.

Mazengarb, C. (1998). Late Neogene structural development of Eastern Raukumara Peninsula: Implications for oil exploration. *New Zealand Petroleum Conference Proceedings, 30 March – 1 April 1998.*

Mazengarb, C. and Speden, I. G. (2000). *Geology of the Raukumara area: scale 1:250,000*. Lower Hutt: Institute of Geological and Nuclear Sciences 1:250,000 geological map 6.

Mazzini, A., Svensen, H., Akhmanov, G. G., Aloisi, G., Planke, S., Malthe-Sorenssen, A., Istadi, B. (2007). Triggering and dynamic evolution of the LUSI mud volcano, Indonesia. *Earth and Planetary Science Letters*, 261, pp.375-388.

Mazzini, A., Svensen, H., Planke, S., Guliyev. I., Akhmanov, G. G., Fallik, T., Banks, D. (2009). When mud volcanoes sleep: Insight from seep geochemistry at the Dashgil mud volcano, Azerbaijan. *Marine and Petroleum Geology, 26(9),* pp. 1704-1715.

Mazzini, A. and Etiope, G. (2017). Mud volcanism: An updated review. *Earth-Science Reviews*, 168, pp.81–112.

Menapace, W., Volker, D., Sahling, H., Zoellner, C., Ferreira, C., Bohrmann, G., Kopf, A. (2017). Long-term in situ observations at the Athina mud volcano, Eastern Mediterranean: Taking the pulse of mud volcanism. *Tectonophysics*, 721, pp.12-27

Miller, B. A.,Schaetzl, R. J. (2012). Precision of Soil Particle Size Analysis using Laser Diffractometry. *Soil Science Society of America Journal*, *76*(5), pp.1719–1727.

Monroe, J, N. (1999). *Fracture-Permeability Development in Organically-Rich Sediments through Methane Generation*. Unpublished PhD Thesis. Texas Tech University. Lubbock, Texas, United States of America.

Moore, P. R., Adams, A. G., Isaac M. J., Mazengarb, C., Morgans, H. E. G., Phillips, C. J. (1986). A revised Cretaceous-early Tertiary stratigraphic nomenclature for eastern North Island. *New Zealand Geological Survey report GI04*. Department of Scientific and Industrial Research. Wellington.

Moore, P. R. (1988). Stratigraphy, composition and environment of deposition of the Whangai Formation and associated Late Cretaceous-Paleocene rocks, Eastern North Island, New

Zealand. *New Zealand Geological Survey Bulletin.* 100. Department of Scientific and Industrial Research. Wellington.

Moore, R. (1991). The chemical and mineralogical controls upon the residual strength of pure and natural clays. *Geotechnique, 41,* pp. 35-47.

Mori, Y., Yoshida, H., Masuda, H. (2012). Particle size analysis by laser diffraction method using reference particles. *Advanced Materials Research, 508,* pp.33–37.

Nadeau, P. H. (1985). The physical dimensions of fundamental clay particles. *Clay Minerals*, *20*(4), pp.499–514.

Neef, G., Bottrill, R. S. (1992) The Cenozoic geology of the Gisborne area (1:50,000 metric sheet Y18AB), North Island, New Zealand. *New Zealand Journal of Geology and Geophysics,* 35(4), pp.515-531.

Nicol, A., Mazengarb, C., Chanier, F., Rait, G., Uruski, C., Wallace, L. (2007). Tectonic evolution of the active Hikurangi subduction margin, New Zealand, since the Oligocene. *Tectonics*, *26*(4), pp.1–24.

Niu, Y., Dzurisin, D., Zhong, Lu. (2019). Interferometric synthetic aperture radar study of recent activity at Shrub mud volcano, Alaska. *Journal of Volcanology and Geothermal Research, 387,* pp.1-12.

Odonne, F., Impert, P., Dupuis, M., Aliyev, A, A., Abbasov, O, R., Baloglanov, E, E., Vendeville, B. C., Gabalda, G., Dominique, R., Bichaid, V., Juste, R., Pain, M., Blouin, A., Dofal, A., Gertauda, M. (2020). Mud volcano growth by radial expansion: Examples from onshore Azerbaijan. *Marine and Petroleum Geology, 122*, 104051

Pettinga, J. R. (2003). Mud volcano eruption within the emergent accretionary Hikurangi margin, southern Hawke's Bay, New Zealand. *New Zealand Journal of Geology and Geophysics*, *46*(1), pp.107–121.

Rahardjo, P, P. (2015). Geotechnical aspects of mud eruption disaster in East Java. *Japanese Geotechnical Society Special Publication. The 15th Asian Regional Conference on Soil Mechanics and Geotechnical Engineering.*

Rait, G. J. (1992). *Early Miocene thrust tectonics on Raukumara Peninsula, north-eastern New Zealand.* Unpublished PhD thesis. Victoria University of Wellington. Wellington, New Zealand.

Reyners, M., Mcginty, P. (1999). Shallow subduction tectonics in the Raukumara Peninsula, New Zealand, as illuminated by earthquake focal mechanisms. *Journal of Geophysical Research, 104(B2),* pp.3025–3034.

Ridd, M. F. (1964). Succession and structural interpretation of the Whangara-Waimata area, Gisborne, New Zealand. *New Zealand Journal of Geology and Geophysics, 7(2),* pp. 279-298.

Ridd, M. F. (1968). Gravity gliding on the Raukumara Peninsula. *New Zealand Journal of Geology and Geophysics, 11,* pp. 547-548

Ridd, M. F. (1970). Mud Volcanoes in New Zealand. *American Association of Petroleum Geologists Bulletin, 54,* pp. 601 to 616.

Roberts, S, K. (2011). *Mud Volcano Systems: Structure, Evolution and Processes*. Unpublished PhD Thesis. Durham University. Durham, United Kingdom.

Rogozhin, E, A. (2005). 'Mud Volcanic Manifestations in the Maximum Shaking Areas of Strong Earthquakes', in Martinelli, G., Panahi, B. (eds). *Mud Volcanoes, Geodynamics and Seismicity*. Springer, Dordrecht, The Netherlands, 3, pp.105-110.

Ryzak, M., Beiganowski, A. (2011). Methodical aspects of determining soil particle-size distribution using the laser diffraction method', *Journal of Plant Nutrition and Soil Science,* 174(4), pp. 624-633.

Scherwath, M., Kopp. H., Flueh, E. R., Henrys, S. A., Sutherland, R., Stagpoole, V. M., Barker, D. H. N., Reyners, M. E., Bassett, D. G., Planert, L., Dannowski, A. (2010). Fore-arc deformation and underplating at the northern Hikurangi margin, New Zealand. *Journal of Geophysical Research.* 115, B06408.

Sciarra, A., Cantucci, B., Ricci, T., Tomonaga, Y., Mazzini, A. (2019). Geochemical Characterization of the Nirano mud volcano, Italy. *Applied Geohemistry*, 102, pp.77-87.

Selby, M. J., 1993. *Hillslope Materials and Processes.* Oxford University Press, Oxford.

Sherard, J. L., Decker, R. S., Dunningan, L. P., Steele, E. F. (1976). Identification and nature of dispersive soils. *Journal of Geotechnical Engineering*, 102, pp. 277-301.

Skempton, A, W. (1953). The Colloidal Activity of Clays. *Proceedings of the 3rd International Conference on Soil Mechanics and Foundation Engineering*. London, Vol 1, pp. 57-61

Sobkowicz, J. C., Morgenstern, N. R. (1984). The undrained equilibrium behaviour of gassy sediments. *Canadian Geotechnical Journal, 21(3)*, pp 439-448.

Speden, I. (2004). Geological hazard and risk assessment in the Wheatstone Road – Sponge Bay area, Gisborne City. *Institute of Geological & Nuclear Sciences science report, 2004/29.*

Standards New Zealand. (1986). *Methods for Testing Soils for Civil Engineering Purposes (NZS 4402:1986).* Wellington: Standards Association of New Zealand.

Standards New Zealand. (2011). *Timber Framed Buildings (NZS 3604:2011).* Wellington: Standards Association of New Zealand.

Stanley, A. (2019). Geochemical Fingerprinting Sediments of Waimata Tributaries by LA-ICP-MS. *John Tunnicliffe (Rivers).* University of Auckland.

Starodub, N. F. (2005). Biosensor Control of Acute Total Toxicity of Water and Soil Polluted by Polycyclic Aromatic Hydrocarbons, in Martinelli, G. and Panahi, B (eds), *Mud Volcanoes, Geodynamics, and Seismicity.* Springer, Netherlands, pp.221-226.

Stewart, S. A., Davies, R. J. (2006). Structure and emplacement of mud volcano systems in the South Caspian Basin. *AAPG Bulletin* 2006, 90(5), pp. 771–786.

Stockwell, M. J. (1977). Determination of allowable bearing pressure under small structures. New Zealand Engineering.

Sutherland, R., Stagpoole, V., Uruski, C., Kennedy, C., Bassett, D., Henrys, S., Flueh, E. R. (2009). Reactivation of tectonics, crustal underplating, and uplift after 60 Myr of passive subsidence, Raukumara Basin, Hikurangi-Kermadec fore arc, New Zealand: Implications for global growth and recycling of continents. *Tectonics*, *28*(5), pp.1–23.

Tanikawa, W., Sakaguchi, M., Wibowo, H. T., Shimamoto, T., Tadai, O. (2010). Fluid transport properties and estimation of overpressure at the Lusi mud volcano, East Java Basin. *Engineering Geology,* 116, pp.73-85

Terzaghi, K., Peck R. B. (1948). *Soil Mechanics In Engineering Practice*. John Wiley & Sons, New York,

Uhlemann, S., Smith, A., Chambers, J., Dixon, N., Dijkstra, T., Haslam, E., Meldrum, P., Merritt, A., Gunn, D., Mackay, J. (2016). Assessment of ground-based monitoring techniques applied to landslide investigations. *Geomorphology, 253*, pp. 438-451.

Wentz, R., Traylen, N., Fairclough, A., Ashfield, D. (2016). 'Module 2: Geotechnical Investigations for earthquake engineering', in *Earthquake geotechnical engineering practice.* New Zealand Geotechnical Society and Ministry of Business, Innovation and Development.

Yassir, N. A. (1989*). Mud volcanoes and the behaviour of overpressured clays and silts.* Unpublished Doctoral Thesis. University College London. London, United Kingdom.

Zeyen, H., Pessel, M., Ledesert, B., Herbert, R., Bartier, D., Sabin, M., Lallement, S. (2011). 3D electrical resistivity imaging of the near-surface structure of mud-volcano vents. *Tectonophysics*, 509, pp. 181-190.

APPENDIX A: FIELD GUIDES

NZ GEOTECHNICAL SOCIETY INC

SOIL > field guide sheet

FIELD DESCRIPTION OF SOIL

SEQUENCE OF TERMS – fraction – colour – structure – strength – moisture – bedding – plasticity – sensitivity – additional

GRAIN SIZE CRITERIA

TYPE	COARSE								FINE		ORGANIC
	Boulders	Cobbles	Gravel			Sand			Silt	Clay	Organic Soil
			coarse	medium	fine	coarse	medium	fine			
Size Range (mm)	200	60	20	6	2	0.6	0.2	0.06	0.002		
Graphic Symbol											

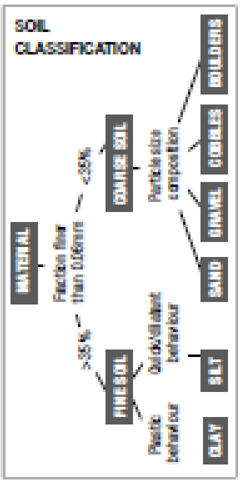

PROPORTIONAL TERMS DEFINITION (COARSE SOILS)

Fraction	Term	% of Soil Mass	Example
Major	(....) [UPPER CASE]	≥ 50 [major constituent]	GRAVEL
Subordinate	(....) y [lower case]	20 – 50	Sandy
Minor	with some .... with minor	12 – 20 5 – 12	with some sand with minor sand
	with trace of (or slightly)....	< 5	with trace of sand (slightly sandy)

DENSITY INDEX (RELATIVE DENSITY) TERMS

Descriptive Term	Density Index (R_D)	SPT "N" value (blows / 300 mm)	Dynamic Cone (blows / 100 mm)
Very dense	> 85	> 50	> 17
Dense	65 – 85	30 – 50	7 – 17
Medium dense	35 – 65	10 – 30	3 – 7
Loose	15 – 35	4 – 10	1 – 3
Very loose	< 15	< 4	0 – 2

Note: • No correlation is implied between Standard Penetration Test (SPT) and Dynamic Cone Test values. • SPT "N" values are uncorrected. • Dynamic Cone Penetrometer (Scala)

CONSISTENCY TERMS FOR COHESIVE SOILS

Descriptive Term	Undrained Shear Strength (kPa)	Diagnostic Features
Very soft	< 12	Easily exudes between fingers when squeezed
Soft	12 – 25	Easily indented by fingers
Firm	25 – 50	Indented by strong finger pressure and can be indented by thumb pressure
Stiff	50 – 100	Cannot be indented by thumb pressure
Very stiff	100 – 200	Can be indented by thumb nail
Hard	200 – 500	Difficult to indent by thumb nail

ORGANIC SOILS/ DESCRIPTORS

Term	Description
Topsoil	Surficial organic soil layer that may contain living matter. However topsoil may occur at greater depth, having been buried by geological processes or man-made fill, and should then be termed a buried topsoil.
Organic clay, silt or sand	Contains finely divided organic matter; may have distinctive smell; may stain; may oxidise rapidly. Describe as for inorganic soils.
Peat	Consists predominantly of plant remains. ***Firm***: Fibres already compressed together ***Spongy***: Very compressible and open stucture ***Plastic***: Can be moulded in hand and smears in fingers ***Fibrous***: Plant remains recognisable and retain some strength ***Amorphous***: No recognisable plant remains
Rootlets	Fine, partly decomposed roots, normally found in the upper part of a soil profile or in a redeposited soil (e.g. colluvium or fill)
Carbonaceous	Discrete particles of hardened (carbonised) plant material.

PLASTICITY (CLAYS & SILTS)

Term	Description
High plasticity	Can be moulded or deformed over a wide range of moisture contents without cracking or showing any tendency to volume change
Low plasticity	When moulded can be crumbled in the fingers; may show quick or dilatant behaviour

MOISTURE CONDITION

Condition	Description	Granular Soils	Cohesive Soils
Dry	Looks and feels dry	Run freely through hands	Hard, powdery or friable
Moist	Feels cool, darkened in colour	Tend to cohere	Weakened by moisture, but no free water on hands when remoulding
Wet			Weakened by moisture, free water forms on hands when handling
Saturated	Feels cool, darkened in colour and free water is present on the sample		

GRADING (GRAVELS & SANDS)

Term	Description	
Well graded	Good representation of all particle sizes from largest to smallest	
Poorly graded	Limited representation of grain sizes - further divided into:	
	Uniformly graded	Most particles about the same size
	Gap graded	Absence of one or more intermediate sizes

NZ GEOTECHNICAL SOCIETY INC

This field sheet has been taken from and should be used and read with reference to the document FIELD DESCRIPTION OF SOIL AND ROCK. Guideline For the Field Classification and Description of Soil and Rock for Engineering Purposes. NZ Geotechnical Society Inc, December 2005. **www.nzgeotechsoc.org.nz**

Appendix A. 1: *NZGS soil field guide sheet by NZ Geotechnical Society Inc (2005), page 2. Used for filed soil descriptions.*

APPENDIX B: SCANNING ELECTRON MICROSCOPE IMAGES

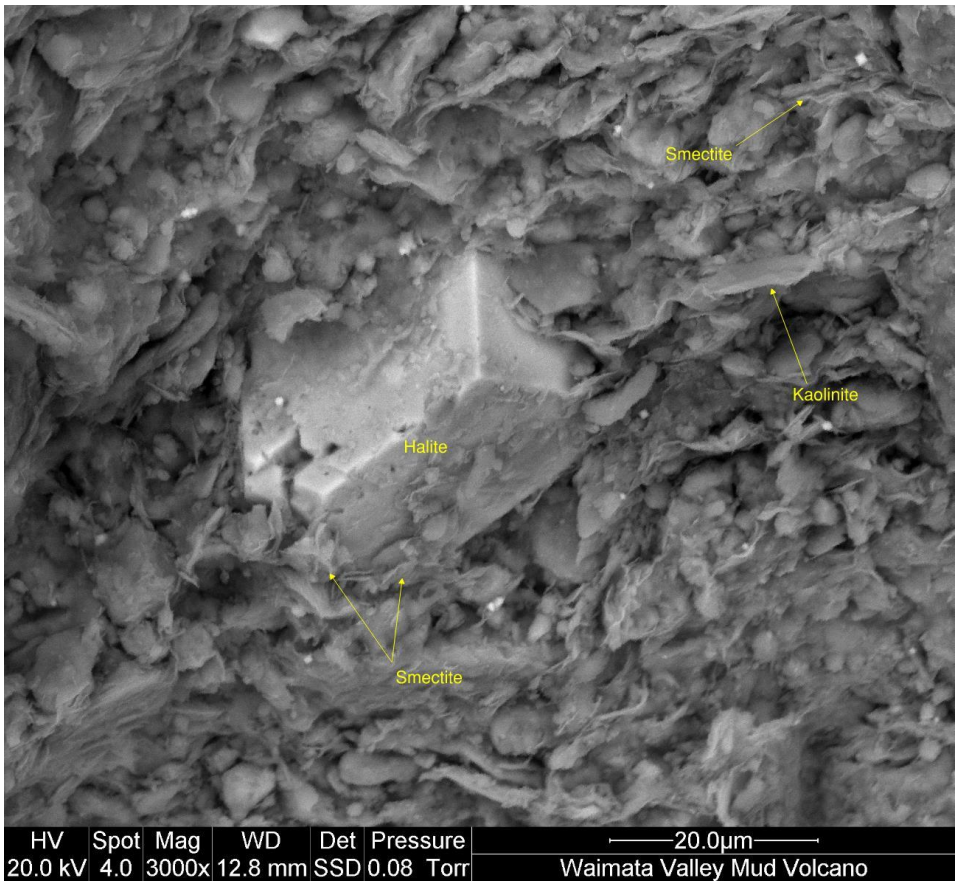

Appendix B. 1: *Halite crystal within matrix comprised of platy clay minerals. Smectite identified by wavy 'flame-like' texture, Kaolinite identified by planar, staked, hexagonal structure.*

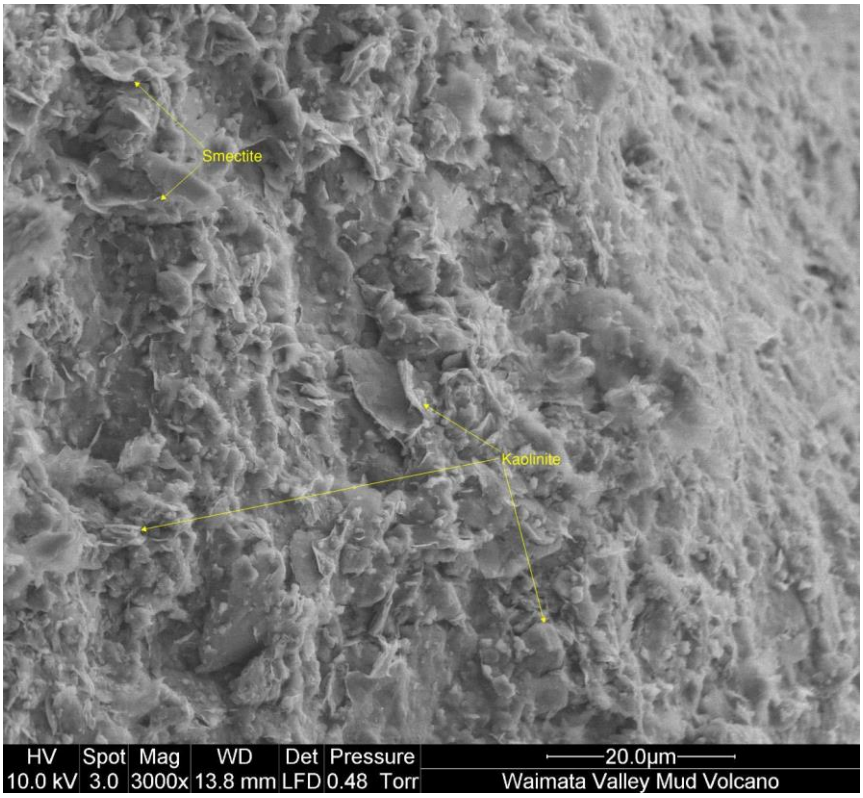

Appendix B. 2: *Wavy smectite clays and stacked, planar Kaolinite clays.*

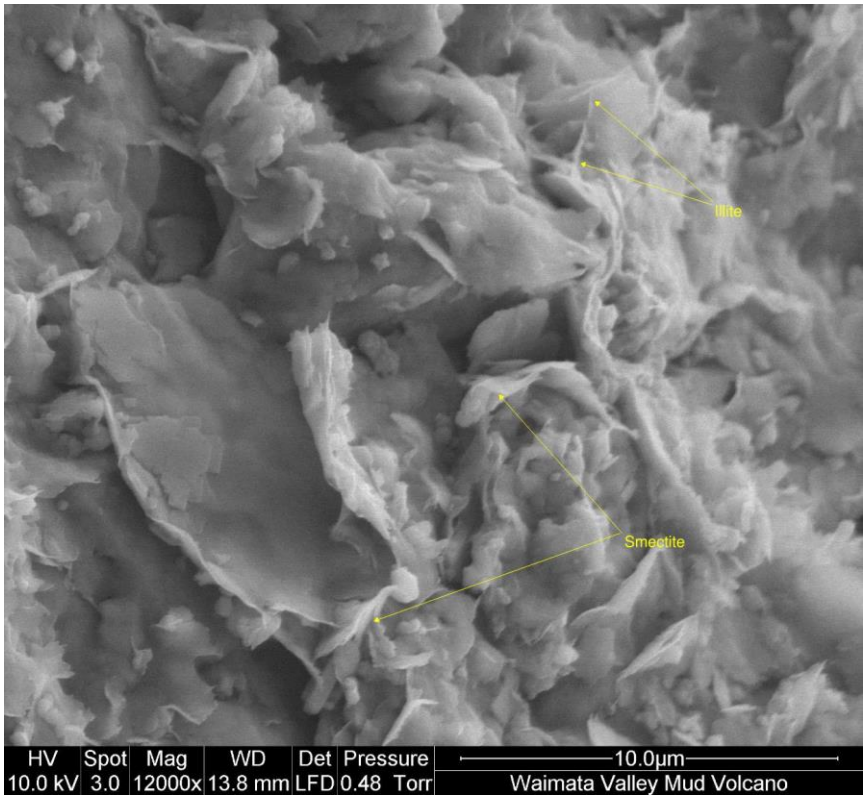

Appendix B. 3: *Wavy smectite clays and fibrous illite clays*

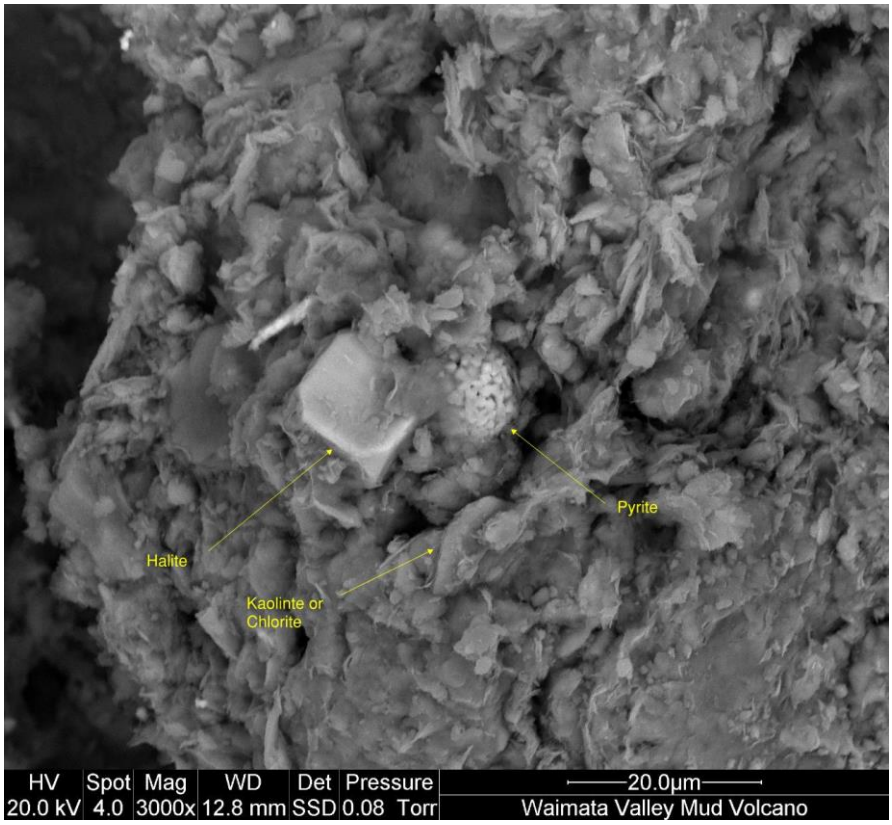

Appendix B. 4: *Halite any pyrite crystals forming within clay matrix. Hexagonal clay crystals either Kaolinite or Chlorite.*

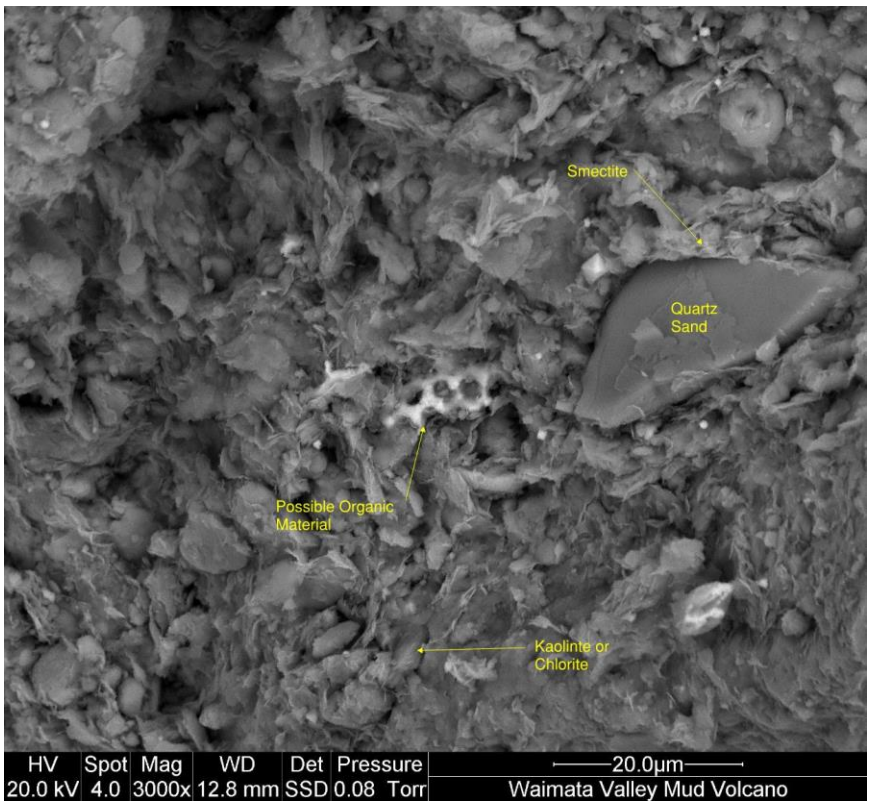

Appendix B. 5: *Fine quartz sand within clay matrix of smectite and kaolinite and/or chlorite. Smectite identified by wavy texture, kaolinite/chlorite identified by stacked, hexagonal texture.*

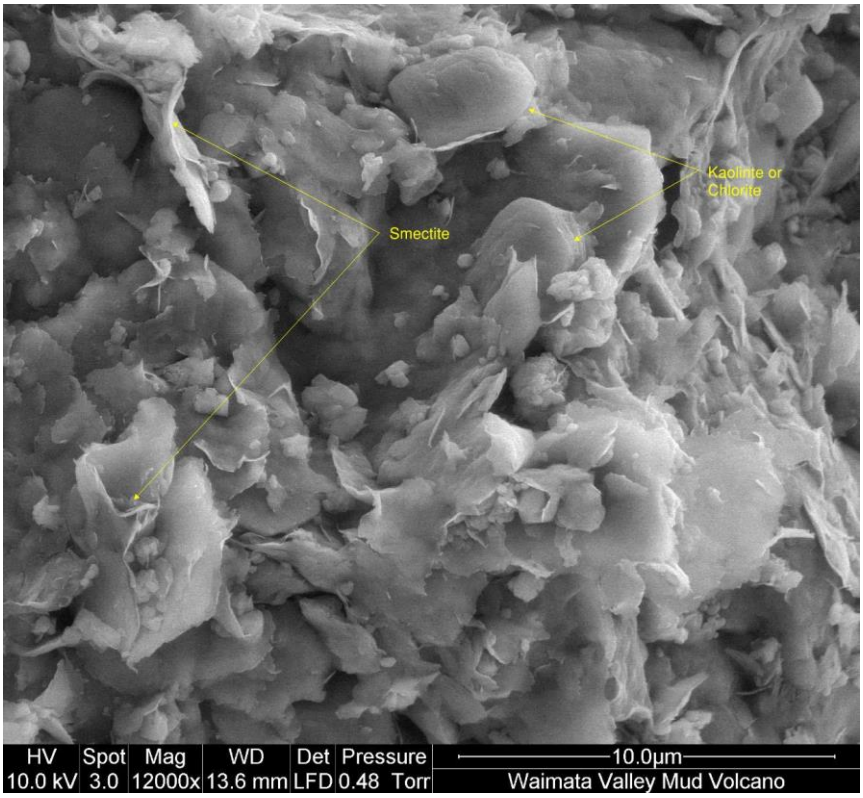

Appendix B. 6: *Clay matrix comprised of wavy 'flame-like' smetitic clays, and hexagonal, stacked, Kaolinite and/or chlorite.*

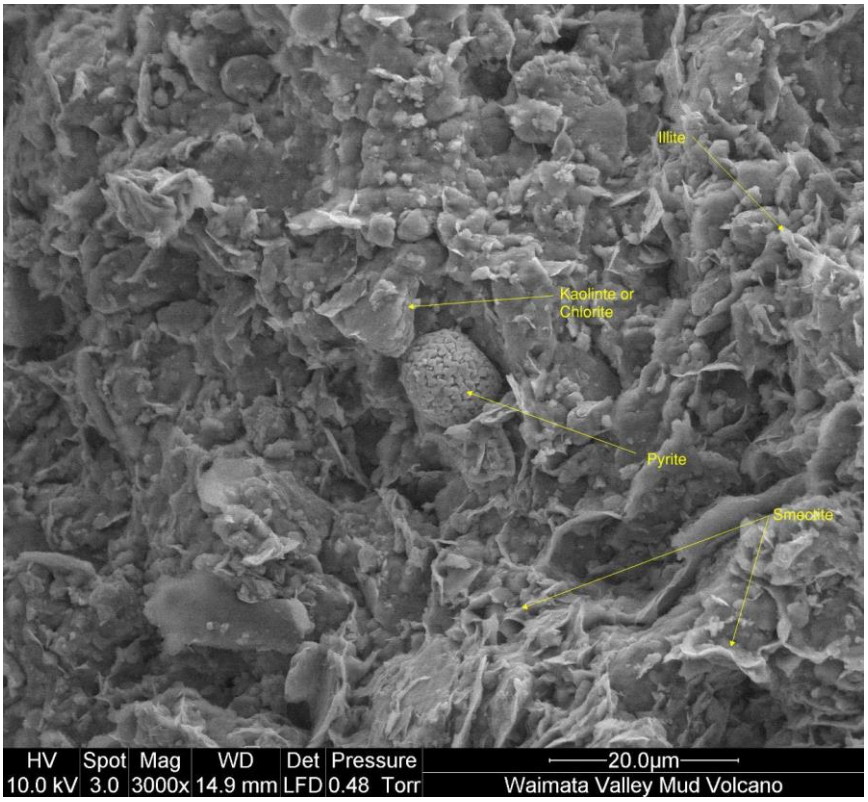

Appendix B. 7: *Pyrite crystal within clay matrix comprising of smectite, illite, and Kaolinite and/or chlorite.*

APPENDIX C: GEOTECHNICAL DATA

Number of Blows								
HA1	HA2	HA3	HA4	HA5	HA8	HA9	HA10	Depth (mm)
1	1	1	1	1	1	1	1	50
0	1	1	1	1	1	0	1	100
0	0	1	1	0	1	0	0	150
0	0	0	0	0	1	0	0	200
1	0	0	0	0	0	0	0	250
0	0	0	0	0	0	0	0	300
0	0	0	0	0	0	0	0	350
0	0	0	0	0	0	0	0	400
0	0	0	0	0	0	0	0	450
0	0	0	0	0	0	0	0	500
1	0	0	0	0	0	0	0	550
2	0	0	0	0	0	0	0	600
	0	1	0	0	0	0	0	650
	0	3	0	0	0	0	0	700
	0	5	1	0	1	0	0	750
	0	2	0	1	1	0	0	800
	1	1	0	1	1	0	0	850
	0		0	2		0	1	900
	0		0			0	0	950
	0		0			0	1	1000
	0		0			0	0	1050
	0		1			0	1	1100
	0		1			0	0	1150
	0		0			0	0	1200
	0		0			1	1	1250
	2		1			3	0	1300
	2		1			1	1	1350
	1		0			0	0	1400
	1		1			1	1	1450

			0			1	1	1500
			1			0	1	1550
			0			1	1	1600
			1			0	2	1650
			1			1	1	1700
			1			0	1	1750
			2			1	2	1800
			0			1	1	1850
			1			0		1900
			1			1		1950
						1		2000
						1		2050
						0		2100
						1		2150
						1		2200
						0		2250
						1		2300
						1		2350
						1		2400
						1		2450
						1		2500
						1		2550
						1		2600
						1		2650
						1		2700
						1		2750
						1		2800
						2		2850
						1		2900

Appendix C. 1: *Scala penetrometer results from various test positions*

Job No:	EARTHSCI794
Project:	Waimata Valley Mud Volcano
Calc:	AHL
Date:	#####
Check:	
Date:	

Description: Simplistic Slide model Sheet No:

Infinite Slope

Data				Results		
Gamma	kN/m3		17	Uplift	U	19.41
Phi	Deg		13	Normal Force: Soil		33.63
Cohesion	kPa		0	Normal Force: Ext Loads		0.00
				Total Normal Force		14.22
Fail S Depth	m	D	2	**Net Resistance**	R	3.28
Water Depth	m	Dw	0	Down Slope Force: Soil		3.53
Fail S Slope	Deg	S	6	Down Slope Force: Ext Loads		0.00
Ext Loads	kN/m	V	0	**Net Driving F**	F	3.53
	kN/m	H	0			
					FOS	**0.93**

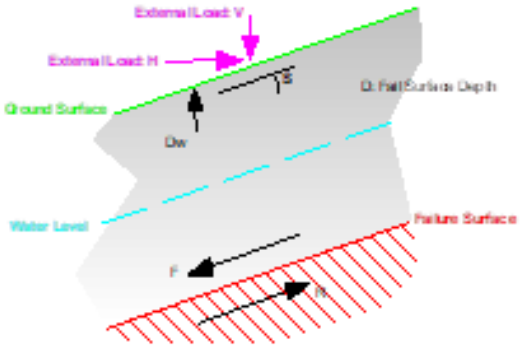

Note: Depths measured below Ground Level

Updated: 2016.12.09

Appendix C. 2: *Infinite Slope analysis using measured soil parameters*

Mastersizer Grading																			
	HA3		HA4		HA8		HA10 0.5m		TP1 (Vent)		HA6 0.5m		TP2 (Vent)		HA5 1.0m		HA9 1.0m		HA5 0.5m
sieve	0.3m	sieve	0.5m	sieve	0.5m	sieve	0.5m	sieve	1.0m	sieve	0.5m	sieve	0.0m	sieve	1.0m	sieve	1.0m	sieve	0.5m
8	100	8	100	8	100	8	100	8	100	8	100	8	100	8	100	8	100	8	100
4	100	4	100	4	100	4	100	4	100	4	100	4	100	4	100	4	100	4	100
2	100	2	100	2	100	2	100	2	100	2	100	2	100	2	100	2	100	2	100
1	100	1	100	1	100	1	100	1	100	1	100	1	99.98	1	100	1	100	1	100
0.5	100	0.5	100	0.5	100	0.5	99.37	0.5	100	0.5	100	0.5	99.46	0.5	99.95	0.5	100	0.5	99.68
0.25	99.9	0.25	98.51	0.25	99.97	0.25	88.61	0.25	100	0.25	98.83	0.25	98.68	0.25	93.93	0.25	99.45	0.25	90.81
0.125	98.31	0.125	90.09	0.125	99.68	0.125	73.24	0.125	99.71	0.125	93.76	0.125	98.68	0.125	79.69	0.125	96	0.125	81.5
0.063	94.68	0.063	81.58	0.063	98.73	0.063	65.64	0.063	97.47	0.063	89.15	0.063	94.68	0.063	62.7	0.063	91.2	0.063	78.83
0.031	89.46	0.031	72.81	0.031	94.4	0.031	62.77	0.031	90.59	0.031	83.12	0.031	84.39	0.031	46.88	0.031	85.38	0.031	76.51

0.016	80.68	0.016	62.95	0.016	83.89	0.016	58.48	0.016	78.8	0.016	72.62	0.016	70.67	0.016	36.01	0.016	76.45	0.016	69.67
0.008	67.57	0.008	52.39	0.008	67.46	0.008	45.98	0.008	56.39	0.008	57.8	0.008	55.67	0.008	27.98	0.008	61.96	0.008	57.7
0.004	49.09	0.004	36.08	0.004	45.96	0.004	28.62	0.004	34.17	0.004	39.79	0.004	37.98	0.004	19.12	0.004	42.16	0.004	40.73
0.002	27.19	0.002	19.27	0.002	23.96	0.002	14.15	0.002	16.45	0.002	21.14	0.002	19.92	0.002	9.99	0.002	21.57	0.002	22.07
0.001	0	0.001	0	0.001	0	0.001	0	0.001	0	0.001	0	0.001	0	0.001	0	0.001	0	0.001	0

Appendix C. 3: *Particle size analysis data extracted from Malvern Mastersizer 3000 used to create particle size analysis curves*

APPENDIX D: ICP-MS DATA

Marjor Elements, PPM																
SelectionLabel	Na	Mg	Al	Si	P	K	Ca	Ti	Fe							
AR-MV1	50966.67	23500	162466.7	427700	36273.33	41603.33	19863.33	8566.667	68500							
MS-MV1	32236.67	18533.33	145700	378033.3	11726.67	34430	6553.333	6158	52220							
MS-MV2	23306.67	21280	157066.7	422600	17070	35676.67	11056.67	5971	54780							
WV-MV	48436.67	23200	157360	423733.3	34000	38000	18916.67	8625.333	61933.33							
Trace Elements, PPM																
SelectionLabel	V	Cr	Mn	Co	Ni	Cu63	Cu65	Zn	Sr	Zr	Mo	Cd	Cs	Ba	Pb	U
AR-MV1	300.6667	169.5667	286.9333	11.77	55.2	52.16667	51.03333	193.5333	806.3333	164.3333	2.836667	0.007667	4.92	826.8667	14.73667	2.479
MS-MV1	234.4333	141.1667	134.7	11.5	45.73333	63.83333	61.63333	154.2333	186.1	114.6667	1.42	0.006567	4.011	578.4	13.29333	1.636667

MS-MV2	247	164.0667	125.6667	16.05	61.93333	70.36667	67.8	229.0667	438.3	114.0333	1.556667	0.010633	3.862	427.9667	9.56	1.765
WV-MV	274	186.4667	272.3333	12.08667	63.3	53.63333	53.16667	194.7333	700	153.3667	2.475	0.007	5.923333	792.7667	19.17667	2.224667
Rare Earth Elements, PPM																
SelectionLabel	Y	La	Ce	Nd	Sm	Eu	Tb	Dy	Yb							
AR-MV1	19.07333	17.51667	42.96667	15.7	3.583333	0.840667	0.444	3.143333	2.59							
MS-MV1	13.70333	11.82667	29.20667	10.43333	2.426667	0.573	0.286	2.233333	1.896667							
MS-MV2	13.80667	11.42333	28.64667	10.21667	2.36	0.56	0.287	2.25	1.956667							
WV-MV	16.57333	22.4	41.88333	16.71	3.006667	0.858	0.442	2.656667	2.6							

Appendix D. 1: *Elemental concentrations measured using ICP-MS. Data for Mangaehu and Arakihi Rd Mud Volcanoes (AR-MV, MS-MV1, MS-MV2) from Stanley (2019). Data from WV-MV measured as part of this study.*